NASA/TM—1998-206979

# Summary Report of Mission Acceleration Measurements for MSL–1

## STS–83, Launched April 14, 1997
## STS–94, Launched July 1, 1997

Milton E. Moskowitz and Kenneth Hrovat
Tal-Cut Company, North Olmsted, Ohio

Peter Tschen and Kevin McPherson
Lewis Research Center, Cleveland, Ohio

Maurizio Nati
European Space Research and Technology Center, Noordwijk, The Netherlands

Timothy A. Reckart
Tal-Cut Company, North Olmsted, Ohio

National Aeronautics and
Space Administration

Lewis Research Center

May 1998

Available from

NASA Center for Aerospace Information
7121 Standard Drive
Hanover, MD 21076
Price Code: A06

National Technical Information Service
5287 Port Royal Road
Springfield, VA 22100
Price Code: A06

# SUMMARY REPORT OF MISSION ACCELERATION MEASUREMENTS FOR MSL-1

## STS-83, launched April 14, 1997
## STS-94, launched July 1, 1997


Authors:

Milton E. Moskowitz
*Tal-Cut Company*
*North Olmsted, Ohio*

Kenneth Hrovat
*Tal-Cut Company*
*North Olmsted, Ohio*

Peter Tschen
*NASA Lewis Research Center*
*Cleveland, Ohio*

Kevin McPherson
*NASA Lewis Research Center*
*Cleveland, Ohio*

Maurizio Nati
*European Space Research and Technology Center*
*Noordwijk, The Netherlands*

Timothy A. Reckart
*Tal-Cut Company*
*North Olmsted, Ohio*

## Abstract

The microgravity environment of the Space Shuttle Columbia was measured during the STS-83 and STS-94 flights of the Microgravity Science Laboratory (MSL-1) mission using four different accelerometer systems: the Orbital Acceleration Research Experiment (OARE), the Space Acceleration Measurement System (SAMS), the Microgravity Measurement Assembly (MMA), and the Quasi-Steady Acceleration Measurement (QSAM) system.

All four accelerometer systems provided investigators with acceleration measurements downlinked in near-real-time. Data from each system was recorded for post-mission analysis. The OARE measured the Shuttle's acceleration with high resolution in the quasi-steady frequency regime below about 0.1 Hz. The SAMS provided investigators with higher frequency acceleration measurements up to 25 Hz. The QSAM and MMA systems provided investigators with quasi-steady and higher frequency (up to 100 Hz) acceleration measurements, respectively.

The microgravity environment related to various Orbiter maneuvers, crew activities, and experiment operations as measured by the OARE and MMA is presented and interpreted in section 8 of this report.

## Table of Contents

## List of Tables



## List of Figures

## Abbreviations and Acronyms

| | |
|---|---|
| A/D | analog-to-digital |
| APS | Alternate Payload Specialist |
| APU | auxiliary power unit |
| ASTRE | Accelerometre Spatiale Triaxiale Electrostatique |
| Astro/PGBA | Astro/Plant Generic Bioprocessing Apparatus |
| CDR | Commander |
| CG | Center of Gravity |
| CM-1 | Combustion Module-1 |
| CSLM | Coarsening in Solid-Liquid Mixtures |
| DAP | Digital Autopilot |
| dB | decibel |
| DCE | Droplet Combustion Experiment |
| DCP | Data Collection Processor |
| DLR | Deutsche Forschungsanstalt fur Luft und Raumfahrt (German Aerospace Research Establishment) |
| EDT | Eastern Daylight Time |
| EST | Eastern Standard Time |
| ESA | European Space Agency |
| ESTEC | European Space Research and Technology Center |
| EXPRESS | Expedite the Processing of Experiments to Space Station |
| FCS | Flight Control System |
| FEP | Front End Processor |
| FES | Flash Evaporator System |
| g | acceleration due to normal Earth gravity (9.81 $m/s^2$) |
| $g_o$ | 9.81 $m/s^2$ |
| GMT | Greenwich Mean Time (day/hour:minute:second) |
| GSE | Ground Support Equipment |
| HRM | High Rate Multiplexer |
| Hz | Hertz |
| IML-2 | Second International Microgravity Laboratory |
| IVIS | Inertial Vibration Isolation System |
| IWG | Investigator Working Group |
| JSC | Johnson Space Center |
| KSC | Kennedy Space Center |
| LeRC | Lewis Research Center |
| LIF | Large Isothermal Furnace |
| LMS | Life and Microgravity Sciences |
| LSP | Laminar Soot Processes |
| LVLH | Local Vertical Local Horizontal |
| μg | microgravity (1/1,000,000 of $g_o$) |
| mg | milligravity (1/1,000 of $g_o$) |
| MET | Mission Elapsed Time (day/hour:minute:second) |
| MEWS | Mission Evaluation Workstation System |
| MGBX | Microgravity Glovebox |
| MMA | Microgravity Measurement Assembly |
| MRD | Microgravity Research Division |

| | |
|---|---|
| MS | Mission Specialist |
| MSFC | Marshall Space Flight Center |
| MSL-1 | First Microgravity Science Laboratory |
| MSP | Microgravity Sensor Package |
| OARE | Orbital Acceleration Research Experiment |
| OMS | Orbital Maneuvering System |
| P | Pitch |
| PAO | Public Affairs Office |
| PCG | Protein Crystal Growth |
| PHaSE | Physics of Hard Spheres Experiment |
| PI | Principal Investigator |
| PIMS | Principal Investigator Microgravity Services |
| PLT | Pilot |
| POCC | Payload Operations Control Center |
| PRCS | Primary Reaction Control System |
| PS | Payload Specialist |
| PSD | Power Spectral Density |
| QSAM | Quasi-Steady Acceleration Measurement |
| QTH | Quasi-Steady Three-Dimensional Histogram |
| R | Roll |
| RCS | Reaction Control System |
| RMS | Root-Mean-Square |
| rpm | revolutions per minute |
| RSS | Root-Sum-of-Squares |
| SAMS | Space Acceleration Measurement System |
| SIMO | simultaneous supply water and waste water |
| SOFBALL | Structure of Flame Balls at Low Lewis-number |
| STS | Space Transportation System |
| TBE | Teledyne Brown Engineering |
| TEMPUS | Tiegelfreies Elecktromagnetisches Prozessieren Unter Schwerelosigkeit (Electromagnetic Containerless Processing Facility) |
| TSC | Telescience Support Center |
| TMF | Trimmean Filter |
| TSH | Triaxial Sensor Head |
| VRCS | Vernier Reaction Control System |
| VV | Velocity Vector |
| WWW | World Wide Web |
| X, Y, Z | Generic coordinate system axes |
| $X_{h,1}, Y_{h,1}, Z_{h,1}$ | MMA MSP-1 coordinate system axes |
| $X_{h,2}, Y_{h,2}, Z_{h,2}$ | MMA MSP-2 coordinate system axes |
| $X_{h,3}, Y_{h,3}, Z_{h,3}$ | MMA MSP-3 coordinate system axes |
| $X_{h,4}, Y_{h,4}, Z_{h,4}$ | MMA MSP-4 coordinate system axes |
| $X_{h,A}, Y_{h,A}, Z_{h,A}$ | SAMS TSH A coordinate system axes |
| $X_{h,B}, Y_{h,B}, Z_{h,B}$ | SAMS TSH B coordinate system axes |
| $X_{h,C}, Y_{h,C}, Z_{h,C}$ | SAMS TSH C coordinate system axes |
| $X_b, Y_b, Z_b$ | Orbiter Body coordinate system axes |
| $X_o, Y_o, Z_o$ | Orbiter Structural coordinate system axes |
| $X_{OARE}, Y_{OARE}, Z_{OARE}$ | OARE coordinate system axes |
| Y | Yaw |

**Acknowledgments**

The authors would like to thank the entire PIMS team, who provided acceleration environment interpretation during the mission, and real-time support with the SAMS team. We would also like to thank the crew of Columbia for their great work, and their insight during their Lewis Research Center visit.

A large portion of the interpretation in this report would not have been possible without the information provided by a number of individuals. We gratefully acknowledge Martin O'Toole of the Analex Company, who provided CM-1 gas chromatograph pump operation data. John Caruso (NASA LeRC), for his help in determining the CSLM run-times, and for telling us about the use of the MGBX circulation fans during the CSLM experiment runs. Daniel A. Catalano and Tony Johnson (Analex Corporation) for providing us with fan performance and other information from the DCE experiment. Dee Dee Westbrook, Wayne Wright, Brian Matisak, and Gary M. Rowe (Teledyne-Brown Engineering) for compiling the As-Flown timelines. Joerg Piller (DLR) for his positive identification of the TEMPUS water pump signature from both the IML-2 and MSL-1 missions. Victoria A. Lavergne (NASA JSC, Crew Office) for her information about Dyna-Bands and Dyna-Band exercise. Christian T. Lant (PHaSE Lead Functional Engineer) and Michael Shoemaker (PHaSE Project Lead), ADF, Inc., for detailed PHaSE mixer operational descriptions and timeline information. Alex Hoehn (BioServe Space Technologies, and University of Colorado) for identification of the Astro/PGBA air circulation pump. Tomas Hernandez and Donnie McCaghren (Teledyne-Brown Engineering), for helping to identify the MGBX circulation fan signature. Jeff Eggers, Cathy Jorgensen, and Jennifer Keller (ADF, Inc., SAMS group), for diagnosing and explaining the SAMS data anomalies. Robby Estep (United Space Alliance - JSC) for his information about Orbiter water dump systems.

## 1. Introduction and Purpose

Microgravity science experiments are conducted on the NASA Orbiters to take advantage of the reduced gravity environment resulting from the continuous free-fall state of a low Earth orbit. Accelerometer systems are flown on the Orbiters to record the microgravity environment. This environment is composed of quasi-steady accelerations (aerodynamic drag, venting forces, etc.), higher frequency accelerations (experiment equipment, Orbiter systems, crew activity, structural modes, etc.), and transient disturbances (thruster firings, crew activities, etc.).

The First Microgravity Science Laboratory (MSL-1) was launched on April 4, 1997 as the prime payload of the STS-83 flight aboard the Space Shuttle Columbia. Due to a fuel cell problem, the Orbiter returned to Earth on April 8, 1997, and landed at KSC. The MSL-1 experiments were given a second flight as STS-94, using the same vehicle, crew, and experiment facilities. STS-94 flew from July 1 to July 17, 1997. Throughout this report, both the STS-83 and STS-94 flights will be referred to using the "MSL-1" designation. Unless otherwise noted, discussions will refer to STS-94. The MSL-1 payload was dedicated to microgravity sciences, which included combustion, fluid physics, material processing, and life sciences disciplines. Two accelerometer systems managed by the NASA Lewis Research Center (LeRC) supported the MSL-1 mission: the Orbital Acceleration Research Experiment (OARE), and the Space Acceleration Measurement System (SAMS). These accelerometers were funded by the Microgravity Research Division (MRD) of the NASA Office of Life and Microgravity Sciences and Applications. In addition, the Microgravity Measurement Assembly (MMA) and the Quasi-Steady Acceleration Measurement (QSAM) system, both sponsored by the Microgravity Research Division, collected acceleration data as a part of the MSL-1 mission. The MMA was funded and designed by the European Space Agency in the Netherlands (ESA/ESTEC), and the QSAM system was funded and designed by the German Space Agency (DLR).

The Principal Investigator Microgravity Services (PIMS) project at the NASA Lewis Research Center (LeRC) supports Principal Investigators (PIs) of the microgravity science community as they evaluate the effects of acceleration on their experiments. PIMS' primary responsibility is to support NASA-sponsored investigators in the area of acceleration data analysis and interpretation.

This report was prepared and published by PIMS in order to furnish interested experiment investigators with a guide for evaluating the acceleration environment during the MSL-1 mission. Section 2 of this report provides an overview of the MSL-1 mission, payloads, and the experiments manifested on the payloads. Section 3 describes the coordinate systems used in this report. Section 4 describes the accelerometer systems flown on MSL-1, and discusses the means by which they recorded data and provided data to the users. Section 5 discusses the experiments which PIMS supported in real-time. Section 6 discusses specific analysis techniques which were applied to the accelerometer data. Section 7 briefly discusses the SAMS data anomalies encountered during STS-83. Section 8 describes the microgravity environment of Columbia during STS-94. Appendix A describes how OARE and SAMS data can be accessed through the Internet. Appendices B, C, and D, which are included on the attached CD-ROM and on the Internet, provide color spectrograms of MMA data at the Rack 10, 9, and 3 locations, respectively. Appendix E provides accelerometer system contact information. Appendix F contains a user comment sheet. Users are encouraged to complete this form and return it to the authors.

## 2. Mission Overview

The MSL-1 experiments were first launched on April 4, 1997 at 2:20 p.m. EST as the primary payload of the STS-83 flight aboard the Space Shuttle Columbia. Due to a fuel cell problem, the mission was shortened and Columbia landed on April 8, 1997 at 2:34 p.m. EDT at KSC. The MSL-1 experiments were given an historic second chance for flight. At 2:02 p.m. EDT on July 1, 1997, Columbia launched the STS-94 flight from the NASA Kennedy Space Center. Landing of STS-94 occurred at 6:47 a.m. EDT on July 17, 1997, at KSC. Both missions operated with the same vehicle, crew, and experiment facilities.

In terms of time conventions used in this report, the Greenwich Mean Time (GMT) corresponding to the STS-83 and STS-94 launches were 094/19:20:32 and 182/18:01:59, respectively. Nose landing gear touchdown were at GMT 098/18:33:23 for STS-83, and GMT 198/10:46:45 for STS-94. The mission elapsed time (MET) always starts at 000/00:00, corresponding to liftoff time. STS-83 landed at MET 003/23:12:51 and STS-94 landed at MET 015/16:44:46. Both GMT and MET are recorded in day/hour:minute:second format.

MSL-1 was a cooperative effort between international governmental partners, academic institutions, and industries to enhance the knowledge of various disciplines in microgravity science such as combustion, fluid physics, and materials science. Figure 1 is a schematic of the Spacelab module that shows the location of the experiment facilities. A list of MSL-1 experiments and facilities is shown in Table 1. Some facilities have multiple experiments and Principal Investigators. Table 2 shows a listing of payloads and affiliations. The seven member crew (listed in Table 3) was divided into two shifts (designated red and blue), enabling microgravity experiments to be conducted around the clock.

**Table 1. Experiments and Facilities**

| *Experiments and Facilities* | *Location* | *Contact* | *Affiliation* |
|---|---|---|---|
| Combustion Module-1 (CM-1)<br>*2 experiments* | Spacelab Rack 8 | Roy Hager | NASA Lewis Research Center, Cleveland, OH |
| Coarsening in Solid-Liquid Mixtures (CSLM) | Spacelab Rack 12 | Peter Voorhees | Northwestern University, Chicago, IL |
| Droplet Combustion Experiment (DCE) | Spacelab Rack 10 | Forman Williams | University of California, San Diego, CA |
| Expedite the Processing of Experiments to the Space Station (EXPRESS Rack)<br>*2 experiments* | Spacelab Rack 7 | Annette Sledd | NASA Marshall Space Flight Center, Huntsville, AL |
| Large Isothermal Furnace (LIF)<br>*6 experiments* | Spacelab Rack 9 | Thomas Glasgow<br>Alfonso Velosa | NASA Lewis Research Center, Cleveland, OH |
| Space Acceleration Measurement System (SAMS) | Spacelab Center Aisle | Ron Sicker | NASA Lewis Research Center, Cleveland, OH |
| Middeck Glovebox<br>*4 experiments* | Spacelab Rack 12 | David Jex | NASA Marshall Space Flight Center, Huntsville, AL |
| Electromagnetic Containless Processing Facility (TEMPUS)<br>*10 experiments* | Spacelab Rack 3 | Wolfgang Dreier | German Space Agency (DARA) |
| Protein Crystal Growth (PCG)<br>*3 experiments* | Spacelab Middeck | Keith Higginbotham | NASA Marshall Space Flight Center, Huntsville, AL |
| Microgravity Measurement Assembly (MMA) | Spacelab Rack 3 | Maurizio Nati | European Space Agency (ESA) |
| Quasi-Steady Acceleration Measurement (QSAM) System | Spacelab Rack 3 | Hans-Ewald Richter | German Aerospace Research Establishment (DLR) |

**Table 2. Payloads**

| *Payload* | *Location* | *Contact* | *Affiliation* |
|---|---|---|---|
| MSL-1 | Cargo Bay | Mike Robinson | Marshall Space Flight Center, Huntsville, AL |
| Cryogenic Flexible Diode (CRYOFD) | Cargo Bay | Susan Olden | Goddard Space Flight Center, Greenbelt, MD |
| Orbital Acceleration Research Experiment (OARE) | Keel Bridge | William Wagar | NASA Lewis Research Center, Cleveland, Ohio |

**Table 3. Crew**

| *Crewmember* | *Position* | *Team* |
|---|---|---|
| James D. Halsell | Commander | Red |
| Susan L. Still | Pilot | Red |
| Janice E. Voss | Mission Specialist -1, Payload Commander | Blue |
| Michael L. Gernhardt | Mission Specialist -2 | Blue |
| Donald A. Thomas | Mission Specialist -3 | Red |
| Roger K. Crouch | Payload Specialist -1 | Blue |
| Gregory T. Linteris | Payload Specialist -2 | Red |

## 3. Coordinate Systems

Five coordinate systems are discussed in this report: Orbiter structural, Orbiter body, OARE sensor, SAMS sensor, and MMA sensor.

In the Orbiter structural coordinate system ($X_o$, $Y_o$, $Z_o$), the direction from nose to tail of the Orbiter is $+X_o$, the direction from port wing to starboard wing is $+Y_o$, and the direction from the Orbiter belly to the top of the Orbiter fuselage is $+Z_o$. The origin of this coordinate system is at the tip of the external fuel tank, as illustrated in Figure 2. This coordinate system is usually used to specify the location of equipment within the vehicle.

In the Orbiter body coordinate system ($X_b$, $Y_b$, $Z_b$), the direction from tail to nose of the Orbiter is $+X_b$, the direction from port wing to starboard wing is $+Y_b$, and the direction from the top of the fuselage to the Orbiter belly is $+Z_b$. The origin of this coordinate system is at the Orbiter's center of gravity, and is typically used as the navigational reference frame. The Orbiter body coordinate system is shown in Figure 3.

In the OARE coordinate system ($X_{OARE}$, $Y_{OARE}$, $Z_{OARE}$), the direction from tail to nose of the Orbiter is $+X_{OARE}$, the direction from the Orbiter belly to the top of the Orbiter fuselage is $+Y_{OARE}$, and the direction from port wing to starboard wing is $+Z_{OARE}$. The origin of the OARE coordinate system is at the OARE sensor proofmass centroid. A description of the OARE instrument is given in Section 4.1.

The SAMS sensor and MMA sensor coordinate systems are specific to each sensor head. This results in three possible coordinate systems for the SAMS data, and four systems for the MMA data. SAMS sensor head notation is denoted with a capital axis, a subscript "h" (to denote head), and a capital letter to denote which sensor head (i.e. A, B, or C). MMA sensor head notation is denoted with a capital axis, a subscript "h" (to denote head), and a number to denote sensor number (i.e. 1, 2, 3, or 4).

Table 4 shows a compilation of the various coordinate systems, and may be used as a cross-reference between the systems.

**Table 4. Comparison of Coordinate Systems**

| Orbiter Struct. | Orbiter Body | OARE Sensor | SAMS TSH A | SAMS TSH B | SAMS TSH C | MMA MSP 1 | MMA MSP 2 | MMA MSP 3 | MMA MSP 4 |
|---|---|---|---|---|---|---|---|---|---|
| $+X_O$ | $-X_b$ | $-X_{OARE}$ | $+Z_{h,A}$ | $+Y_{h,B}$ | $-Z_{h,C}$ | $+X_{h,1}$ | $+Z_{h,2}$ | $-Y_{h,3}$ | $-X_{h,4}$ |
| $+Y_O$ | $+Y_b$ | $+Z_{OARE}$ | $-X_{h,A}$ | $+Z_{h,B}$ | $+X_{h,C}$ | $+Y_{h,1}$ | $-Y_{h,2}$ | $-Z_{h,3}$ | $-Y_{h,4}$ |
| $+Z_O$ | $-Z_b$ | $+Y_{OARE}$ | $-Y_{h,A}$ | $+X_{h,B}$ | $-Y_{h,C}$ | $+Z_{h,1}$ | $-X_{h,2}$* | $+X_{h,3}$ | $-Z_{h,4}$ |

* The sign for this entry has been inverted based upon an unknown data anomaly reported by the MMA group. This is under investigation, contact the MMA group for further details.

## 4. Accelerometer Systems

Four accelerometer systems measured the microgravity and vibration environment of the Orbiter Columbia during the MSL-1 mission: the Orbital Acceleration Research Experiment (OARE), the Space Acceleration Measurement System (SAMS), the Microgravity Measurement Assembly (MMA), and the Quasi-Steady Acceleration Measurement (QSAM) System.

### 4.1 Orbital Acceleration Research Experiment (OARE)

The OARE was designed to measure quasi-steady accelerations from below $1x10^{-8}$ g up to $2.5x10^{-3}$ g. The OARE consists of an electrostatically suspended proofmass sensor, an in-flight calibration subsystem, and a microprocessor for in-flight experiment control, processing, and storage of flight data [1-7]. The sensor's output acceleration signal was filtered using a Bessel filter with a cutoff frequency of 1 Hz for the $X_{OARE}$-axis, and 0.1 Hz for the $Y_{OARE}$- and $Z_{OARE}$-axes. The output signal was discretized at 10 samples per second. These data were processed and digitally filtered with an adaptive trimmean filter (TMF) prior to electronic storage onboard the instrument. Simultaneously, the unprocessed data were recorded on the Orbiter's payload tape recorder and routed to the Spacelab High Rate Multiplexer (HRM). Using the HRM interface, the unprocessed OARE data were downlinked from the Orbiter, and sent to the PIMS Ground Support Equipment (GSE) at the NASA Lewis Research Center's Telescience Support Center (TSC). The PIMS team subsequently processed and displayed the OARE data for the PIs on the World Wide Web in near-real-time.

The OARE was mounted to the floor of Columbia's cargo bay on a keel bridge, close to the Orbiter's center of gravity. The location and orientation of the sensor with respect to the Orbiter structural coordinate system are given in Table 5 and Figure 4. In this report, the OARE data are presented in Orbiter body coordinates. The sign convention used is consistent with a frame of reference fixed to the Orbiter, meaning that a forward thrust of the Orbiter is recorded as a negative $X_b$ acceleration because a free particle would appear to translate in the negative $X_b$-axis direction relative to the Orbiter's acceleration in the positive $X_b$-axis direction. OARE data for STS-83 are available from MET 000/00:10 through OARE power-down around MET 002/06:29. OARE data for STS-94 are available from MET 000/00:10 through MET 015/15:01. Appendix A describes how these data can be accessed using the Internet.

**Table 5. OARE Sensor Head Location and Orientation**

| OARE Sensor | | Sample Rate: 10 samples/second |
|---|---|---|
| Location: Orbiter Cargo Bay Keel Bridge | | Frequency: 0 to 1 Hz |
| ORIENTATION | | LOCATION |
| Orbiter Structural Axis | Sensor Axis | Structural Coordinates |
| $X_O$ | $-X_{OARE}$ | $X_O$ = 1153.3 in |
| $Y_O$ | $Z_{OARE}$ | $Y_O$ = -1.3 in |
| $Z_O$ | $Y_{OARE}$ | $Z_O$ = 317.8 in |

### 4.2 Space Acceleration Measurement System (SAMS)

The SAMS was developed to measure the low-gravity environment of the Orbiters in support of microgravity science payloads. STS-94 was the 18th flight of a SAMS unit on a Shuttle. The SAMS configuration for MSL-1 consisted of three remote triaxial sensor heads (TSHs), connecting cables, and a central processing unit with a data recording system using standard commercial hard drives that have been upgraded for space use. The main unit was located in the center aisle of the Spacelab module. The locations of the SAMS unit and its sensor heads are shown in Figures 5a, 5b, and 5c.

For the STS-83 flight, three TSHs (located at Racks 8, 9, and 12) were connected to the main unit. During post-flight analysis of the data, it was concluded that SAMS TSH A data were corrupt. Due to the short turnaround time between flights, the exact problem could not be localized, and SAMS TSH A was disconnected prior to the STS-94 flight. Further investigation showed that the TSH A data were corrupt due to an inadvertent zeroing of the data, resulting from the closing of the zeroing relays inside the head. These data were unrecoverable [8].

Two sensors (TSH B and C) were connected for the STS-94 flight. Real-time data downlink indicated sporadic anomalies with TSH B. Post-mission analysis showed that TSH B experienced inadvertent gain changes, and inadvertent zeroing of the data [8]. At the time of this printing, the PIMS group is currently working to recover portions of this corrupt data. The signals from the triaxial sensor heads were filtered by lowpass filters with cutoff frequencies of 25 Hz (TSH B, located in Rack 12) and 2.5 Hz (TSH C, located in Rack 9). These signals were then sampled at 125 and 12.5 samples per second, respectively. The data were simultaneously downlinked and recorded onboard the shuttle. In this report, the SAMS data are presented in terms of the Orbiter structural coordinate system. The SAMS data sign convention is such that a forward thrust of the Orbiter is recorded as a negative $X_o$ acceleration. We refer to this sign convention as an inertial frame of reference fixed to a point in space. The locations of the SAMS heads with respect to the Orbiter structural coordinate system are given in Table 6. More detailed descriptions of the SAMS accelerometers are available in the literature [9-15].

**Table 6. SAMS Sensor Head Locations and Orientations**

| Unit B, TSH A | | Sample Rate: 125 samples/second |
|---|---|---|
| S/N: 821-42 | | Facility: CM-1 |
| Location: Rack 8 | | Frequency: 25 Hz |
| ORIENTATION | | LOCATION |
| Orbiter Structural Axis | Sensor Axis | Structural Axis |
| $X_O$ | $+Z_{h,A}$ | $X_O$ = 1034.89 in |
| $Y_O$ | $-X_{h,A}$ | $Y_O$ = 64.01 in |
| $Z_O$ | $-Y_{h,A}$ | $Z_O$ = 418.23 in |

| Unit B, TSH B | | Sample Rate: 125 samples/second |
|---|---|---|
| S/N: 821-22 | | Facility: MGBX |
| Location: Rack 12 | | Frequency: 25 Hz |
| ORIENTATION | | LOCATION |
| Orbiter Structural Axis | Sensor Axis | Structural Axis |
| $X_O$ | $+Y_{h,B}$ | $X_O$ = 1118.77 in |
| $Y_O$ | $+Z_{h,B}$ | $Y_O$ = 34.88 in |
| $Z_O$ | $+X_{h,B}$ | $Z_O$ = 393.57 in |

| Unit B, TSH C | | Sample Rate: 12.5 samples/second |
|---|---|---|
| S/N: 821-10 | | Facility: LIF |
| Location: Rack 9 | | Frequency: 2.5 Hz |
| ORIENTATION | | LOCATION |
| Orbiter Structural Axis | Sensor Axis | Structural Axis |
| $X_O$ | $-Z_{h,C}$ | $X_O$ = 1079.38 in |
| $Y_O$ | $+X_{h,C}$ | $Y_O$ = 69.45 in |
| $Z_O$ | $-Y_{h,C}$ | $Z_O$ = 405.72 in |

Troubleshooting efforts after STS-94 determined there was a logic problem on the Data Collector Processor (DCP) board. Data transfers between the DCP and the Front-End Processor (FEP) board had a side effect of producing inadvertent bus-level commands to the boards controlling the sensor heads. The inadvertent commands caused gain changes and closing of the zeroing relays inside the affected heads, thereby corrupting the data. The frequency of occurrence of this effect and the number of channels affected was found to increase with temperature. The result on the data were that for the inadvertent zeroing, those portions of data are unrecoverable. The result for inadvertent gain changes is that the data were collected at less than optimum gain, but are recoverable [8].

For STS-83, 331 MB of valid SAMS data are available between MET 000/07:36 and MET 002/14:40. For STS-94, 2.2 GB of valid SAMS data are available between MET 007/03:33 and MET 015/05:25. Appendix A describes how these data can be accessed using the Internet.

### 4.3 Microgravity Measurement Assembly (MMA)

The MMA is a microgravity monitoring system capable of providing investigators and the Orbiter crew with real-time display of acceleration detected by up to seven sensor heads. These sensor heads consist of six Microgravity Sensor Packages (MSPs) and one Accelerometre Spatiale Triaxiale Electrostatique (ASTRE). The MSPs are triaxial micromechanical sensors, each with dedicated analog-to-digital (A/D) electronics, capable of measuring acceleration disturbances in the 0.1 to 100 Hz range. The ASTRE is an electrostatically suspended proofmass sensor, designed to measure quasi-steady disturbances of frequencies below 1 Hz. The ASTRE and one MSP reside within the MMA unit, and the remaining MSPs can be located remotely within the Spacelab module [1,16,17].

MMA has flown previously on the STS-55 (Spacelab D-2) and STS-78 (LMS) missions. The ASTRE sensor was previously flown only on the LMS mission. For MSL-1, four of the possible seven sensor heads were used, consisting of three MSPs and the ASTRE. The MMA main unit (containing one MSP and the ASTRE) were located in Rack 3 of the Spacelab module. The remaining two MSP sensor heads were located at the DCE (Rack 10) and the LIF (Rack 9) facilities within the Spacelab module. Figures 5a, 5b, and 5c show the approximate locations of MMA sensors for the MSL-1 mission.

Throughout the MSL-1 mission, data from the MMA sensors were downlinked to the ground via the HRM and the Experiment Computer Input/Output device. The HRM data were stored by the MMA Ground Station in the MSFC Payload Operations Control Center (POCC). The MMA team displayed the data via the World Wide Web in both the time and frequency domains, using either near-real-time or playback data.

For STS-83, approximately 2.8 gigabytes of MMA data are available between MET 000/06:24:31 and MET 002/20:01:50. For STS-94, over 17 gigabytes of MMA data from are available between MET 000/05:48:22 and MET 015/03:28:04. For MMA data access, the reader is referred to the MMA point-of-contact team member, listed in Appendix E.

### 4.4 Quasi-Steady Acceleration Measurement (QSAM) System

The QSAM system, first flown on STS-65 (IML-2), was developed by the German Aerospace Research Establishment (DLR) to detect accelerations from quasi-steady up to 50 Hz. For the quasi-steady range, QSAM advertises a resolution of $9.7 \times 10^{-7}$ g, and a resolution of $4.8 \times 10^{-5}$ g for frequencies up to 50 Hz. In order to assess the quasi-steady acceleration level, QSAM suppresses the sensor's bias and noise by rotating the sensor's sensitive axis. QSAM utilizes four rotating sensors to allow for a three-dimensional quasi-steady acceleration detection. An additional package with stationary (non-rotating) sensors provides measurements for frequencies up to 50 Hz [18].

During the MSL-1 mission, QSAM was located in Rack 3 (next to the TEMPUS facility). Throughout the MSL-1 mission, data from the QSAM sensors were downlinked to the ground via the HRM and the Experiment Computer Input/Output device. The HRM data were stored and displayed by the QSAM Ground Station in the MSFC Payload Operations Control Center (POCC). The PIMS team displayed the data on the World Wide Web via a remote POCC terminal emulator. For a complete set of QSAM data from the MSL-1 missions, the reader is referred to the QSAM point-of-contact team member, listed in Appendix E.

## 5. Real-Time Support on the First Microgravity Science Laboratory

Prior to flight, PIMS worked with Project Scientists and Principal Investigators (PIs) from the MSL-1 experiment teams to determine the appropriate acceleration data support for real-time and post-mission analysis. Accelerometer systems (placement of sensor heads, frequency characteristics, etc.) and real-time acceleration data displays were discussion topics during the MSL-1 Investigator Working Group (IWG) meetings. In particular, PIMS had the opportunity to work closely with the Structure of Flame Balls at Low Lewis-number (SOFBALL) and the Coarsening in Solid-Liquid Mixtures (CSLM) experiment teams.

The SAMS real-time displays on the Internet included acceleration versus time plots (for the $X_o$-, $Y_o$-, and $Z_o$-axes), and a color spectrogram for the root-sum-of-squares (RSS) combination of the three axes for the TSH B (MGBX), and TSH C (LIF) data. The color spectrograms served as an overview of the recent microgravity environment. These plots allowed the PIMS team to determine exercise activity, and alert the TEMPUS experiment team in near-real-time when exercise was currently underway. This real-time feedback allowed the TEMPUS group to closely monitor and control their critical experiment activities, attempting to minimize the impact of acceleration disturbances on their experiment.

In addition to the nominal SAMS display described above, a customized analysis display was developed for the CSLM experiment. This customized analysis contained plots of root-mean-square (RMS) acceleration versus time for five different frequency intervals. The total range of these frequency intervals was from 0.05 to 25 Hz. The specific intervals were chosen based upon discussions between the CSLM and PIMS groups.

The near-real-time OARE processing provided the capability to map the OARE data from the OARE instrument location to each of the facility locations in the Spacelab module, and to the Orbiter's center of gravity. In order to compute the effective quasi-steady acceleration at the various experiment facilities, the Orbiter's attitude data (body rates and angles) were extracted from the Orbiter's telemetry downlink and stored on PIMS Ground Support Equipment (GSE) located at NASA LeRC's Telescience Support Center (TSC). Prior to mapping the data to each of the facility locations, the OARE data were scale factor and bias compensated, and digitally filtered with an adaptive trimmean filter (TMF). The resultant data were the quasi-steady accelerations at each facility location. OARE real-time displays made available on the World Wide Web were acceleration versus time plots at each facility location for the $X_b$-, $Y_b$-, and $Z_b$-axes. In addition, raw (10 samples per second) OARE data were stored and processed throughout the mission in support of the SOFBALL experiment.

### 5.1 Structure of Flame Balls at Low Lewis-number (SOFBALL) Experiment

The SOFBALL experiment studied the interactions of chemical reactions with heat and mass transport for fuel-lean gas flames near their extinction limit. The proposed federal emission standards for the year 2000 and beyond are the primary driving force for gaining insight into the combustion process under fuel-lean conditions. Currently, the behavior of premixed gas flames near their extinction or stability limits is not well understood. A simple configuration (such as the SOFBALL experiment) is required to conduct further studies [19].

In a microgravity environment, reduced buoyant convection helps to emphasize other transport mechanisms, such as thermal and mass diffusion. A low Lewis number (high mass diffusivity and low thermal diffusivity) is required for complete combustion of a fuel-lean system near its extinction limits. In addition, it has been shown that many near-limit phenomena are influenced by buoyant convection. A microgravity environment is required to obtain a spherical symmetry, which avoids buoyancy-induced extinction of the flame balls. Flame balls are the simplest configuration to correlate theoretical, numerical, and experimental studies of the interaction between chemical and transport processes in flames near their extinction limits [19].

The SOFBALL PI was Professor Paul Ronney of the University of Southern California, and the hardware was developed by the NASA Lewis Research Center in Cleveland, Ohio. The investigation was supported by the Microgravity Research Division, Office of Life and Microgravity Sciences and Applications of NASA Headquarters. The SOFBALL experiment was conducted in the Combustion Module-1 (CM-1) facility. During the mission, the CM-1 apparatus was shared between two combustion experiments: SOFBALL and Laminar Soot Processes (LSP).

One of SOFBALL's objectives was to determine whether the flame ball motion was due to the non-zero gravity level encountered in the Spacelab module. Professor Ronney had requested PIMS to provide near-real-time, raw (10 samples per second) OARE acceleration data that were mapped to the CM-1 location for each of the SOFBALL runs. These OARE data were used as inputs to a SOFBALL numerical model which helped determine if the flame ball motion was buoyancy-induced.

### 5.2 Coarsening in Solid-Liquid Mixtures (CSLM) Experiment

The CSLM experiment examined the dynamics of the solid particle growth process within a two phase solid-liquid mixture. Coarsening is a phenomenon whereby small particles lose atoms to larger particles, causing the larger particles to grow. Coarsening occurs in many metallurgical systems. In their solid state, high-temperature turbine blade superalloys undergo coarsening at the operating temperature of the turbine. Coarsening also occurs in liquid-liquid and liquid-vapor systems, such as the growth of quartz droplets in molten steel and the growth of liquid droplets from the vapor phase which occurs inside rain clouds. A sound understanding of the coarsening process that predict the structures of alloys could lead to a wide range of commercial applications [20].

Recent theories suggest a strong dependence between the coarsening rate and particle volume fraction. In a terrestrial environment, coarsening experiments can only be performed with high volume fractions since the formation of solid skeletal structure can prevent particle sedimentation. In a microgravity environment, reduced buoyant convection helps to reduce particle sedimentation. The reduction of particle sedimentation allows the opportunity for this experiment to be performed over a wide range of particle volume fractions. The reduced buoyant convection also provides a diffusion-controlled process during coarsening. A liquid lead-tin alloy system is most ideal for this experiment since a reliable database of the thermophysical parameters that are required for comparison between theory and experiment is available [20].

The PI for the CSLM experiment was Professor Peter Voorhees of the Northwestern University. The experiment hardware was developed by the NASA Lewis Research Center in Cleveland, Ohio. The investigation was supported by the Microgravity Research Division, Office of Life and Microgravity Sciences and Applications of NASA Headquarters. Following a successful peer-review process, the CSLM experiment was selected from the NASA Materials Science Research Announcement. The CSLM experiment was conducted in the Microgravity Glovebox (MGBX) facility, and was the primary user of the MGBX facility.

One of the CSLM experiment requirements was to ensure that the coarsening process remained diffusion-controlled, which is believed to be possible only below 10 μg for frequencies less than 5 Hz. Professor Voorhees requested PIMS to provide near-real-time, root-mean-square acceleration data over five frequency ranges for each of the CSLM runs. The five frequency ranges chosen were: 0.01 to 6.5 Hz, 6.5 to 10 Hz, 10 to 15 Hz, 15 to 20.5 Hz, and 20.5 to 25 Hz.

## 6. Accelerometer Data Analysis

Post-flight, the SAMS group is responsible for SAMS data reduction, whereby the data are corrected for pre-mission bias calibration offsets, and compensated for temperature and gain related errors of bias, scale factor, and axial misalignment. The resulting units of acceleration are g's where 1 g = 9.81 m/s$^2$ (the nominal acceleration due to Earth's gravity). The data were orthogonally transformed from the SAMS TSH coordinate systems ($X_h$, $Y_h$, $Z_h$) to the Orbiter structural coordinate system ($X_o$, $Y_o$, $Z_o$).

The OARE data presented here have been compensated for temperature, bias, and scale factors errors, and were orthogonally transformed to the Orbiter Body Coordinate System ($X_b$,$Y_b$, $Z_b$). A detailed discussion of this processing may be found in [7].

The MMA and QSAM telemetry data streams were recorded on CD media by the Data Reduction group at MSFC. PIMS processed select portions of the MMA data using telemetry conversion algorithm descriptions supplied by the MMA group. The MMA data were calibrated for temperature changes and offset biases detected during flight.

After the data reduction phase, additional data analyses were applied to the SAMS, OARE, and MMA data to characterize the acceleration environment of the Orbiter. Some data analysis techniques are more applicable to data from one accelerometer than the other. For example, frequency domain analysis is typically not performed on quasi-steady acceleration measurements. The particular processing technique used also depends upon the type of information desired.

### 6.1 Time Domain Analysis

The time domain analysis technique used in this report for the high-frequency data is acceleration versus time. For low-frequency time domain analysis, plots of trimmean acceleration versus time, raw acceleration versus time, and Quasi-Steady Three-Dimensional Histogram (QTH) plots are provided. The notation for all the data analysis discussed here is defined in the Abbreviations and Acronyms list, located at the beginning of this document.

#### 6.1.1 Acceleration versus Time

These are plots of the acceleration (in units of g or μg) versus time. This type of plot yields the most precise accounting of the variation of acceleration magnitude as a function of time.

### 6.1.2 Trimmean Acceleration versus Time

A trimmean filter was applied to OARE data to reject transient, higher magnitude accelerations from analysis aimed at measuring the quasi-steady accelerations. This filtering procedure ranks the collected data in order of increasing magnitude, measures the deviation of the resulting distribution from a normal distribution, and deletes (trims) an adaptively determined amount of the data. The mean of the remaining data is calculated, and this value is assigned to the beginning of the time interval analyzed [7]. For this report, the trimmean filter was applied to 50 seconds of data every 25 seconds. Further information on this procedure may be found in [6,7].

### 6.1.3 Quasi-Steady Three-Dimensional Histogram

This type of analysis results in a visualization of the low frequency acceleration vector alignment, projected onto three orthogonal planes (for example, the top, front, and side view of the Orbiter). The time series is analyzed using a two-dimensional histogram method where the percentage of time the acceleration vector magnitude falls within a two-dimensional bin is plotted as a color. Areas showing colors toward the red end of the colorbar indicate higher occurrences of the acceleration vector magnitude falling within that area. Conversely, areas showing colors toward the blue end are indicative of a lower number of occurrences. A color of white indicates virtually no occurrences falling within that area. This type of plot provides a summary of the quasi-steady acceleration vector magnitude and direction for the time period analyzed. Timing of acceleration events cannot be extracted from this type of plot.

## 6.2 Frequency Domain Analysis

Transformation of acceleration data into the frequency domain is typically performed to gain more insight about the microgravity environment, and to help identify potential acceleration disturbance sources. The frequency domain analyses and displays used in this report include: acceleration power spectral density (PSD) versus frequency, and acceleration power spectral density versus frequency versus time (spectrogram). Frequency domain analyses are performed on SAMS or MMA MSP data, but are not performed on OARE or MMA ASTRE data due to the relative lack of pertinent frequency information in the quasi-steady regime.

### 6.2.1 Power Spectral Density (PSD) versus Frequency

Spectral analysis is performed on time series data to identify the relative magnitudes of sinusoidal signals that compose the series. The basis of this computation is the Fourier transform, which indicates the magnitude of each frequency (sinusoid) present in the time history signal. The PIMS team uses the PSD as a basis for frequency domain analysis. The PSD (reported in units of $g^2/Hz$) is derived from the discrete Fourier transform of a time series such that Parseval's relation is satisfied: the RMS of a time signal is equal to the square root of the integral of the PSD across the frequency band represented by the original signal. Stated mathematically:

For even N:

$$PSD(m) = \begin{cases} \frac{2|F(m)|^2}{N U f_s} & [g^2/Hz] \text{ for } m = 1,2,...,(N/2)-1 \\ \frac{|F(m)|^2}{N U f_s} & [g^2/Hz] \text{ for } m = 0 \text{ and } m = (N/2) \end{cases}$$

and for odd N:

$$PSD(m) = \begin{cases} \frac{2|F(m)|^2}{N U f_s} & [g^2/Hz] \text{ for } m = 1,2,...,(N-1)/2 \\ \frac{|F(m)|^2}{N U f_s} & [g^2/Hz] \text{ for } m = 0 \end{cases}$$

where

$$U = \frac{1}{N} \sum_{n=0}^{N-1} w_n^2$$

$|F(m)|$ is the magnitude of the one-sided Fast Fourier Transform, $f_s$ is the sampling rate, and N is the number of data points in the time series.

Spectral averaging is often used to produce PSDs that represent the average spectral content of a time period of interest. The PSDs resulting from k successive intervals are calculated, and the k resulting spectral series are averaged together on a point-by-point basis. This averaging technique is often referred to as Welch's Averaged Periodogram Method. Signal stationarity is an underlying assumption when spectral averaging is performed. While the microgravity environment of Earth-orbiting laboratories is not stationary, there are periods when the environment does not change significantly. Variations in spectral content are subject to averaging when the acceleration spectrum is non-stationary.

### 6.2.2 Power Spectral Density versus Frequency versus Time (Spectrogram)

Spectrograms provide a roadmap of how acceleration signals vary with respect to both time and frequency. As such, they are particularly useful for identifying when certain activities (such as exercise, pumps, etc.) began or ended. To produce a spectrogram, PSDs are computed for successive time intervals. The PSDs are oriented vertically on the page such that frequency increases from bottom to top. PSDs from successive time slices are spread horizontally across the page such that time increases from left to right. Each time-frequency bin is assigned a color corresponding to the base 10 logarithm of the PSD magnitude at that time and frequency.

### 6.2.3 Spectrogram Decoder Tool

The microgravity environment of the Orbiter is dynamic; the start and stop of various equipment and activities are not always timelined or predictable. To facilitate the analysis of over 15 days of acceleration data, such as those collected for this mission, it is often useful to have a tool that indicates the source of significant disturbances for a specific time and frequency. The decoder tool (Figure 6) was included as an aid to help track spectral components that are attributable to specific disturbances over time. The dimensions and orientation of this decoder tool are such that when it is overlayed on the appendix spectrograms, with the alignment marks as indicated, the markers along the vertical axis (the frequency axis) give indication for the presence or absence of the specified disturbance source. Time can then be read off the abscissa of the spectrogram plot. Note that size and tic location should match scale of Appendix spectrograms. Scale decoder tool cut-out with photocopier if needed. Table 7 shows a tabular representation of Figure 6.

**Table 7. Select Acceleration Disturbances Below 100 Hz**

| *Frequency Range (Hz)* | *Known Disturbance* |
|---|---|
| 17.0 | Ku-band antenna dither fundamental |
| 31.8 - 32.0 | Astro/PGBA |
| 34.0 | Ku-band antenna dither 2nd harmonic |
| 42.6 - 43.0 | TEMPUS |
| 44.2 - 44.6 | Astro/PGBA |
| 45.0 - 45.3 | Astro/PGBA |
| 46.1 | CM-1 Gas Chromatograph vacuum pump |
| 51.0 | Ku-band antenna dither 3rd harmonic |
| 54.7 | CM-1 Gas Chromatograph vacuum pump |
| 63.3 - 63.7 | Astro/PGBA |
| 65.1 - 65.6 | PHaSE |
| 66.3 - 66.9 | PHaSE |
| 67.4 - 67.8 | PHaSE |
| 73.6 - 74.9 | DCE |
| 81.7 - 81.9 | DCE |
| 85.5 - 86.1 | TEMPUS |
| 86.2 - 86.7 | PHaSE |
| 89.9 - 90.1 | PHaSE |

## 7. Description of STS-83 SAMS Data Anomalies

During the STS-83 flight, SAMS TSH A (Rack 8, CM-1 location) experienced data acquisition problems. During the mission, telemetry data indicated that the acceleration data were corrupt. Due to the short time between the STS-83 and STS-94 flights, ground-based troubleshooting efforts failed to find the cause of the problem, and TSH A was disconnected from the main unit to guard against potential damage.

Troubleshooting after the STS-94 flight traced the anomaly to a logic problem on the data collector processor board. Data transfers between this board and the front-end processor board inadvertently produced bus-level commands to the sensor head controller boards. These inadvertent commands caused gain changes and closing of the zeroing relays inside the affected sensor head, corrupting the data.

Further analysis showed that these inadvertent bus-level commands were sensitive to both temperature and loading of the bus. With the removal of TSH A (for the STS-94 flight), the bus loading was changed, and this caused sporadic corruption of the TSH B data for the STS-94 flight. For further details, contact the SAMS group at the NASA Lewis Research Center.

## 8. Columbia Microgravity Environment (STS-94)

The microgravity environment of an orbiting space laboratory such as the Shuttle has many components. The quasi-steady microgravity environment is related to orbital phenomena such as aerodynamic drag and rotational motion, and to gravity gradient effects based upon the location-of-interest's distance from the Orbiter's center of gravity. In addition to these quasi-steady accelerations, all ongoing operations of crew life-support systems and activities, and operations of the Orbiter, crew, carrier, and experiments have transient and vibratory components that contribute to the overall acceleration environment.

The remainder of this section discusses the acceleration environment recorded during the STS-94 flight of Columbia, including accelerations related to Orbiter attitude, Orbiter venting operations, a variety of experiment-specific fans, pumps, and compressors, crew exercise, and crew quiet periods.

The Appendices provide an overview of the microgravity vibration environment during the STS-94 mission. Appendices B, C, and D present color spectrograms of the MMA MSP-3, MSP-4, and MSP-1 data, respectively. These appendices are on the enclosed CD-ROM, and on the PIMS Internet Web page (see http://www.lerc.nasa.gov/WWW/MMAP/PIMS/HTMLS/reportlist.html). Adobe Acrobat Reader 2.1 or higher is required to access the PDF files of these plots. Also on the enclosed CD-ROM, are mission summary reports for: SPACEHAB-5 (STS-79), LMS (STS-78), USMP-3 (STS-75), and USML-2 (STS-73).

### 8.1 Orbiter Attitude

A summary plot of the OARE data for the entire STS-94 mission is provided in Figure 7. The MSL-1 mission was flown using a two-shift crew. This fact manifests itself in the absence of prolonged quiet periods in Figure 7 as would be expected for sleep periods. The distinction between the two primary attitudes (-ZN/55ROLL and -ZN/+XV55ROLL) during the MSL-1 mission are not readily apparent from the acceleration versus time plot.

A Quasi-Steady Three-Dimensional Histogram (QTH) of the trimmean filtered OARE data recorded throughout the mission is provided in Figure 8. Initial inspection of the plot suggests a single attitude throughout the mission. Closer inspection of the $X_b$- versus $Y_b$-axis (lower left) plot indicates an oval-shaped area of concentration, instead of the expected circular area signature of a single attitude observed in previous missions [1]. This oval-shaped concentration is a direct result of the similarity between the two primary attitudes flown during the mission. The -ZN/55ROLL ([pitch,yaw,roll]=[180.0,0.0,55.0]) attitude orients the Orbiter's tail into the velocity vector with a 55 degree roll. The attitude -ZN/+XV55ROLL ([pitch,yaw,roll] = [0.0,0.0,235.0]) orients the Orbiter's nose into the velocity vector with a 235 degree roll. The similarities in these two primary MSL-1 attitudes results in their three-dimensional projections sharing nearly the same space, resulting in the oval-shaped concentration observed in Figure 8.

### 8.2 Venting Operations

The Orbiter Food, Water, and Waste Management Subsystem provides storage and dumping capabilities for potable and waste water [21]. Supply and waste water dumps are performed using nozzles located on the port side of the Orbiter. Water dumps from these nozzles are expected to cause a steady acceleration of about $4.0 \times 10^{-7}$g in the negative $Y_b$-direction [22]. Figures 9 and 10 show a simultaneous supply water/waste water (SIMO) dump and a supply water dump alone, respectively. In addition to the expected $Y_b$-axis effects, these water dumps show unexpected effects in the $Z_b$-axis. These unexpected $Z_b$-axis effects have been present in the OARE data for all microgravity missions since USML-2 (STS-73). The explanation for these $Z_b$-axis contributions is unknown.

The availability of the MMA ASTRE data from MSL-1 (see Table 4, for the ASTRE coordinate system, MMA MSP-2 column) allows for a comparison between the OARE and ASTRE sensors and their ability to detect events in the quasi-steady acceleration realm. For this comparison, both sensors' data sets were subjected to a trimmean filter utilizing a 50 second sliding window reporting a filtered acceleration reading every 25 seconds. These trimmean filter parameters represent the standard parameters used for processing the raw (10 sample per second) OARE data. Figures 11 and 12 are comparisons of OARE and ASTRE data (mapped to the ASTRE location in Rack 3) during a supply water dump and SIMO dump, respectively. Both quasi-steady acceleration measurement systems indicate the expected $Y_b$-axis effects and the unexpected effects in the $Z_b$-axis discussed previously.

### 8.3 Microgravity Glovebox (MGBX) Circulation Fans

The PIMS group has performed an acceleration characterization of the fans which were used in the old glovebox facility [23,24]. The MSL-1 mission provided the opportunity for PIMS to characterize the acceleration levels which were related to the new MGBX fan operations. For this characterization, the crew were asked to cycle the MGBX fans on and off, and voice down the times for the switch throws. Adequate time between switch throws was allowed for the accelerometer systems to record data. The fans cycled were interface fans 1 and 2, as well as the workarea circulation fan.

The MGBX checkout procedure (performed during MET day 001) called for the workarea circulation fan to be used, at a speed setting of 5. The fan settings range from 1 through 7, with higher numbers indicating higher speeds. Figure 13 shows a 1-hour color spectrogram of MMA MSP-3 data for a portion of the time frame of the MGBX checkout procedure. Recall that the MMA MSP-3 sensor utilized a lowpass cutoff filter of 100 Hz, therefore all data above 100 Hz have been attenuated, and will appear artificially low in magnitude. Notice the acceleration signals that plateau at 63.5, 66.5, 98.6, and 127.0 Hz. These start around t=2 minutes, and cease around t=55 minutes. These signals are related to the operation of the MGBX workarea circulation fan, and an integration of the PSDs show them to range in magnitude up to 180 $\mu g_{RMS}$. This fan speed setting was utilized for the CSLM experiment runs during this mission.

Two runs were made of the MGBX fan characterization procedure (using a circulation fan setting of 7). The first was performed between MET 002/14:25 and 002/14:34, and the second between MET 014/19:57 and 014/20:05. Although the exact impact is unknown, the MGBX filter covers were installed during the first run. Presumably, this accounts for the fact that no acceleration signals were identified as being circulation-fan specific during this test. The second run, however, showed two acceleration signals that are related to the MGBX circulation fan's use at the speed setting of 7. Figure 14 shows a color spectrogram (imaged with the same frequency and magnitude limits as Figure 13) for the period covering the second MGBX fan characterization activity. Notice the signals at 71 and 104 Hz (having acceleration magnitudes of 200 and 100 $\mu g_{RMS}$, respectively) which are active between t=12 and t=15 minutes in this plot. Note that the higher frequency signal is above the cutoff frequency for the sensor head, thus the measured acceleration level is lower than the actual acceleration level.

The cause for a lower number of signals at the higher speed is most likely due to varying harmonics based upon the fundamental operating frequency of the fan at the two speeds. The higher speed setting resulting in a higher frequency is consistent with expectations (i.e. a fan must rotate more quickly in order to circulate more air for a given period of time).

### 8.4 Crew Exercise

In order to maintain physical fitness, each crew member must perform some type of physical exercise throughout the mission. This is normally accomplished with one exercise period per person per day. During STS-94, two primary types of exercise were performed: pedaling on the ergometer or stretching a Dyna-Band.

The ergometer is a recumbent bicycle-like device, with the crew member's pedaling motion being the primary exertion. During the MSL-1 mission, the ergometer was isolated using the Inertial Vibration Isolation System (IVIS) on the flight deck of the Orbiter. Past PIMS analyses [24] have shown that ergometer exercise typically produces acceleration disturbances around 2-3 Hz ("two-per-rev" associated with the pedaling frequency), and 1-1.5 Hz (corresponding to the crew member's shoulders rocking side-to-side). The recorded magnitude of these disturbances is a function of the crew member, the type of vibration isolation (if any), the location of the ergometer, and the structural transmission path between the exercise and measurement locations.

A Dyna-Band is a flat, 6-inch wide, 3-foot long latex band. According to Victoria A. Lavergne (NASA JSC, Code CB), "The band can be wrapped around the hands for upper body work or [used] for lower body conditioning." This type of exercise was Roger Crouch's (PS-1) primary exercise method during the MSL-1 mission.

Table 8 is a list of the crew exercise times for the STS-94 mission. This table was generated by analyzing the color spectrogram plots from MMA MSP-3. The crew member column was completed based on notes from the PIMS logbook (denoted by a '†'), and from the STS-94 As-Flown Experiment Timeline (denoted by a '*') [25].

A comparison of the accelerations imparted by various crew members shows the similarities and differences between the crew members' exercise characteristics. The periods shown in Table 8 were analyzed in the frequency domain to produce cumulative root-mean-square (RMS) acceleration versus frequency plots. The frequency domain data for all of a single crew member's exercise periods were averaged on a point-by-point basis. The results of these averages are shown in Figure 15.

Note that the line corresponding to MS-3 is significantly higher in the 0-4 Hz region. Due to the cumulative nature of the plots (and the first few points being higher for this trace), this observation is not related to the exercise from this crew member. This increased level is caused by impulsive disturbances in acceleration data, which cause a broad-band increase, particularly in the DC-component.

## Table 8. STS-94 Exercise Period Overview

| *Time (MET)* | *Crew* | *Time (MET)* | *Crew* |
|---|---|---|---|
| 000/21:40 - 000/22:10 | Don* | 008/09:15 - 008/09:42 | Mike† |
| 000/22:25 - 000/23:00 | Greg* | 008/10:22 - 008/10:58 | Janice† |
| 001/03:05 - 001/03:25 | Janice† | 008/12:03 - 008/12:30 | Jim† |
| 001/08:19 - 001/09:00 | Mike† | 008/12:36 - 008/13:02 | Don† |
| 001/13:00 - 001/13:30 | Jim† | 008/21:10 - 008/21:40 | Greg† |
| 001/13:40 - 001/14:10 | Don† | 008/21:41 - 008/22:00 | Susan† |
| 001/16:00 - 001/16:20 | Susan* | 009/08:18 - 009/08:50 | Mike† |
| 001/22:05 - 001/22:40 | Greg† | 009/09:36 - 009/10:05 | Janice† |
| 002/09:15 - 002/09:45 | Mike* | 009/10:19 - 009/10:50 | Don† |
| 002/10:20 - 002/10:55 | Janice* | 009/12:58 - 009/13:21 | Jim† |
| 002/12:38 - 002/13:10 | Don* | 009/13:23 - 009/14:00 | Greg† |
| 002/16:20 - 002/16:55 | Jim† | 009/22:00 - 009/22:10 | Susan† |
| 002/21:40 - 002/22:05 | Susan* | 009/22:20 - 009/22:40 | Susan† |
| 002/23:05 - 002/23:35 | Greg* | 010/10:10 - 010/10:40 | Don or Roger* |
| 003/09:38 - 003/10:10 | Mike† | 010/10:50 - 010/11:20 | Janice† |
| 003/10:55 - 003/11:22 | Janice* | 010/11:25 - 010/11:55 | Don or Roger* |
| 003/12:15 - 003/12:42 | Jim* | 010/12:10 - 010/12:40 | Jim† |
| 003/12:55 - 003/13:20 | Don* | 010/12:45 - 010/13:28 | Greg† |
| 003/21:10 - 003/21:40 | Susan* | 010/22:35 - 010/22:55 | Susan† |
| 003/21:45 - 003/22:25 | Greg* | 011/10:20 - 011/10:53 | Janice† |
| 004/04:45 - 004/05:00 | Roger* | 011/11:00 - 011/11:30 | Mike or Roger* |
| 004/09:15 - 004/09:42 | Mike† | 011/12:05 - 011/12:40 | Jim* |
| 004/10:23 - 004/11:00 | Janice* | 011/12:45 - 011/13:20 | Don* |
| 004/12:22 - 004/12:55 | Jim* | 011/21:30 - 011/22:10 | Susan† |
| 004/13:20 - 004/13:50 | Greg† | 011/22:18 - 011/23:00 | Greg† |
| 004/17:00 - 004/17:30 | Don* | 012/08:00 - 012/08:30 | Roger† |
| 004/22:10 - 004/22:35 | Susan† | 012/09:20 - 012/09:50 | Don† |
| 005/10:15 - 005/10:43 | Mike* | 012/11:20 - 012/11:55 | Janice† |
| 005/11:08 - 005/11:28 | Janice* | 012/14:00 - 012/14:38 | Greg† |
| 005/12:25 - 005/12:55 | Jim* | 012/21:00 - 012/21:30 | Susan† |
| 005/15:58 - 005/16:25 | Don* | 012/22:03 - 012/22:38 | Jim† |
| 005/21:45 - 005/22:20 | Susan* | 013/10:40 - 013/11:03 | Mike* |
| 005/22:35 - 005/23:15 | Greg† | 013/11:20 - 013/11:50 | Janice† |
| 006/10:00 - 006/10:35 | Janice† | 013/14:15 - 013/14:20 | Greg* |
| 006/10:58 - 006/11:23 | Mike* | 013/14:25 - 013/15:20 | Don† |
| 006/12:25 - 006/12:55 | Jim* | 013/16:30 - 013/16:55 | Susan† |
| 006/13:10 - 006/13:41 | Don* | 013/17:00 - 013/17:25 | Jim† |
| 006/13:50 - 006/14:32 | Greg† | 014/09:40 - 014/10:10 | Mike* |
| 006/22:00 - 006/22:20 | Susan† | 014/13:20 - 014/13:50 | Janice* |
| 007/09:05 - 007/09:35 | Mike† | 014/13:55 - 014/14:25 | Greg* |
| 007/10:22 - 007/10:45 | Janice* | 014/14:30 - 014/15:05 | Don† |
| 007/11:58 - 007/12:30 | Jim† | 014/16:13 - 014/16:17 | Jim† |
| 007/12:40 - 007/13:10 | Don† | 014/16:25 - 014/16:50 | Jim† |
| 007/21:30 - 007/21:55 | Susan† | 014/18:22 - 014/18:40 | Susan† |
| 007/22:36 - 007/23:15 | Greg† | | |

†: Crew notation from PIMS Data Logbook, *: Crew notation from As-Flown Timeline

None of the crew members shows a particularly strong shoulder-sway peak around the 1-1.5 Hz region, however increased slopes in this frequency region are evident (see CDR, MS-1, and PS-2 traces in Figure 15). The pedaling frequency for CDR, PLT, MS-3, and one of PS-1's ergometer periods are in the 2.5-3 Hz region, which is consistent with past mission exercise data. The pedaling frequency for MS-1 is around 3 Hz. The pedaling frequency for MS-2, one of PS-1's ergometer periods, and PS-2 is in the 3-3.5 Hz region, which is higher than normally noted, but not out of family. Continuing up through the spectrum, all crew members show a heightened response at about 4.5 Hz, which is close to one of the vehicle's structural modes. Some crew members (PLT, MS-1, MS-2, and PS-1) show a strong upper frequency around 5.5 Hz, which is also close to a structural mode.

As seen from this analysis, there are similarities (twin peaks at pedaling and shoulder-sway frequencies), and there are differences between the crew members in both the frequency and intensity of their exercise characteristics. Such similarities and differences between crew members are to be expected, and these are consistent with similar comparisons from previous missions.

### 8.5 Public Affairs Office (PAO) Events/Quiet Periods

During a typical Shuttle mission, a number of demonstration and/or question-and-answer periods are scheduled. These are timelined as Public Affairs Office (PAO) events, and normally take place with some or all of the crew gathered in a single area, such as the flight deck. These PAO events tend to quiet the microgravity environment because crew activity is reduced from nominal conditions, so the crew is less likely to impart push-off and impact transients on the Orbiter's structure. In addition, crew conferences and briefings occur with similar quieting of the acceleration environment.

During this mission, there were at least 11 PAO events that took place with a nominal duration of about 15 minutes each. Table 9 enumerates the MET start and stop times of some selected PAO/quiet periods.

**Table 9. Selected PAO/Quiet Periods**

| *Activity* | *MET Start* | *MET Stop* | *Comments* | *Figure Reference* |
|---|---|---|---|---|
| PAO Event | 02/00:00:50 | 02/00:18:02 | All 7 crew on flight deck | Figure 16 (a) |
| PAO Event | 11/17:55:36 | 11/18:10:26 | With 4 crew members (red shift) | Figure 16 (b) |
| Crew Conference | 13/12:48:00 | 13/13:12:51 | All 7 crew members | Figure 16 (c) |
| Deorbit Brief | 14/12:01:00 | 14/12:12:47 | All 7 crew members | Figure 16 (d) |

Color spectrograms for SAMS TSH B (mounted under the glovebox in Rack 12) that encompass the 4 periods specified in Table 9 are shown in Figure 16. Note that below about 10 Hz, the tendency of the spectrograms is toward the blue range of the scale for the excerpt times listed in Table 9. The upper left plot shows this most clearly. This exemplifies the quieting effect that is expected from diminished crew activity. For the time periods spanned by the spectrograms of Figure 16, the RMS acceleration values measured by SAMS TSH B decrease from a median value of approximately 167 $\mu g_{RMS}$, during nominal crew activity, to about 123 $\mu g_{RMS}$, while the crew was less active. During such quiet periods, Orbiter structural modes around 5 Hz and the Ku-band antenna dither at 17 Hz dominate the acceleration spectra.

The quasi-steady microgravity environment measured by OARE exhibits a noticeable quieting during PAO events. Figure 17 illustrates the effect of the crew conference of Figure 16(c) event on the quasi-steady acceleration environment. During this event, the reduced crew activity level leads to a noticeably quieter microgravity environment. This particular event involved the entire STS-94 crew and consequently minimized the effects of crew activity on the microgravity environment.

### 8.6 Physics of Hard Spheres Experiment (PHaSE)

The Physics of Hard Spheres Experiment (PHaSE) was designed for integration in the Expedite the Processing of Payloads to Space Station (EXPRESS) Rack on the MSL-1 mission. The objective of this experiment was to characterize the nucleation and growth of colloidal crystals driven purely by the configurational entropy of tailored hard spheres. The PHaSE payload was comprised of three separate hardware assemblies: the test section, the avionics section, and a power drawer. The test section housed the instrument portion of the payload, which contained (among other things) sample cells and a mixer. The mixer employed a belt system that oscillated the sample cells in order to homogenize them prior to the start of an experiment sequence [26].

#### 8.6.1 PHaSE Activation/Deactivation

Activation of the PHaSE facility was performed by MS-3 around MET 000/16:30 [25]. Figure 18 shows the 60-94 Hz region of a color spectrogram of MMA MSP-4 data (LIF Location, Rack 9). Notice the five signals which start just before t=35 minutes on this plot (MET 000/16:34). Figure 19 shows an analogous plot for the MSP-3 data (DCE Location, Rack 10). Table 10 summarizes the five frequencies which were excited, and the change in RMS acceleration levels which were measured by the sensor heads for each of these bands.

**Table 10. Comparison of RMS Acceleration Levels Before and After PHaSE Activation, MMA MSP-3 (Rack 10), and MMA MSP-4 (Rack 9) Data**

| | RMS Acceleration Increase [$\mu g_{RMS}$] | |
|---|---|---|
| ***Frequency Range [Hz]*** | ***MSP-3*** | ***MSP-4*** |
| 65.1-65.6 | 38.8 | 87.0 |
| 66.3-66.9 | 64.8 | 130.5 |
| 67.4-67.8 | 45.1 | 120.9 |
| 86.2-86.7 | not observed | 39.6 |
| 89.9-90.1 | 14.2 | 126.5 |

Not surprisingly, the MSP-4 sensor (located one rack aft of the EXPRESS Rack) measured higher acceleration increases than did the MSP-3 sensor (located one rack aft, and across the aisle from the EXPRESS Rack).

These five frequencies all disappear abruptly at MET 014/17:13 (corresponding with the PHaSE deactivation period performed by MS-3) [25]. A color spectrogram of this deactivation time (using MMA MSP-4 data) is shown in Figure 20. Note the cessation of the five PHaSE-attributed spectral components at about the 13-minute mark.

### 8.6.2 PHaSE Mixer

Operation of the PHaSE mixer imparted a distinct signature in the acceleration data collected by the MMA MSP-4 sensor. This accelerometer was located in Rack 9 of the Spacelab module, which was adjacent to the PHaSE equipment operated in Rack 7 (see Figure 1). Figure 21 shows a spectrogram of MMA MSP-4 data containing a series of mix sequences. The short red horizontal streaks (most prominent in the 80-100 Hz region) are a train of spectral peaks that appear when the mixer is on. Also evident from this spectrogram is the mixer's 50% duty cycle; for nominal operations, the mixer was active for two minutes, then paused for two minutes, and repeated in this manner until mixing was complete. The first such cycle seen in Figure 21 starts just after the 2-minute mark. Detailed examination of the MMA MSP-4 acceleration spectra during PHaSE mixer operations reveals that the strong train of spectral peaks starts at about 71.9 Hz, and has discrete components approximately every 0.9 Hz (with varying degrees of intensity) up to about 97 Hz. Occasionally, concurrent peaks are observed starting at about 38 Hz and appearing approximately every 0.9 Hz up to about 66.5 Hz. The spacing in frequency between the spectral peaks at different times during the mission was sometimes 1.8 Hz instead of 0.9 Hz. Table 11 shows the MET start and stop for 89 time frames when the PHaSE mixer was running.

**Table 11. Start/Stop Times for PHaSE Mixer**

| *MET Start* | *MET Stop* | *MET Start* | *MET Stop* | *MET Start* | *MET Stop* |
|---|---|---|---|---|---|
| 000/17:32:21 | 000/17:34:30 | 001/06:34:12 | 001/06:35:15 | 013/06:44:04 | 013/06:46:08 |
| 000/17:37:37 | 000/17:39:33 | 001/06:37:02 | 001/06:38:04 | 013/07:04:33 | 013/07:06:38 |
| 000/17:41:38 | 000/17:43:34 | 001/06:40:36 | 001/06:41:38 | 013/07:25:03 | 013/07:27:08 |
| 000/17:46:23 | 000/17:48:19 | 001/08:44:15 | 001/08:45:00 | 013/07:45:50 | 013/07:47:55 |
| 000/17:50:15 | 000/17:52:20 | 001/08:46:02 | 001/08:46:56 | 013/08:03:58 | 013/08:06:02 |
| 000/17:54:24 | 000/17:56:20 | 001/08:48:43 | 001/08:50:39 | 013/08:12:17 | 013/08:14:21 |
| 000/17:58:25 | 000/18:00:21 | 001/08:52:43 | 001/08:54:48 | 014/09:48:28 | 014/09:50:33 |
| 000/18:03:55 | 000/18:05:59 | 001/09:06:32 | 001/09:07:34 | 014/09:52:29 | 014/09:54:33 |
| 000/18:07:46 | 000/18:09:24 | 001/09:09:39 | 001/09:10:06 | 014/09:56:29 | 014/09:58:34 |
| 000/18:09:51 | 000/18:11:56 | 001/09:10:50 | 001/09:11:44 | 014/10:10:36 | 014/10:12:49 |
| 000/18:13:52 | 000/18:15:48 | 001/09:14:51 | 001/09:15:53 | 014/10:32:26 | 014/10:34:30 |
| 000/18:20:24 | 000/18:21:35 | 001/11:19:01 | 001/11:19:54 | 014/10:53:31 | 014/10:55:36 |
| 000/19:05:03 | 000/19:06:05 | 001/11:21:32 | 001/11:22:26 | 014/11:15:12 | 014/11:17:17 |
| 000/19:16:02 | 000/19:19:36 | 001/11:25:33 | 001/11:27:20 | 014/11:36:53 | 014/11:38:58 |
| 000/19:20:03 | 000/19:22:08 | 001/11:29:24 | 001/11:31:29 | 014/11:58:52 | 014/12:00:56 |
| 000/19:25:15 | 000/19:27:20 | 001/11:40:33 | 001/11:41:35 | 014/12:20:33 | 014/12:22:37 |
| 000/19:29:24 | 000/19:31:20 | 001/11:44:24 | 001/11:45:27 | 014/12:42:31 | 014/12:44:36 |
| 000/19:49:36 | 000/19:51:41 | 001/13:50:00 | 001/13:51:02 | 014/13:03:55 | 014/13:05:59 |
| 000/19:55:24 | 000/19:56:26 | 001/13:53:52 | 001/13:54:54 | 014/14:28:01 | 014/14:30:06 |
| 000/20:36:50 | 000/20:38:46 | 005/11:51:11 | 005/11:53:16 | 014/14:32:02 | 014/14:34:07 |
| 000/20:40:42 | 000/20:42:46 | 005/11:55:21 | 005/11:57:26 | 014/14:36:02 | 014/14:38:07 |
| 000/20:47:40 | 000/20:49:36 | 013/04:54:10 | 013/04:56:14 | 014/14:46:08 | 014/14:48:13 |
| 000/20:51:41 | 000/20:53:37 | 013/04:58:01 | 013/05:00:06 | 014/15:08:07 | 014/15:10:12 |
| 000/21:00:18 | 000/21:01:20 | 013/05:01:53 | 013/05:03:58 | 014/15:24:27 | 014/15:26:32 |
| 000/21:02:00* | 000/21:04:18 | 013/05:16:26 | 013/05:18:31 | 014/15:43:46 | 014/15:45:50 |
| 000/21:22:17 | 000/21:22:52 | 013/05:26:41 | 013/05:28:46 | 014/16:05:09 | 014/16:07:14 |
| 000/21:26:17 | 000/21:27:20 | 013/05:47:37 | 013/05:49:24 | 014/16:27:08 | 014/16:29:12 |
| 001/06:07:02 | 001/06:08:04 | 013/06:07:49 | 013/06:09:54 | 014/16:46:08 | 014/16:48:13 |
| 001/06:09:33 | 001/06:10:36 | 013/06:28:37 | 013/06:30:33 | 014/17:05:09 | 014/17:07:14 |
| 001/06:13:07 | 001/06:14:01 | 013/06:07:49 | 013/06:09:54 | | |
| 001/06:31:32 | 001/06:32:43 | 013/06:28:37 | 013/06:30:33 | | |

* Start time approximated because of gap in acceleration data.

On September 15, 1997, a crew debrief was held at the NASA Lewis Research Center. When asked about any significant microgravity environment disturbance sources, both Don Thomas and Roger Crouch noted that PHaSE mixer operation was easily noticeable acoustically, and that it sounded something like a washing machine: "thunk-thunk-thunk", with one or two "thunks" per second. Figure 22 shows a 1-minute period of the three orthogonal axes' accelerations recorded by MMA MSP-4 (in MSP coordinates) during the onset of PHaSE mixer operation. Notice the $X_h$- and $Z_h$-axis spikes beginning at about the 18-second mark and occurring about every half-second. These undoubtedly are the "thunks" described by the crew.

In order to quantify the impact of PHaSE mixer operation on the microgravity environment, the acceleration vector magnitude for MMA MSP-4 was plotted for the 10-minute interval shown in Figure 23. As seen in this figure, when the mixer was on, the acceleration vector magnitude was typically between 5 and 6 mg. When the mixer was off, the acceleration vector magnitude was below 3 mg. Across the Spacelab aisle in Rack 10, the MMA MSP-3 sensor registered about 1 mg when the mixer was off and only marginally more when it was on for the time frame shown in Figure 23.

## 8.7 Combustion Module-1 (CM-1)

Microgravity combustion research has practical applications in spacecraft fire safety, combustion diagnostics, soot predictions, and combustion system design. Combustion studies will be an important part of the scientific research conducted on the International Space Station. As part of the preparations for this endeavor, the CM-1 facility was developed to test hardware and experiment approaches in the Spacelab module during the MSL-1 mission. The key concept that CM-1 demonstrated was the accommodation of a variety of combustion experiments through the use of experiment-unique chamber inserts. Each of two different investigations' inserts was installed in the combustion chamber on orbit. These were the Laminar Soot Processes (LSP) experiment and the Structure of Flame Balls at Low Lewis-number (SOFBALL) experiment [27].

### 8.7.1 Mallet Pounding for Setup

As part of the procedure to close the combustion chamber, an astronaut would have to strike a V-band with a rubber mallet. This activity called for the crew member to tap this band 4 times at alternate locations (i.e. opposite corners of a square) using the rubber mallet, see Figure 24.

Figure 25 shows acceleration versus time plots for the MMA MSP-3 sensor (Rack 10 location). Notice that there are four groupings of four-spike sets. Comparisons between the sets also show an axial dependence (i.e. for the $X_h$-axis, the first grouping of spikes is louder than the third grouping of spikes).

In order to compare the MMA measurements for this event (which were recorded with a 100 Hz lowpass filter) and the SAMS data at the MGBX location (recorded with a 25 Hz lowpass filter), a 25 Hz lowpass filter was applied to the MMA data prior to plot production. This filter was achieved by designing a Chebychev type II filter in MATLAB, and implementing a forward and reverse digital filter. The effective filtering from this technique was a Chebychev type II 14th order filter with zero phase distortion.

Figures 26 through 28 show the MMA MSP-3, SAMS TSH B, and MMA MSP-4 data, respectively, all with a 25 Hz lowpass filter applied. Notice that the levels shown by MMA MSP-3 and SAMS TSH B are roughly comparable (around $2 \times 10^{-3}$ g maximum), while the MMA MSP-4 data show less than half of this value. This difference is attributed to the structural path which separates the source location (Rack 8) from the recording locations (Rack 10, Rack 12, or Rack 9). Rack 9, being across the Spacelab aisle, presumably has the furthest structural path between source and recording location.

Analysis of Figure 24, and comparison with the Structural coordinate system (see Figure 2) results in the first two columns of Table 12, detailing the predicted acceleration spike directions. All of these positions have assumed a $+Y_0$ impact, based upon the direction from which the astronaut is able to use the mallet (while facing the CM-1 facility, the astronaut is facing the $+Y_0$ direction).

**Table 12. Predicted Acceleration Spike Directions Due to Mallet Pounding for CM-1 Setup**

| *Position* | *Predicted* | *Observed* |
|---|---|---|
| A | $+X_0$, $+Y_0$, $-Z_0$ | $-X_0$, $+Y_0$, $-Z_0$ |
| B | $-X_0$, $+Y_0$, $+Z_0$ | $+X_0$, $+Y_0$, $+Z_0$ |
| C | $-X_0$, $+Y_0$, $-Z_0$ | $-X_0$, $+Y_0$, $-Z_0$ |
| D | $+X_0$, $+Y_0$, $+Z_0$ | $+X_0$, $+Y_0$, $+Z_0$ |

The third column in Table 12 follows from a close-up look at the acceleration data shown in Figure 25. These observed values document the initial transient direction for each of the axes, transformed from the MMA MSP-3 coordinate system to the Orbiter Structural coordinate system (see Table 4 for more detail).

Note that in Table 12 the predicted and observed directions all match, with the exception of the $X_0$-axis for positions A and B. It should be noted that for these positions, the peak magnitudes in the $X_0$-axis data were relatively small, thus the observed direction was not easily discernible.

### 8.7.2 Gas Chromatograph Vacuum Pump

During the mission, the PIMS group monitored communications between science teams, payload operations control and mission control, and logged information pertinent to the microgravity environment. As a result of this effort, it was noted from the SAMS real-time downlink data that a strong disturbance at about 46 Hz regularly occurred twice during each SOFBALL experiment run. Post-mission, a positive correlation between operation of the internal gas chromatograph vacuum pump and distinct acceleration disturbances at about 46 and 55 Hz was observed. A nominal gas chromatograph analysis sequence consisted of a number of pump on-off cycles. Depending on specifics of the test point, there were between 5 and 10 cycles, which always began with 2 long cycles (these long cycles are those that were observed in the data). The remaining cycles were short cycles. A 5-cycle example is shown in Table 13.

**Table 13. Typical Gas Chromatograph Vacuum Pump Sequence**

| *Cycle* | *Pump Status* | *Duration* |
|---|---|---|
| 1 (long) | ON | 4.25 minutes |
| | OFF | 3.00 minutes |
| 2 (long) | ON | 4.25 minutes |
| | OFF | 3.00 minutes |
| 3 (short) | ON | 10 seconds |
| | OFF | 3.00 minutes |
| 4 (short) | ON | 10 seconds |
| | OFF | 3.00 minutes |
| 5 (short) | ON | 10 seconds |
| | OFF | 3.00 minutes |

To be more precise, a correlation was observed between the disturbance seen in the MMA MSP-3 (located in Rack 10, adjacent to the CM-1 Rack) acceleration data at about 54.7 Hz and the pump's long cycle on-off times. In addition, these data show unequivocal accompaniment of this disturbance by a stronger signal at around 46.1 Hz as shown in Table 14.

Note from Table 14 that the average duration of disturbance #2 was about 4.2 minutes and the gap between the long cycles was about 2.8 minutes. These values match closely with the expected duty cycles called out in Table 13. A typical observed sequence of pump operation is shown in Figure 29. This 20 minute color spectrogram shows MMA MSP-3 data recorded at the Droplet Combustion Experiment (DCE), located at Rack 10 of the Spacelab, adjacent to the CM-1 (Rack 8). Notice the magenta trace that starts just before the 6-minute mark and again just after the 12-minute mark. This signature is referenced in Table 14 as disturbance #1. Concomitant to this is a somewhat less intense disturbance, the orange trace at around 55 Hz. To generalize, disturbance #1 (magenta trace) tends toward a steady-state frequency range of about 44.6 to 47.6 Hz (about 2700 to 2900 rpm), and appears well-controlled in frequency. Disturbance #2 has a nominal frequency of about 54.7 Hz (about 3300 rpm), but is not as well-controlled in frequency as disturbance #1. Disturbance #2 is the signal that shows strong correlation to the gas chromatograph vacuum pump run times in the CM-1 command log. Considering the first 5 occurrences of pump operation shown in Table 14, the RMS acceleration level in the 44 to 49 Hz frequency range more than triples going from about 79.5 $\mu g_{RMS}$ while the pump was off, to about 250 $\mu g_{RMS}$ while the pump was on.

## Table 14. CM-1 Gas Chromatograph Vacuum Pump Operation Times as Detected by MMA MSP-3 (Rack 10 location)

| Disturbance #1 46.1 Hz Signal | | | | Disturbance #2 54.7 Hz Signal | | | |
|---|---|---|---|---|---|---|---|
| Long Cycle #1 | | Long Cycle #2 | | Long Cycle #1 | | Long Cycle #2 | |
| MET Start | MET Stop | MET Start | MET Stop | MET Start | MET Stop | MET Start | MET Stop |
| 006/20:41:32 | 006/20:44:49 | 006/20:48:34 | 006/20:51:46 | 006/20:41:37 | 006/20:45:40 | 006/20:48:32 | 006/20:52:43 |
| 006/22:15:20 | 006/22:18:37 | 006/22:22:14 | 006/22:25:28 | 006/22:15:20 | 006/22:19:22 | 006/22:22:14 | 006/22:26:25 |
| 007/06:40:30 | 007/06:43:50 | 007/06:47:27 | 007/06:50:41 | 007/06:40:58 | 007/06:44:38 | 007/06:47:15 | 007/06:51:35 |
| 007/07:34:07 | 007/07:37:24 | 007/07:40:47 | 007/07:44:13 | 007/07:34:07 | 007/07:38:13 | 007/07:40:24 | 007/07:45:07 |
| 007/09:01:25 | 007/09:04:48 | 007/09:08:25 | 007/09:11:45 | 007/09:01:17 | 007/09:05:40 | 007/09:08:31 | 007/09:12:43 |
| not observed | not observed | not observed | not observed | 007/13:50:24 | 007/13:54:24 | 007/13:57:56 | 007/14:02:13 |
| not observed | not observed | not observed | not observed | 007/14:44:22 | 007/14:48:37 | 007/14:51:17 | 007/14:55:28 |
| not observed | not observed | not observed | not observed | 007/15:49:02 | 007/15:53:02 | 007/15:55:42 | 007/16:00:10 |
| 007/20:14:18 | 007/20:17:15 | 007/20:20:52 | 007/20:23:43 | 007/20:13:55 | 007/20:18:12 | 007/20:21:01 | 007/20:24:41 |
| 007/21:14:26 | 007/21:17:55 | 007/21:21:29 | 007/21:24:49 | 007/21:14:26 | 007/21:18:43 | 007/21:21:35 | 007/21:25:40 |
| 007/22:12:48 | 007/22:16:14 | 007/22:19:54 | 007/22:23:11 | 007/22:12:60 | 007/22:17:11 | 007/22:19:57 | 007/22:24:08 |
| not observed | not observed | not observed | not observed | 008/04:06:39 | 008/04:10:22 | 008/04:13:30 | 008/04:17:42 |
| not observed | not observed | not observed | not observed | 008/07:16:47 | 008/07:21:04 | 008/07:23:58 | 008/07:28:12 |
| 009/02:52:25 | 009/02:55:42 | 009/02:59:25 | 009/03:02:51 | 009/02:52:11 | 009/02:56:36 | 009/02:59:48 | 009/03:03:42 |
| 009/03:59:55 | 009/04:03:10 | 009/04:06:50 | 009/04:10:12 | 009/03:59:55 | 009/04:04:07 | 009/04:06:58 | 009/04:10:58 |
| 009/06:21:22 | 009/06:24:37 | 009/06:28:25 | 009/06:31:42 | 009/06:21:17 | 009/06:25:28 | 009/06:28:31 | 009/06:32:37 |
| 009/07:22:19 | 009/07:25:36 | 009/07:29:42 | 009/07:32:56 | 009/07:22:16 | 009/07:26:34 | 009/07:29:36 | 009/07:33:54 |
| 009/19:23:59 | 009/19:27:25 | 009/19:32:10 | 009/19:35:30 | 009/19:25:19 | 009/19:28:19 | 009/19:32:10 | 009/19:36:22 |
| 009/20:21:52 | 009/20:25:17 | 009/20:29:00 | 009/20:32:20 | 009/20:21:57 | 009/20:26:03 | 009/20:28:55 | 009/20:33:23 |
| 009/21:44:18 | 009/21:47:38 | 009/21:51:15 | 009/21:54:06 | 009/21:44:29 | 009/21:48:35 | 009/21:51:15 | 009/21:55:04 |
| 010/07:14:28 | 010/07:17:40 | 010/07:21:23 | 010/07:24:37 | 010/07:14:48 | 010/07:18:37 | 010/07:21:23 | 010/07:25:34 |
| 010/08:15:22 | 010/08:18:45 | 010/08:22:28 | 010/08:25:42 | 010/08:15:14 | 010/08:19:48 | 010/08:22:28 | 010/08:26:45 |
| 010/09:28:16 | 010/09:31:51 | 010/09:35:28 | 010/09:38:45 | 010/09:28:51 | 010/09:32:45 | 010/09:35:36 | 010/09:39:36 |
| 010/15:13:30 | 010/15:16:50 | 010/15:20:30 | 010/15:23:47 | 010/15:13:42 | 010/15:17:47 | 010/15:20:47 | 010/15:24:45 |
| 010/16:01:29 | 010/16:05:29 | 010/16:08:58 | 010/16:12:12 | 010/16:01:55 | 010/16:06:18 | 010/16:08:58 | 010/16:12:52 |
| 011/09:08:57 | 011/09:12:11 | 011/09:15:48 | 011/09:19:05 | 011/09:09:37 | 011/09:13:08 | 011/09:15:54 | 011/09:20:05 |
| 011/10:07:40 | 011/10:11:06 | 011/10:14:43 | 011/10:17:57 | 011/10:07:40 | 011/10:11:57 | 011/10:14:43 | 011/10:18:54 |
| 011/11:46:53 | 011/11:50:13 | 011/11:53:55 | 011/11:57:15 | 011/11:47:04 | 011/11:51:10 | 011/11:53:55 | 011/11:58:07 |
| 011/14:56:26 | 011/15:01:29 | 011/15:05:06 | 011/15:08:32 | 011/14:56:26 | 011/15:02:26 | 011/15:05:17 | 011/15:09:20 |
| 011/16:00:41 | 011/16:04:07 | 011/16:07:04 | 011/16:09:49 | 011/16:00:52 | 011/16:05:09 | 011/16:06:58 | 011/16:10:47 |
| 011/19:39:16 | 011/19:42:36 | 011/19:46:16 | 011/19:49:39 | 011/19:39:45 | 011/19:43:56 | 011/19:46:25 | 011/19:50:30 |
| 011/20:33:05 | 011/20:36:25 | 011/20:40:02 | 011/20:43:25 | 011/20:33:14 | 011/20:37:31 | 011/20:39:59 | 011/20:44:17 |
| 012/08:01:53 | 012/08:05:10 | 012/08:08:45 | 012/08:12:05 | 012/08:01:53 | 012/08:06:07 | 012/08:08:50 | 012/08:13:02 |
| 012/08:57:29 | 012/09:01:00 | 012/09:04:40 | 012/09:08:03 | 012/08:57:23 | 012/09:01:55 | 012/09:04:40 | 012/09:09:00 |
| 012/21:03:04 | 012/21:06:30 | 012/21:10:01 | 012/21:13:16 | 012/21:03:10 | 012/21:07:21 | 012/21:10:07 | 012/21:14:13 |
| 012/22:05:02 | 012/22:08:28 | 012/22:12:05 | 012/22:15:25 | 012/22:05:08 | 012/22:09:25 | 012/22:12:16 | 012/22:16:16 |
| 013/08:57:06 | 013/09:00:26 | 013/09:04:09 | 013/09:07:29 | 013/08:57:12 | 013/09:01:20 | 013/09:04:09 | 013/09:08:20 |
| 013/09:53:03 | 013/09:56:26 | 013/10:00:03 | 013/10:03:29 | 013/09:53:06 | 013/09:57:23 | 013/10:00:09 | 013/10:04:26 |
| not observed | not observed | not observed | not observed | 013/10:47:00 | 013/10:51:20 | 013/10:54:12 | 013/10:58:13 |
| 013/18:58:58 | 013/19:02:35 | 013/19:06:12 | 013/19:09:32 | 013/18:59:15 | 013/19:03:38 | 013/19:06:12 | 013/19:10:30 |

As discussed in section 5, PIMS worked closely with the SOFBALL experiment team during the STS-94 mission. Pre-mission testing using the KC-135 aircraft demonstrated that the flame balls exhibited a drift velocity proportional to the square root of $gr$, where $g$ is the gravitational acceleration and $r$ is the radius of the flame ball. Given this relationship, the SOFBALL team requested that PIMS provide the SOFBALL team with near real-time raw (10 samples per second) OARE data mapped to the SOFBALL experiment location. These acceleration data were analyzed with SOFBALL radiometry data. The results of one SOFBALL test point (TP 14A) are shown in Figure 30; the effects of the Vernier Reaction Control System (VRCS) activity on the radiometry data are readily apparent. For both periods of VRCS activity (just before the 2-minute mark and just before the 8-minute mark), the radiometry data indicates a distinct change in value. Consequently, the SOFBALL team attempted to avoid VRCS activity during subsequent test points by making use of free drift periods, and they carefully monitored VRCS firings as their experiment periods were initiated.

### 8.8 Effect of Leaving Free Drift

Firings of the Orbiter's Vernier Reaction Control System (VRCS) thrusters result in acceleration impulse disturbances on the order of 100 μg. Occasionally, microgravity PIs request that the Orbiter be placed in a free drift state, during which all thruster firings are inhibited. Such free drift periods result in a quieter microgravity environment (free from thruster disturbances), with the tradeoff that the Orbiter's attitude is no longer under control. To reestablish attitude control following a free drift period, the Digital Autopilot (DAP) compares the current and desired attitudes (roll, pitch, and yaw angles), and begins a series of thruster firings, resulting in a maneuver to the desired attitude. This series of firings typically results in a particularly intense disturbance to the microgravity environment, often for a prolonged period of time. The duration of this increased thruster activity is dependent upon how far the Orbiter had drifted out of the desired attitude.

Figures 31 and 32 show acceleration versus time plots for SAMS TSH C ($f_c$=2.5 Hz, Rack 9 location), and the raw OARE data ($f_c$=1.0 Hz for $X_b$-axis, and 0.1 Hz for the $Y_b$- and $Z_b$-axes, mapped to the Rack 9 location), respectively. Additionally, both plots have a series of indicators (the black circles) to show firings of the VRCS jets. Prior to leaving the free drift period (shortly before t=4.5 minutes in the plot), the Orbiter was in an attitude of (R,P,Y)=(86.6°,179.9°,1.6°). After the series of maneuvers, the Orbiter was back within its deadband tolerance of (R,P,Y)=(55°,180°,0°) by the t=8 minute mark.

Notice that the VRCS firings after t=8 minutes occur less often, and are indicative of nominal attitude maintenance, as opposed to the maneuver firings between t=4 and t=8 minutes. Although free drift is a good way to increase the quality of relatively short microgravity periods, leaving free drift is likely to cause a prolonged period of thruster activity, with the extent and duration of the activity being determined by how far the Orbiter has drifted out of the desired attitude.

### 8.9 Accelerations Related to the Astro/Plant Generic Bioprocessing Apparatus (Astro/PGBA)

Located in the middeck area of the Shuttle Columbia for liftoff and landing, the Astro/Plant Generic Bioprocessing Apparatus (Astro/PGBA) facility was transferred to the EXPRESS Rack (located in Rack 7 of the Spacelab module) for on-orbit operations. The Astro/PGBA facility allows for light and atmospheric control (carbon dioxide, humidity) in the plant growth chamber [27].

Integration of the Astro/PGBA facility into the EXPRESS Rack began around MET 001/20. At MET 001/21:38, the MMA MSP-3 (Rack 10) and MSP-4 (Rack 9) sensors recorded the start of four acceleration signals in the 30-65 Hz region, see Figure 33. In addition to these frequencies, an upper harmonic (centered around 126.9 Hz) was present (not shown in Figure 33). With the exception of the 20 minute period from MET 003/03:07 - 003/03:27 (see Figure 34), these signals remained active until MET 013/20:22. This signal-end time corresponds to the Astro/PGBA de-integration, when the facility was transferred back to the middeck for its landing configuration. Figure 35 shows a PSD plot of the frequencies present in the 30-65 Hz region, during the t=50-60 minute period in Figure 34.

Table 15 shows a listing of the frequencies which were noted, and the root-sum-of-squares (RSS) $\mu g_{RMS}$ which were recorded by the MMA MSP-4 sensor around the turn-off/turn-on activity mentioned above.

**Table 15. Microgravity Effects of the Astro/PGBA Experiment**

| *Frequency (Hz)* | *Without Astro/PGBA* $[\mu g_{RMS}]$ | *With Astro/PGBA* $[\mu g_{RMS}]$ | *Difference* $[\mu g_{RMS}]$ |
|---|---|---|---|
| 31.78 - 31.98 | 23.4 | 66.4 | 43.0 |
| 44.16 - 44.56 | 12.5 | 18.2 | 5.7 |
| 44.97 - 45.26 | 10.8 | 32.4 | 21.6 |
| 63.28 - 63.65 | 30.5 | 786.8 | 756.3 |

The upper harmonic of 126.6 - 127.2 Hz was not included in the above table, as these are above the cutoff frequency of the sensor, making an accurate determination of the $\mu g_{RMS}$ level impractical. The MSP-3 sensor (located across the Spacelab aisle) recorded acceleration levels which were lower than those shown in the above table. This difference is expected, as the MSP-3 sensor was farther away from the Astro/PGBA experiment.

The frequency of the signal centered around 63.5 Hz did not remain constant with respect to time, as may be seen in Figure 33 between MET 002/00:00 and 002/00:30 (the period for which the signal alternates frequencies between 63.8 and 62.9 Hz). This phenomenon was noted in the data throughout the mission as a common occurrence, but not with a regular cycle between events. The majority of these variation periods were under 30 minutes in duration. Information supplied by Alex Hoehn (BioServe Space Technologies) indicate that this alternating acceleration source is a Gillian air compressor. The alternate signatures presumed to be due to a pump back pressure related to the carbon dioxide intake switching process.

### 8.10 Accelerations Related to the Droplet Combustion Experiment (DCE)

The Droplet Combustion Experiment (DCE) was located in Rack 10 of the Spacelab module. This facility provided a closed chamber into which a known oxygen/helium atmosphere could be produced. Syringe-like injectors were used to deploy a single heptane droplet, which was then ignited.

Comparisons between DCE avionics and chamber fan performance [28], DCE activities noted on the as-flown timeline [25], and the MMA color spectrograms [29] have shown two primary acceleration signatures which were coincident with DCE activity times. Figure 36 shows a 6-hour color spectrogram of MMA data from MET 003/12 - 003/18 for the MSP-3 head (DCE Location, Rack 10 of the Spacelab module), with a zoom-in of the 72-84 Hz region. Notice the two signals which start at MET 003/13:00, and end at MET 003/17:00: Signal #1 is in the 73-75 Hz region, Signal #2 is in the 79-82 Hz region. Figure 37 shows a comparison of power spectral density (PSD) plots, for the periods MET 003/17:30-003/17:50 (without the DCE signal, blue trace), and MET 003/16:00-003/16:20 (with the DCE signal, red trace). Notice the increased levels in the 74-75 Hz region, and the 81-82 Hz region. Table 16 shows a listing of the times for which the MMA MSP-3 sensor registered these acceleration signals.

Figures 38 and 39 show analogous figures (same time frames, same axes scaling and colorbar limits as Figures 36 and 37, respectively) for the MMA MSP-4 (LIF location, Rack 9) data. Notice that while the 74-75 Hz signal may be seen in these figures (at a diminished intensity, with a difference of about 6 $\mu g_{RMS}$), there is no evidence of the 79-82 Hz signal in the spectrogram, but the RMS acceleration comparison shows about a 5 $\mu g_{RMS}$ peak difference. Table 17 shows a comparison of the $\mu g_{RMS}$ levels with and without this acceleration source.

**Table 16. DCE Times Determined from Analysis of MMA MSP-3 (Rack 10 location) Data**

| *MET Start* | *MET Stop* | *Duration (hour:minute)* |
|---|---|---|
| 001/07:30 | 001/08:30 | 01:00 |
| 002/00:40 | 002/19:10 | 18:30 |
| 003/01:00 | 003/06:50 | 05:50 |
| 003/13:00 | 003/16:50 | 03:50 |
| 003/18:10 | 004/04:20 | 10:10 |
| 005/01:20 | 005/06:00 | 04:40 |
| 005/13:30 | 005/19:50 | 06:20 |
| 006/01:10 | 006/17:20 | 16:10 |
| 008/12:50 | 008/19:10 | 06:20 |
| 009/14:30 | 009/19:20 | 04:50 |
| 010/19:10 | 010/20:00 | 00:50 |
| 011/02:30 | 011/07:40 | 05:10 |
| 012/04:00 | 012/06:30 | 02:30 |
| 013/03:00 | 013/04:20 | 01:20 |

**Table 17. Comparison of RMS Acceleration Levels Before and During DCE Activity MMA MSP-3 (DCE location, Rack 10) Data**

| | *$\mu g_{RMS}$ Level Without Activity* | *$\mu g_{RMS}$ Level With Activity* | *$\mu g_{RMS}$ Level Difference* |
|---|---|---|---|
| **Signal #1 (73.59 - 74.86 Hz)** | 28.6 | 163.4 | 134.8 |
| **Signal #2 (81.73 - 81.87 Hz)** | 7.6 | 19.6 | 12.0 |

As may be seen in Figure 1, Racks 9 and 10 are directly across the aisle from each-other (and are not in direct physical contact with each-other). The reduced signal intensity supports the conclusion that these signals originated closer to the Rack 9 location than to the Rack 10 location. Comparing Figures 37 and 39, another point of note is that the background acceleration level in the 72-84 Hz region is approximately an order of magnitude higher at the LIF location (Rack 9), compared with the DCE location (Rack 10). The cause for these differing background levels is unknown, but is presumably a localized acceleration phenomenon, which does not appear across the Spacelab aisle.

## 8.11 Accelerations Related to the Electromagnetic Containerless Processing Facility (TEMPUS)

The Electromagnetic Containerless Processing Facility (TEMPUS) allowed metallic samples to be melted without contact with container walls. First flown on the STS-65 (IML-2) mission, TEMPUS was upgraded prior to its MSL-1 flight. Previous PIMS analysis of accelerations related to TEMPUS [24] had shown a very strong (4,000-5,000 $\mu g_{RMS}$) acceleration signal at 4800 rpm (80 Hz). This signal was identified by Joerg Piller of DLR as the TEMPUS facility water pump. PIMS analysis of MMA data from this flight shows a markedly different acceleration signature from the TEMPUS facility.

Figure 40 shows a color spectrogram (zoom-in 30-46 Hz), for the one hour time period beginning at MET 000/14:00. The 42.5-43.0 Hz signal which occurs between t=12 and 44 minutes in this figure is the first occurrence of this acceleration source. The TEMPUS activation procedure was performed during this time frame [25]. An analysis of MMA MSP-4 spectrograms yields the listing of approximate signal-on times seen in Table 18.

**Table 18. TEMPUS Times Determined from Analysis of MMA MSP-4 (Rack 9 location) Data**

| *MET Start* | *MET Stop* | *Duration (hours:minutes)* |
|---|---|---|
| 000/14:00 | 000/14:42 | 00:32 |
| 001/09:40 | 001/10:10 | 00:30 |
| 001/11:00 | 001/15:00 | 04:00 |
| 002/09:40 | 002/10:00 | 00:20 |
| 002/10:10 | 002/12:00 | 01:50 |
| 003/03:00 | 003/21:10 | 18:10 |
| 003/23:50 | 004/15:20 | 15:30 |
| 004/16:30 | 005/14:40 | 22:10 |
| 005/17:00 | 006/03:40 | 10:40 |
| 006/04:00 | 006/08:50 | 04:50 |
| 006/15:00 | 007/17:40 | 26:40 |
| 007/21:20 | 007/21:40 | 00:20 |
| 007/22:10 | 008/09:40 | 11:30 |
| 008/12:10 | 008/21:10 | 09:00 |
| 009/00:10 | 009/09:10 | 09:00 |
| 009/13:10 | 009/21:10 | 08:00 |
| 010/00:40 | 010/10:50 | 10:10 |
| 010/12:50 | 010/21:30 | 08:40 |
| 011/00:00 | 011/11:40 | 11:40 |
| 011/14:10 | 011/19:50 | 05:40 |
| 012/03:40 | 012/14:20 | 10:40 |
| 012/16:40 | 013/01:50 | 09:10 |
| 013/03:40 | 013/11:20 | 07:40 |
| 013/16:00 | 014/00:40 | 08:40 |
| 014/05:40 | 014/16:20 | 10:40 |

As may be seen from Table 18, this signal lasted anywhere from 20 minutes to almost 27 hours, with a nominal duration of about 10 hours.

A comparison between MMA MSP-1 (TEMPUS location) and MSP-4 (LIF location) data yields Figure 41, showing the PSD levels in the 30-46 Hz region for the time period MET 000/14:15 through 000/14:25. Notice that the MSP-1 data shows more than an order of magnitude increase in intensity when compared with the MSP-4 data. An integration of these PSDs in the 42.63-43.03 Hz areas show that the MSP-1 sensor recorded 255 $\mu g_{RMS}$, while the MSP-4 sensor recorded 45 $\mu g_{RMS}$. Along with the signal's start and stop time coincidence with the as-flown timeline, this intensity difference supports the conclusion that this signal is a TEMPUS-related disturbance.

These acceleration results were shown to Joerg Piller (DLR), and both the on/off times and frequency of the signal were confirmed as belonging to the TEMPUS water pump. During the refurbishment of TEMPUS between IML-2 (STS-65, July 1994) and MSL-1 (STS-83/STS-94, April/July 1997), the pump's operating frequency was changed from 4,800 rpm (80 Hz) to 2,500-2,600 rpm (41.7-43.3 Hz). Additionally, isolation methods were utilized to reduce the vibration levels. These modifications resulted in acceleration reduction in excess of 3,500 $\mu g_{RMS}$ Preliminary results from TEMPUS measurements have shown a reduced noise and vibration amplitude, which is partially attributed to this facility modification [30].

### 8.12 Microgravity Measurement Assembly (MMA) Data Comparison

As discussed in section 4.3, the European Space Agency's MMA accelerometer system was flown to provide microgravity monitoring support during the mission. Post-mission, the PIMS group analyzed these data in some detail and this section discusses some significant features and key differences of the microgravity environment as measured by the three MSP sensors.

The spectrogram plots of Appendices B, C, D (for MMA MSP-3, -4, and -1), respectively, were generated with common magnitude (colorbar) axes. As a consequence, a certain portion of the data that fell outside of the limits shown on these colorbars was treated as magnitude saturation. That is, any PSD values which were greater than $10^{-7}$ $g^2$/Hz or less than $10^{-12}$ $g^2$/Hz were imaged as the colors shown at the top or bottom of the colorbar, respectively. As a result, just under 1% of the PSD magnitudes for both MSP-3 and MSP-4 saturated the upper limit, while about 2% of the PSD magnitudes for MSP-1 saturated the upper limit. This higher value for MSP-1 data were ostensibly due to strong spectral peaks in the 60 to 70 Hz range and the broadband excitation at around 50 Hz, which was not present for the other 2 sensors.

A cursory comparison of the Appendices' spectrograms would suggest that much of the vibrational energy was in the 46 to 55 Hz range for MSP-1, the 30 to 36 Hz range for MSP-3, and the 92 to 100 Hz range for MSP-4. In each case, the exact source of the broadband energy has not been identified. A more detailed analysis of the acceleration spectra shows that most of the vibrational energy recorded by the MSP-1 and MSP-4 sensors was concentrated in spectral peaks (horizontal red lines on the spectrograms) in the 60 to 70 Hz range. Both of these accelerometers were on the port side of the Spacelab module, near the EXPRESS rack, where the sources of these spectral peaks originated (see sections 8.6 and 8.9 for details). Table 19 quantifies the RMS acceleration levels for select frequency bands, as measured by the three MMA sensors.

**Table 19. Comparison of MMA RMS Acceleration for Select Frequency Bands**

| | *Median $\mu g_{RMS}$ Acceleration for MMA Sensor* | | |
|---|---|---|---|
| **Frequency Range (Hz)** | **MSP-1** | **MSP-3** | **MSP-4** |
| 16.93 - 17.13 | 86.1 | 104.5 | 73.8 |
| 30 - 36 | 192.9 | 263.9 | 140.4 |
| 46 - 55 | 997.4 | 80.7 | 76.1 |
| 60 - 70 | 2058.1 | 275.0 | 1064.9 |
| 70 - 100 | 351.5 | 108.3 | 620.8 |
| 92 - 100 | 109.7 | 45.2 | 509.7 |
| 0.02 - 100* | 2371.7 | 486.5 | 1284.0 |

* the data were demeaned and the frequency resolution used was approximately 0.02 Hz

In order to generate this table, the RMS accelerations for the frequency bands indicated were computed approximately every minute for the 3-hour period from MET 004/18:00 to 004/21:00. The medians were then computed, and these values are shown in the table.

Figure 42 shows the RMS acceleration versus time values used to compute the medians shown in the first row of Table 19. The particular disturbance investigated here arises from the Ku-band antenna, which dithers at about 17 Hz. This antenna was located on the forward bulkhead (starboard side) of the Orbiter's cargo bay, and its mechanical dithering serves as an interesting benchmark for comparison of RMS acceleration levels. As expected, the MSP-3 sensor (the only MMA accelerometer on the starboard side of the Spacelab module) registered the strongest vibrations (104.5 $\mu g_{RMS}$), while the MSP-4 sensor (the aft-most MMA sensor on the port side) registered the weakest vibrations (73.8 $\mu g_{RMS}$) in the 16.93 to 17.13 Hz frequency range. As always, the Ku-band antenna dither was nearly incessant during the mission. Another continuous source of accelerations were the Orbiter structural modes.

In the structural mode regime (the 3.5 to 10 Hz range for this analysis), one might expect the energy to be rather evenly distributed throughout the Orbiter. The median RMS accelerations calculated for this regime for the 6-hour period from MET 013/06:00 to 013/12:00 were as follows: 86.0 $\mu g_{RMS}$ for MSP-1, 56.7 $\mu g_{RMS}$ for MSP-3, and 64.7 $\mu g_{RMS}$ for MSP-4. Unlike the Ku-band antenna dither and the Orbiter structural modes, crew exercise periods occurred sporadically throughout the mission.

For the two crew exercise periods between MET 013/10:40 and 013/12:00, the median RMS acceleration value for the 1 to 3.5 Hz band for MSP-1 was 92.2 $\mu g_{RMS}$, while the other two MSPs' values were slightly greater than 69 $\mu g_{RMS}$. The MSP-1 sensor was the forward most of the three, and therefore closest to the exercise equipment located on the flight deck. This suggests marginal gains in the microgravity environment quality for the portion of the acceleration spectrum in the exercise band (the 1 to 3.5 Hz range for this analysis) for locations toward the aft of the Orbiter. Higher in the acceleration spectrum, experimental equipment always plays an important role in shaping the microgravity environment. Oscillations imparted by equipment such as pumps, mixers, and fans can be quite intense, and tend to be localized.

A comparison of the impact of the CM-1 gas chromatograph vacuum pump can be gleaned from Figure 43. This figure shows the RMS acceleration versus time plot for the frequency range 45.7 to 47.5 Hz (recall from section 8.7.2 that this vacuum pump imposed a disturbance at about 46 Hz). The pump cycled on and off four times during the time frame MET 013/08:30 to 013/10:30, as indicated by the arrows. From this figure, the baseline (pump off) RMS acceleration for both MSP-3 and MSP-4 was about 30.4 $\mu g_{RMS}$; for MSP-1, the baseline was about 165.0 $\mu g_{RMS}$. The higher value for MSP-1 is attributed to the broadband excitation discussed earlier. When the pump turned on, MSP-4 (blue trace) measured an increase up to about 83.5 $\mu g_{RMS}$, which was minor relative to the MSP-1 (red trace) and MSP-3 (green trace) changes, which both stepped up to well over 200 $\mu g_{RMS}$ during pump operation. With respect to the transmissibility of this disturbance, intuition would suggest that MSP-3 (in Rack 10, adjacent to the pump's rack) would show the highest RMS acceleration during pump operation, while the other two sensors (both across the Spacelab aisle) would show a somewhat lower magnitude. The MSP-4 data supports this expectation, but the MSP-1 data does not. The cause for this discrepancy is unknown at this time.

During PHaSE mixer operation times during the period from MET 013/06:00 to 013/08:30, the median RMS accelerations (for the 71 to 97 Hz range) for MSP-4 approached about 1 $mg_{RMS}$, while the MSP-1 and MSP-3 values were both below 0.5 $mg_{RMS}$. The higher value for MSP-4 was expected since it was mounted in Rack 9, adjacent to the rack that housed the PHaSE mixer.

A final comparison of experimental equipment was performed for the MGBX circulation fan, which was located in Rack 12. For the frequency range from 93 to 97 Hz, the region in which the MGBX circulation fan's oscillations resided for the period MET 013/09:00 to 013/12:00, the median RMS acceleration values were 72, 235, and 235 $\mu g_{RMS}$ for MSP-1, -3, and -4, respectively. These values are in accordance with the proximity of these sensors to the MGBX facility. MSP-1 was farthest removed, MSP-3 was in the rack adjacent to the MGBX, and MSP-4 was just across the aisle.

For this mission, the MMA sensors collected simultaneous measurements at three distributed locations throughout the Spacelab module with common cutoff frequencies, thus providing a unique insight into the transmission of microgravity disturbances. This distributed accelerometer system enabled a crude profile to be formed detailing the impact of various microgravity disturbances at the three sensor locations. Rudimentary RMS acceleration comparisons corroborated the localization of certain disturbances, such as those caused by PHaSE, CM-1, and Astro/PGBA (see sections 8.6, 8.7, and 8.9 for further localization details). Simultaneous high frequency (up to 100 Hz) acceleration measurements at multiple locations have proven to be an effective tool for investigating the localization, identification, and transmissibility of acceleration disturbance sources.

## 9. Summary

Analysis of the acceleration data collected during STS-94 showed that the microgravity environment for this mission was shaped by the usual variety of acceleration disturbance sources. Quasi-steady effects resulting from Orbiter attitude, venting operations, crew activity, etc. comprised the low-frequency regime, while oscillatory effects resulting from crew exercise, experiment-related equipment operations, and vehicle subsystem operations governed the high-frequency regime. Transient effects (primarily thruster firings) were also key components of the overall microgravity environment.

The MMA data presented a unique opportunity for the PIMS group to analyze the microgravity environment of the Orbiter using three distributed high-frequency (100 Hz) sensor heads. Comparisons of accelerations recorded by the three sensors helped to localize acceleration sources, thus assisting with their identification and classification.

PIMS real-time support of this mission included monitoring of the acceleration environment and logging of pertinent information, monitoring communications between experiment teams, payload operations control, mission control, and the crew, monitoring downlink video, discussions with experiment teams, and the creation of custom-made real-time displays and processes for the CSLM and SOFBALL experiment teams.

Low-frequency acceleration variations result from changes in the Orbiter's attitude. Primarily, these accelerations are due to aerodynamic drag, gravity gradient, and rotational effects within the Orbiter. Atmospheric density changes resulting from day/night transitions cause variations, which have been seen in the past, and have been noted for this mission. Vehicle venting operations (such as water dumps) produce a quasi-steady shift of the acceleration vector, related to the venting force and direction. Typical acceleration changes are on the order of -0.4 μg and -1.5 μg for the $Y_b$-axis (water dump and SIMO dump respectively), and 0.8 μg and 1.7 μg for the $Z_b$-axis (water dump and SIMO dump respectively), for venting operations.

Accelerations related to crew activity and Orbiter system operations have been noted. Specifically, crew exercise produced acceleration disturbances resulting from a shoulder-sway motion (1-1.5 Hz), the fundamental pedalling frequency (2.5-3 Hz), and harmonics of these frequencies. Exercise for this mission were typically on the order of 100-200 $\mu g_{RMS}$. PAO events and crew conferences were shown to be quieter microgravity periods, lasting for up to 30 minutes at a time, with a nominal 40 $\mu g_{RMS}$ quieting of the acceleration environment. The 17 Hz dither of the Orbiter's Ku-band communication antenna was present throughout the mission, with magnitudes around 75-105 $\mu g_{RMS}$. The distributed nature of the three MMA sensor heads allowed the magnitude variations of this signal to be seen as a function of distance from the disturbance source.

A number of acceleration sources were identified which were related to experiment or facility operations. Some of note include the MGBX workarea circulation fans (63.5, 66.5, 98.6, and 127.0 Hz with magnitudes up to 180 $\mu g_{RMS}$), the PHaSE mixer (2000-3000 μg vector magnitude increase), the CM-1 gas chromatograph vacuum pump (46 and 55 Hz, 170 $\mu g_{RMS}$ magnitude), the Astro/PGBA air circulation pump (31.8, 44.4, 45.0, and 63.5 Hz, ranging between 5 and 750 $\mu g_{RMS}$ in magnitude), and the TEMPUS water pump (42.5-43 Hz, 250 $\mu g_{RMS}$ magnitude). Some other sources include one or more unidentified components on the PHaSE and the DCE experiments.

Direct correlations were made by the SOFBALL team between their radiometry data and firing of the VRCS thrusters. PIMS provided an analysis showing the microgravity effects of leaving free drift. This showed there were an increased number of thruster firings as the Orbiter maneuvered back to the desired attitude.

Correlations between the MMA ASTRE sensor were made with the OARE sensor. For the venting operations (water and SIMO dumps) shown in this report, both instruments measured approximately the same magnitude and direction for the acceleration vector (about -0.4 μg and -1.5 μg for the $Y_b$-axis, and 0.8 μg and 1.7 μg for the $Z_b$-axis for water dump and SIMO dumps, respectively).

Utilization of high-frequency data from three MMA sensor heads enabled a unique opportunity for the localization and identification of a number of disturbance sources. This proved to be an invaluable tool for the analysis and interpretation of the MSL-1 microgravity environment.

## 10. References

[1] R. Hakimzadeh, K. Hrovat, K.M. McPherson, M.E. Moskowitz, and M.J.B. Rogers, Summary Report of Mission Acceleration Measurements for STS-78, January 1997, pp 1-18.

[2] R.C. Blanchard, M.K. Hendrix, J.C. Fox, D.J. Thomas and Y.J. Nicholson, Orbital Research Experiment, J. Spacecraft and Rockets, Vol. 24, No. 6, (1987) 504-511.

[3] R.C. Blanchard, J.Y. Nicholson and J.R. Ritter, STS-40 Orbital Acceleration Research Experiment Flight Results During a Typical Sleep Period. NASA Technical Memorandum 104209, January 1992.

[4] R.C. Blanchard, J.Y. Nicholson, J.R. Ritter, Preliminary OARE Absolute Acceleration Measurements on STS-50. NASA Technical Memorandum 107724, February 1993.

[5] R.C. Blanchard, J.Y. Nicholson, J.R. Ritter and K.T. Larman, OARE Flight Maneuvers and Calibration Measurements on STS-58. NASA Technical Memorandum 109093, April 1994.

[6] Canopus Systems, Inc., OARE Technical Report 149, STS-78 (LMS-1) Final Report. CSI-9604, September 1996.

[7] Canopus Systems, Inc., OARE Technical Report 151, STS-94 (MSL-1) Final Report. CSI-9704, August 1997.

[8] Jeff Eggers, SAMS Group, Personal Communication

[9] R. DeLombard, B.D. Finley, Space Acceleration Measurement System, Description and Operations on the First Spacelab Life Sciences Mission. NASA Technical Memorandum 105301, November 1991.

[10] R. DeLombard, B.D. Finley and C.R. Baugher, Development of and Flight Results from the Space Acceleration Measurement System (SAMS). NASA Technical Memorandum 105652, January 1992.

[11] C.R. Baugher, G.L. Martin and R. DeLombard, Low-Frequency Vibration Environment for Five Shuttle Missions, NASA Technical Memorandum 106059, March 1993.

[12] M.J.B. Rogers, C.R. Baugher, R.C. Blanchard, R. DeLombard, W.W. Durgin, D.H. Matthiesen, W. Neupert and P. Roussel, A Comparison of Low-Gravity Measurements Onboard Columbia During STS-40. Microgravity Science and Technology VI/3 (1993), 207-216.

[13] B.D. Finley, C. Grodsinsky and R. DeLombard, Summary Report of Mission Acceleration Measurements for SPACEHAB-01, STS-57. NASA Technical Memorandum 106514, March 1994.

[14] M.J.B. Rogers and R. Delombard, Summary Report of Mission Acceleration Measurements for STS-62. NASA Technical Memorandum 106773, November 1994.

[15] SAMS Experiment Brochure, B-0339A, NASA Lewis Research Center, February 1997.

[16] I. Gerhard, Microgravity Measurement Assembly (MMA)-a Centralized Onboard Measurement Facility, Microgravity Measurement Group Conference, Huntsville, Alabama, September 22-24, 1993.

[17] I. Gerhard and C. Gilbert, Microgravity Measurement Assembly (MMA) Description and Performance Summary, Deutsche Aerospace / ERNO Raumfahrttechnik GmbH, Feb. 1993.

[18] MSL-1 Homepage, http://snail.msfc.nasa.gov/spacelab/msl1/msl$mslall.html

[19] SOFBALL Experiment Brochure, B-0772, NASA Lewis Research Center, February 1997.

[20] CSLM Experiment Brochure, B-0775, NASA Lewis Research Center, March 1997.

[21] Shuttle Operational Data Book, Volume 1, JSC-08934, Rev. E, Johnson Space Center, Houston, TX, January 1988

[22] M. J. B. Rogers, B. P. Matisak, and J. I. D. Alexander, Venting Force Contributions-Quasi-steady accelerations on STS-50. Microgravity Science and Technology VII/4 (1995) 293-295

[23] M.J.B. Rogers and R. Delombard, Summary Report of Mission Acceleration Measurements for STS-73. NASA Technical Memorandum 107269, July 1996.

[24] R DeLombard, K. McPherson, K. Hrovat, M. Moskowitz, M. J. B. Rogers and T. Reckart, Microgravity Environment Description Handbook, NASA Technical Memorandum 107486, July 1997.

[25] Teledyne Brown Engineering, MSL-1, STS-94, As-Flown Experiment Timeline, 410RPT0922, August 1997.

[26] http://sven.lerc.nasa.gov/projects/Phase/phase.overview.hardware.html

[27] NASA's Microgravity Science Laboratory: Illuminating the Future (MSL-1 Color Brochure)

[28] Dan Catalano, Analex Coorporation, Personal Communication

[29] M. Moskowitz, K. Hrovat, P. Tschen, K. McPherson, M. Nati and T. Reckart, Summary Report of Mission Acceleration Measurements for MSL-1, Appendix B, NASA Technical Memorandum 206979, March 1998.

[30] Joerg Piller, DLR, Personal Communication

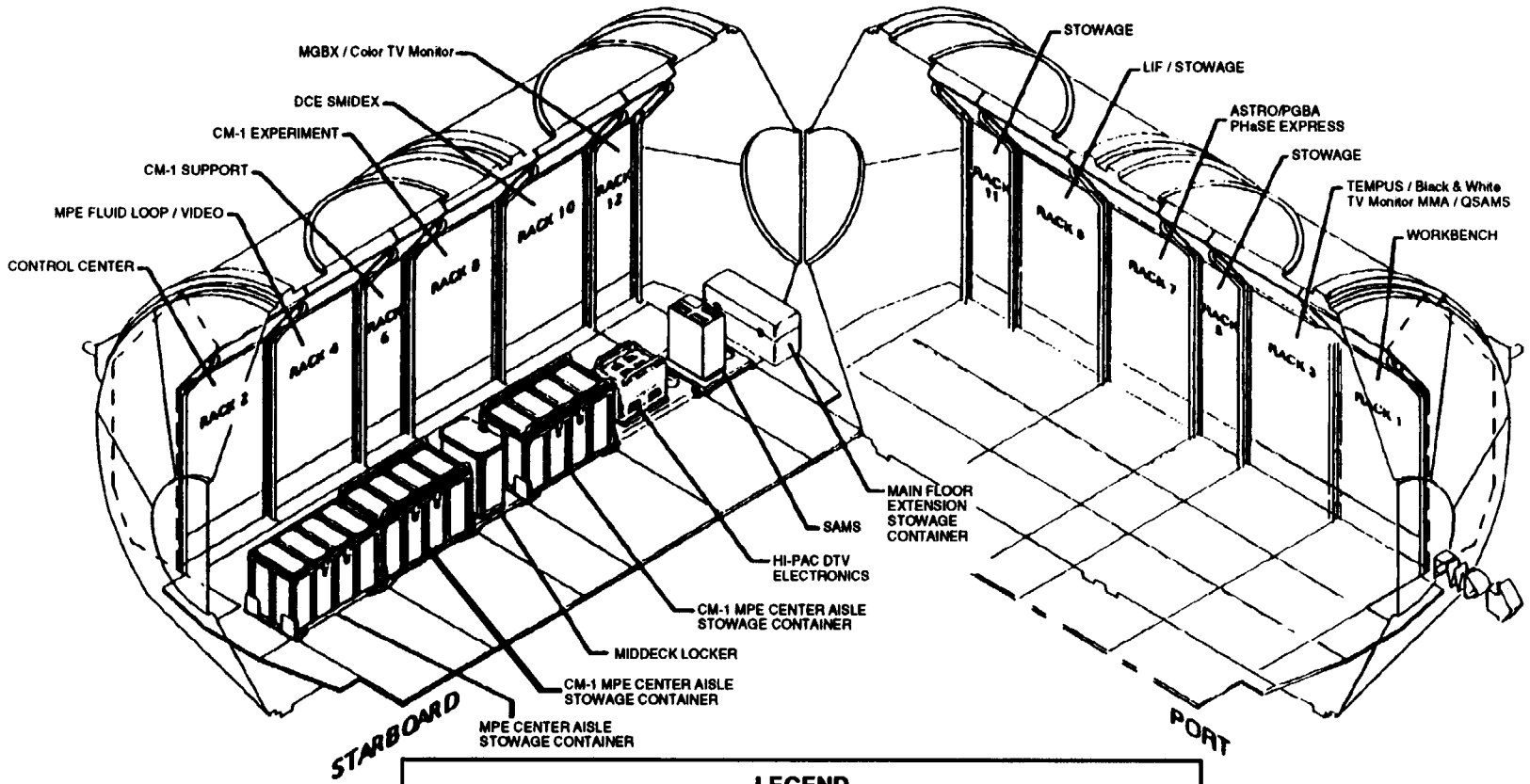


**LEGEND**

| | |
|---|---|
| Astro/PGBA | - Astro/Plant Growth Bioprocessing Apparatus |
| CM-1 | - Combustion Module |
| DCE | - Droplet Combustion Experiment |
| PHaSE | - Physics of Hard Spheres |
| SAMS | - Space Acceleration Measurement System |
| EXPRESS | - EXpedite the PRocessing of Experiments to the Space Station |
| OARE | - Orbital Acceleration Research Experiment |
| MGBX | - Middeck Glovebox |
| PCG-STES | - Protein Crystal Growth-Single Locker Thermal Enclosure System |
| QSAM | - Quasi-Steady Acceleration Measurement |
| TEMPUS | - Electromagnetic Containerless Procesing Facility |
| MMA | - Microgravity Measurement Assembly |
| LIF | - Large Isothermal Furnace |

MSL-1 MODULE EQUIPMENT OVERVIEW

Figure 1. Orthogonal View of the Spacelab for MSL-1.

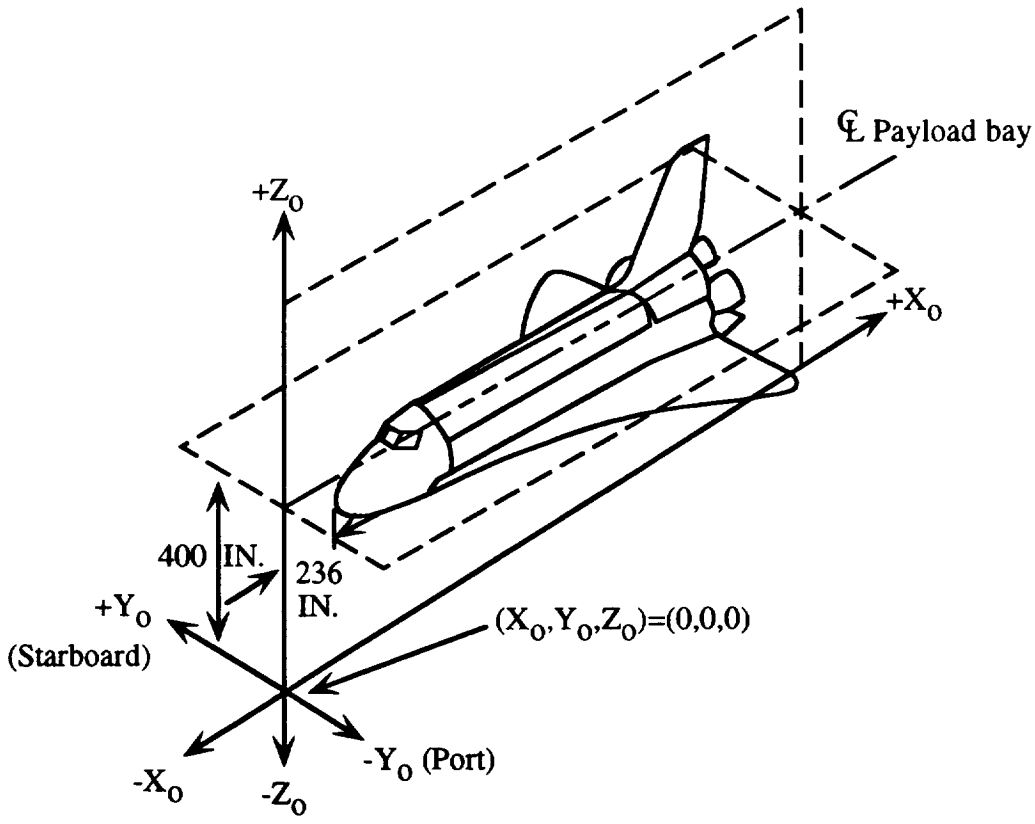


Figure 2. Orbiter Structural Coordinate System.

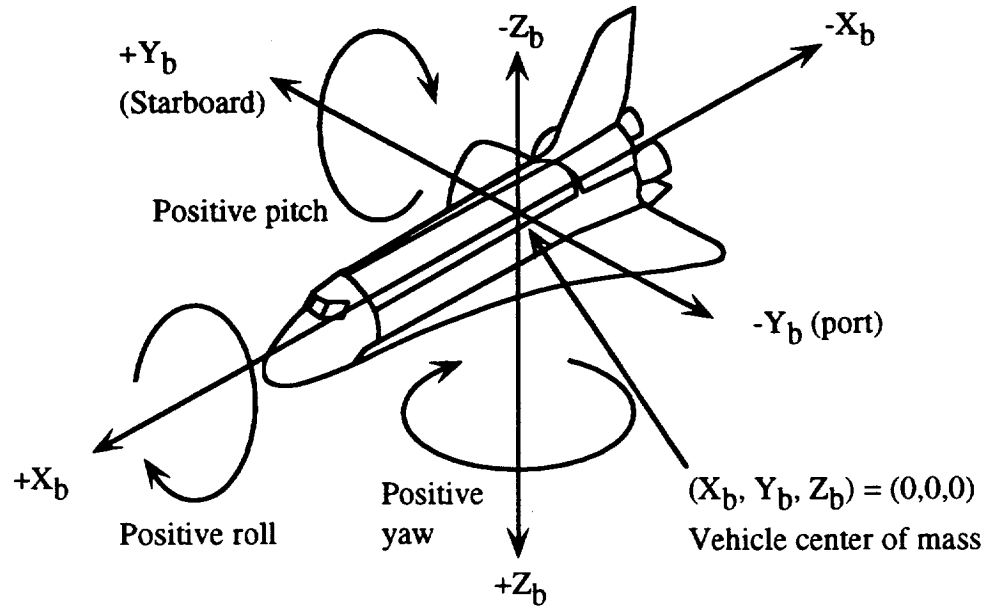


Figure 3. Orbiter Body Coordinate System.

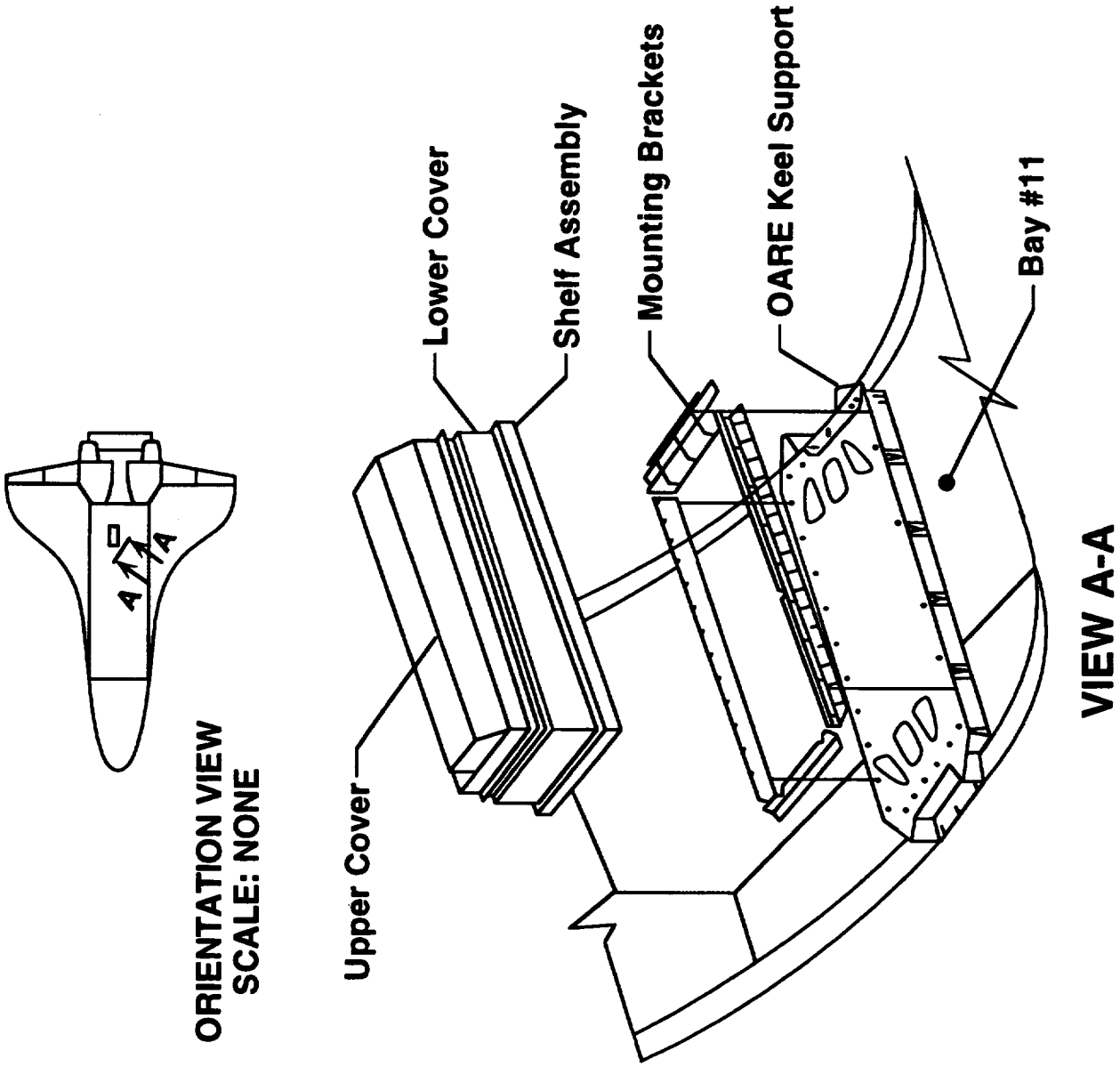


Figure 4. OARE Instrument Location for MSL-1.

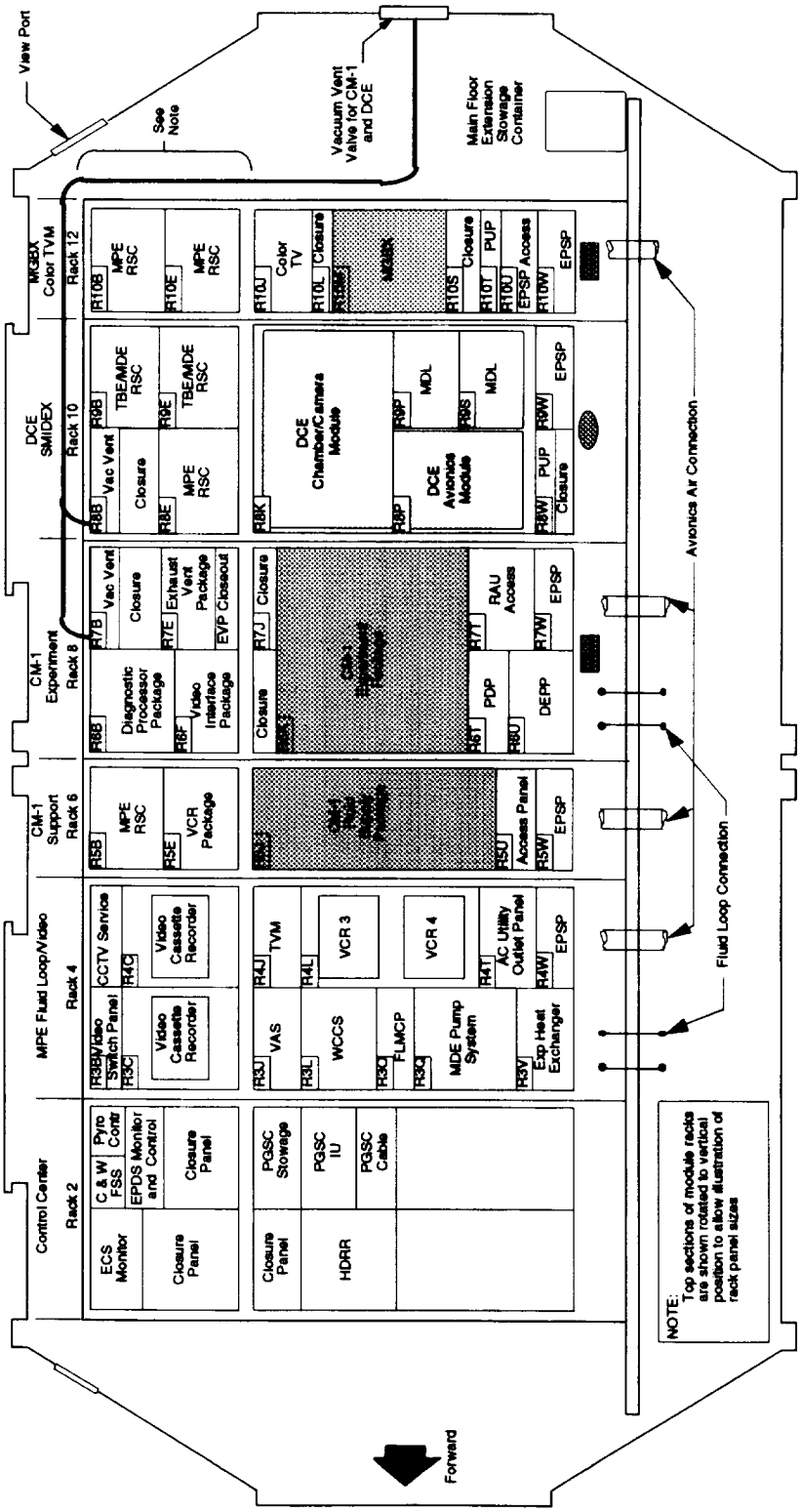


NOTE: 1. Rack Stowage Container (RSC) designations are for reference only.

2. SAMS Sensor Head locations: Rack 8 CM-1 Experiment Package Support Structure (25 hz) and Rack 12 MGBX Facility (25 hz).

3. MMA Sensor located on DCE Chamber/Camera Backplate.

Figure 5a. Spacelab Layout, Starboard View.

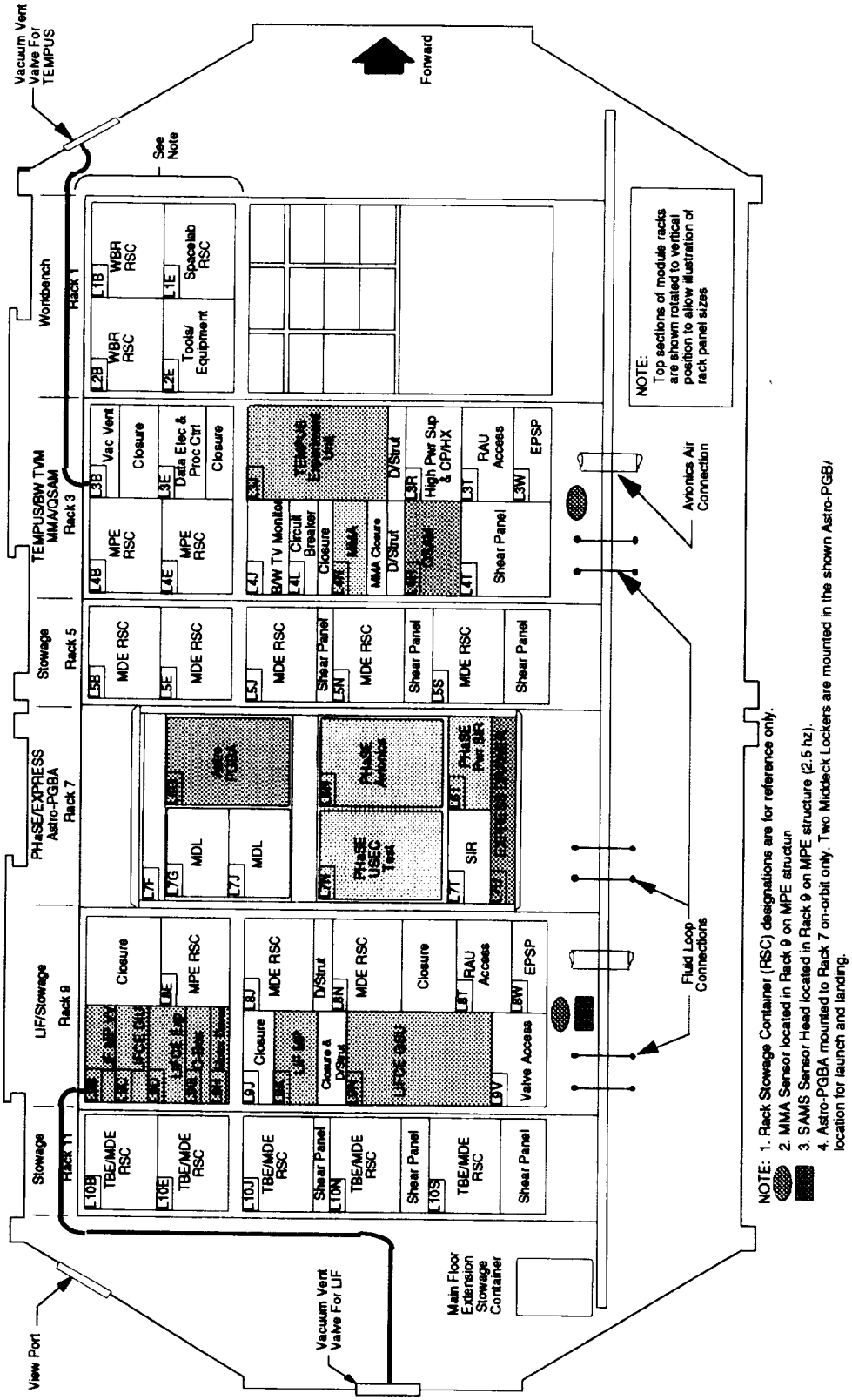


Figure 5b. Spacelab Layout, Port Side View.

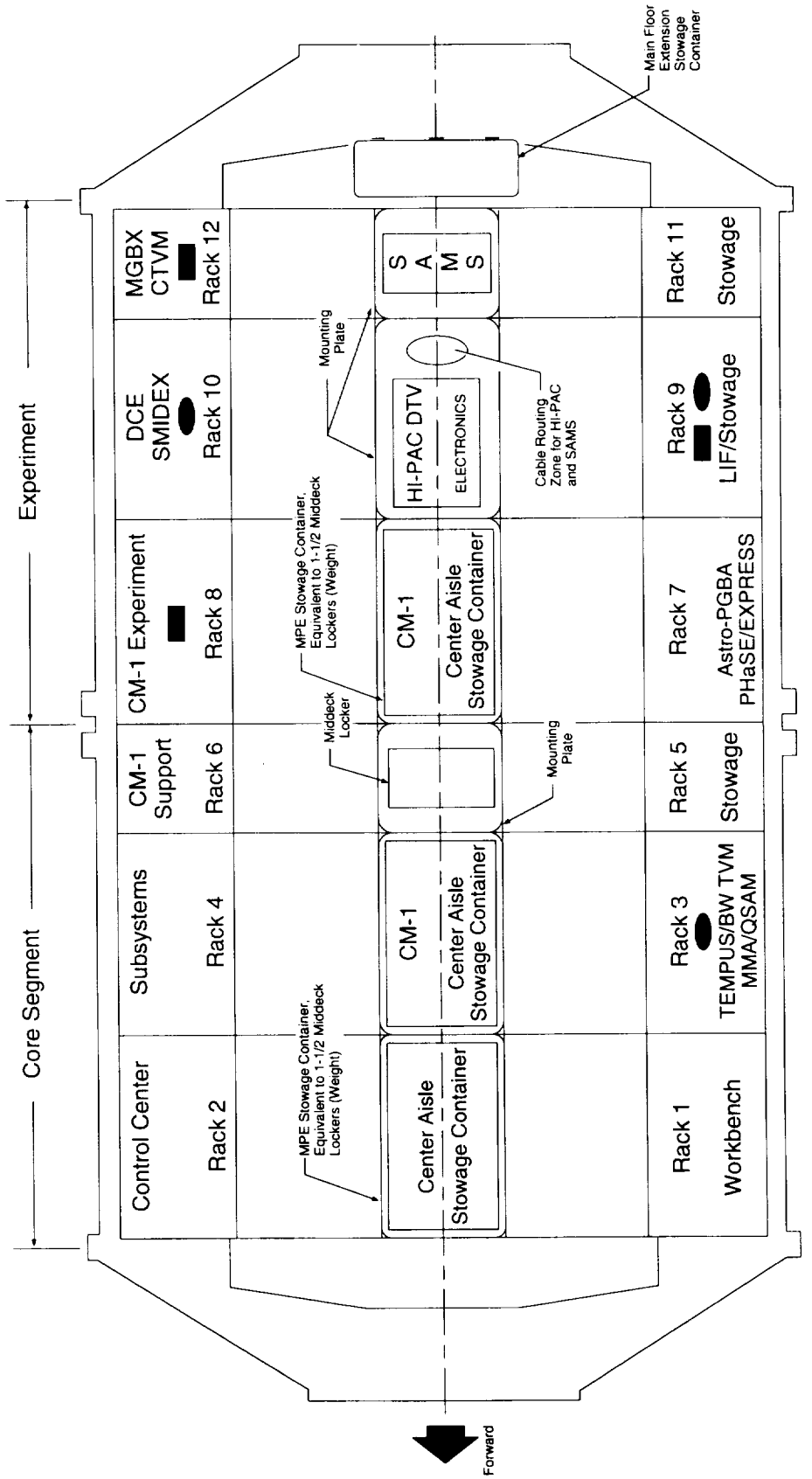


Figure 5c. Spacelab Layout, Center Aisle.

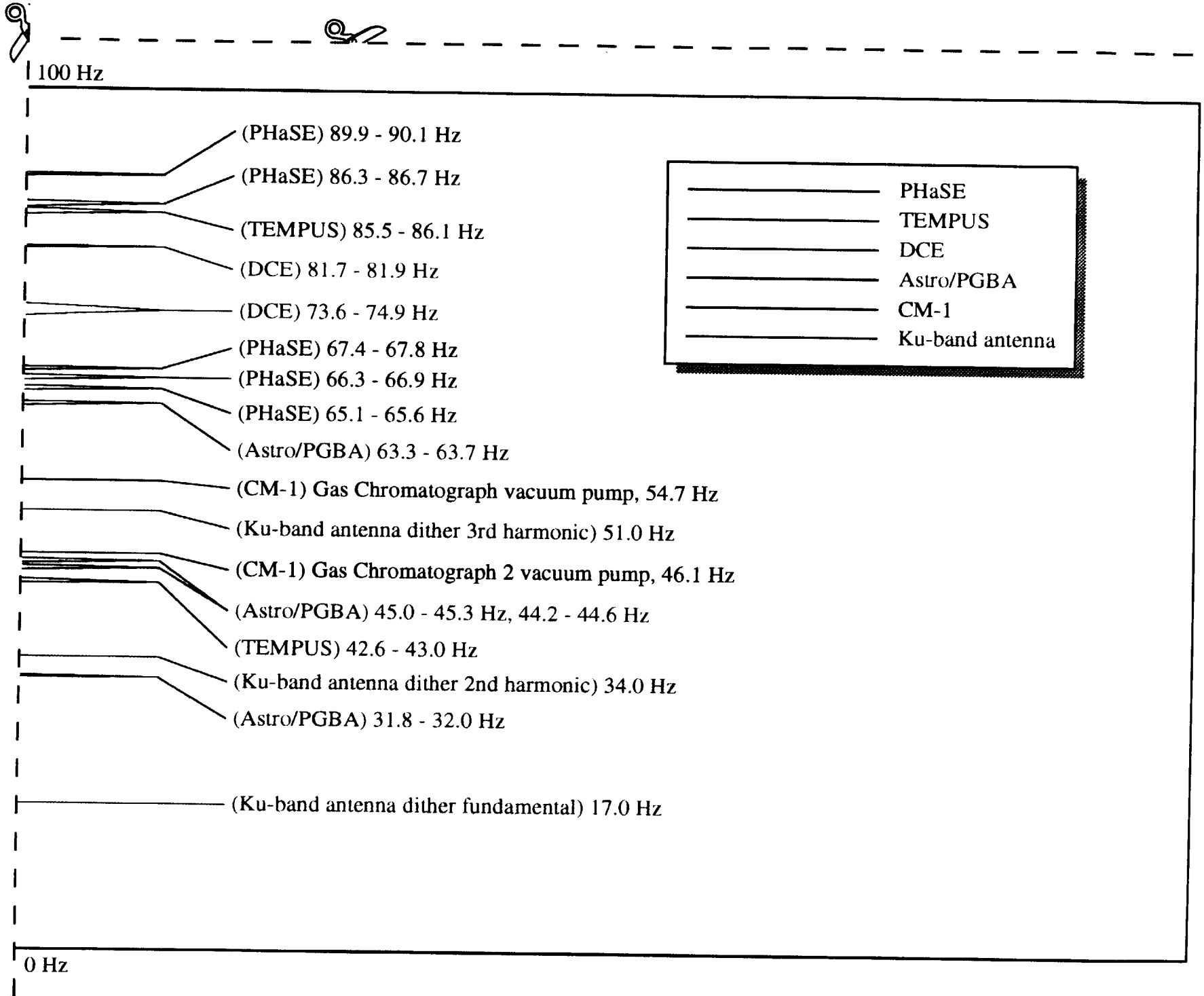


Figure 6. Approximate Location of Select Microgravity Disturbance Sources, Based Upon Appendix Plot Dimensions.

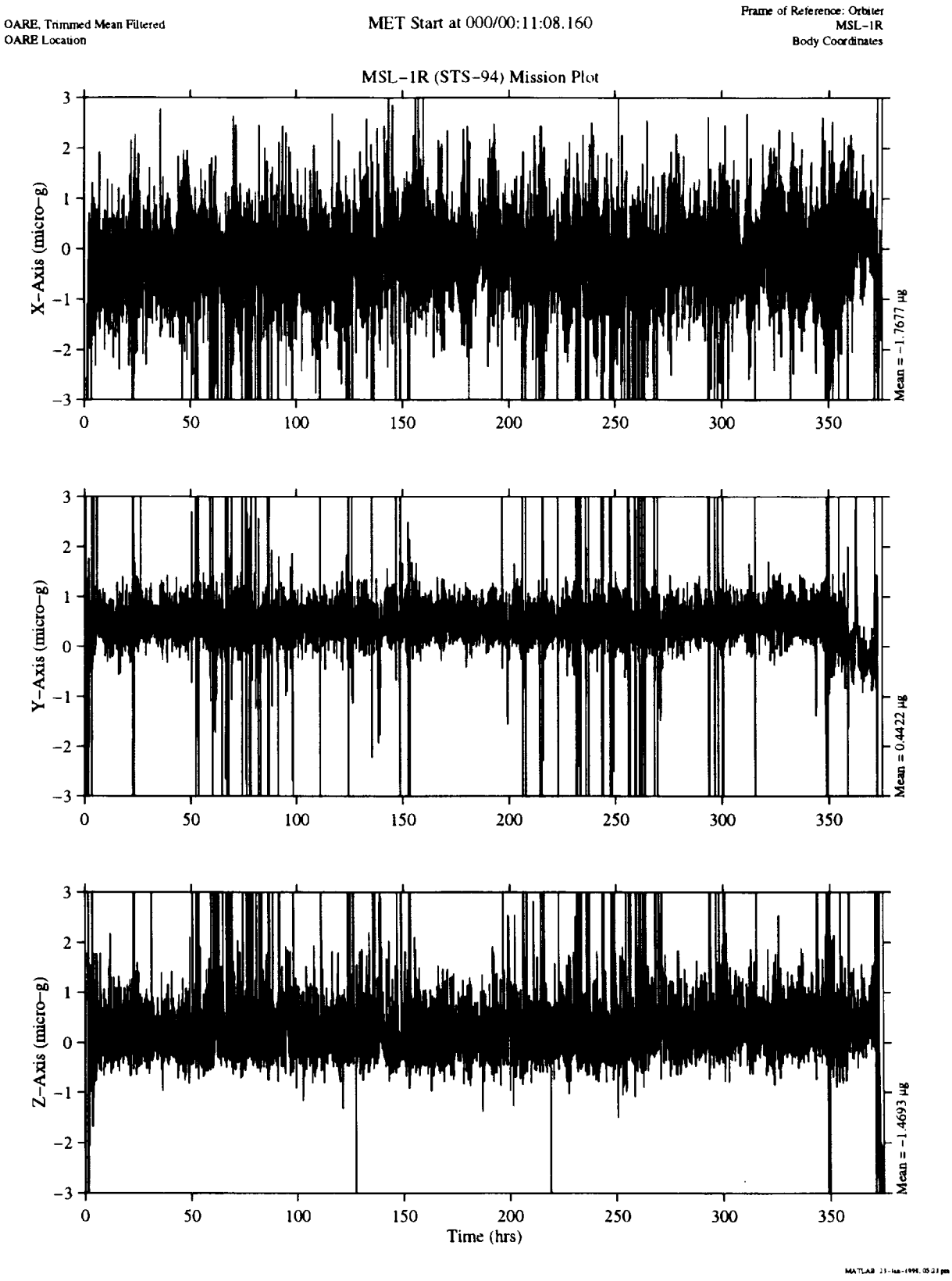


Figure 7. Trimmean Filtered OARE Data for the STS-94 Flight.

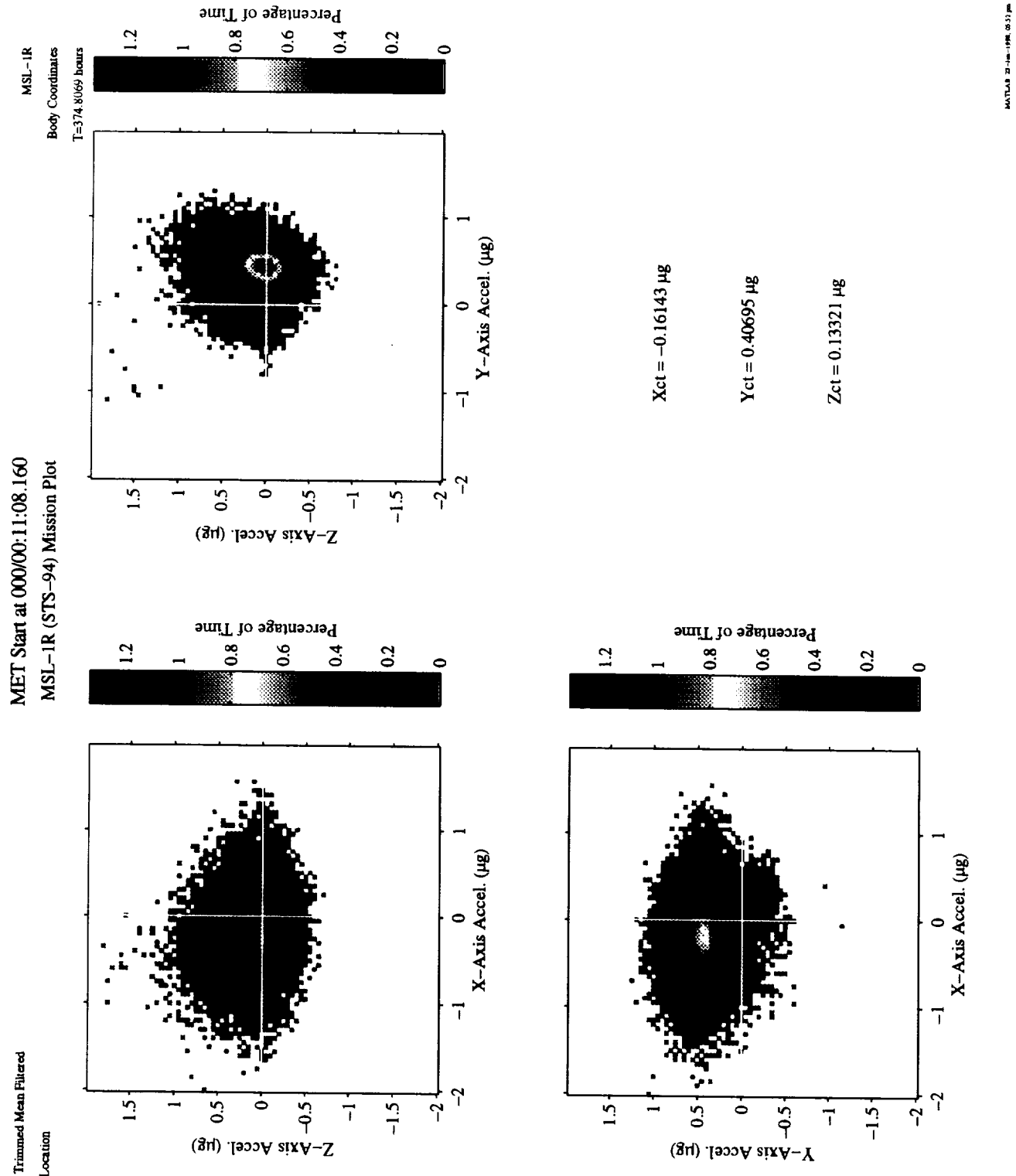


Figure 8. Quasi-steady Three-dimensional Histogram of Trimmean Filtered OARE Data for the STS-94 Flight.

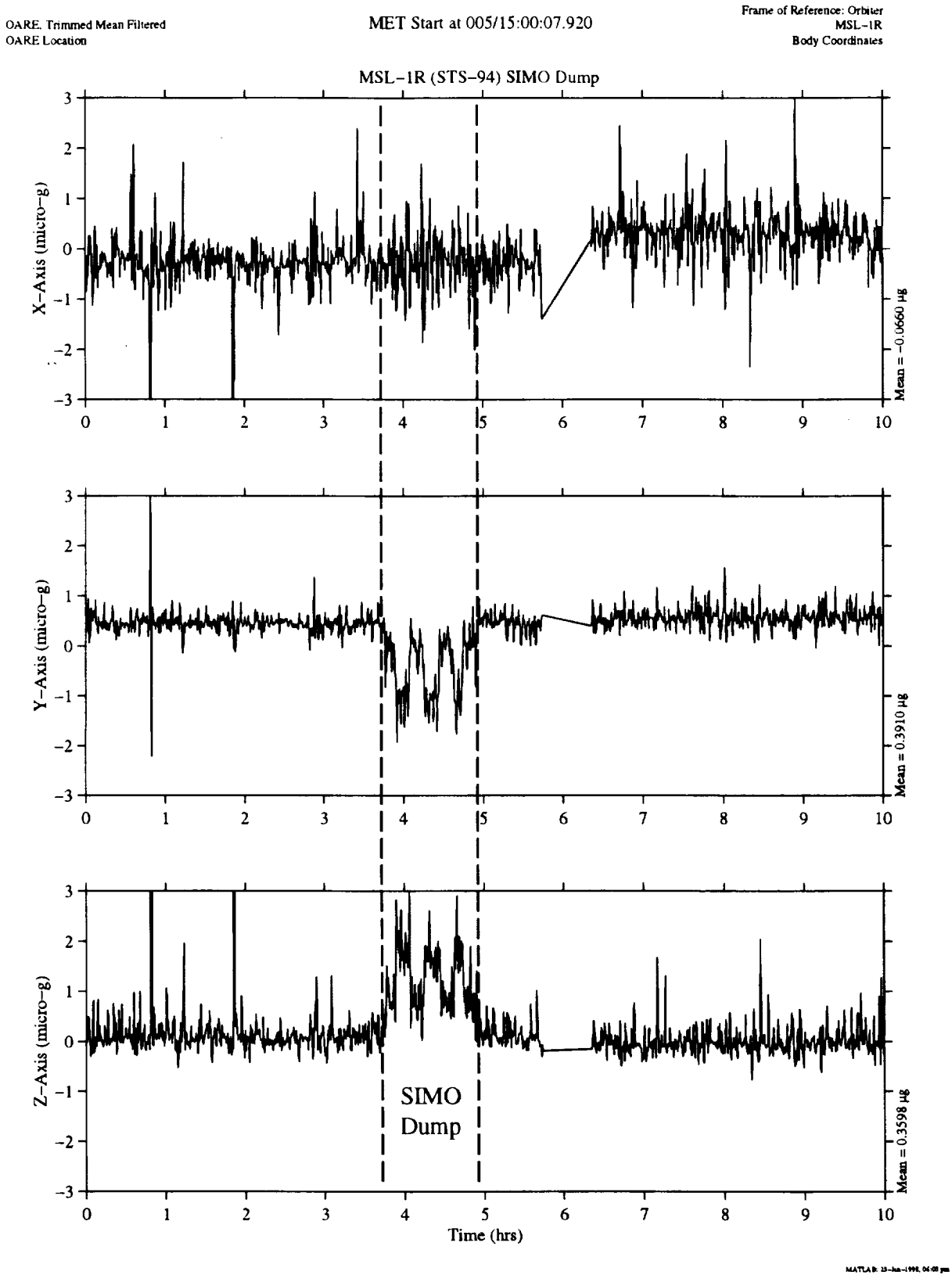


Figure 9. OARE Data Collected During a Simultaneous Supply and Waste Water Dump at MET 005/15:00.

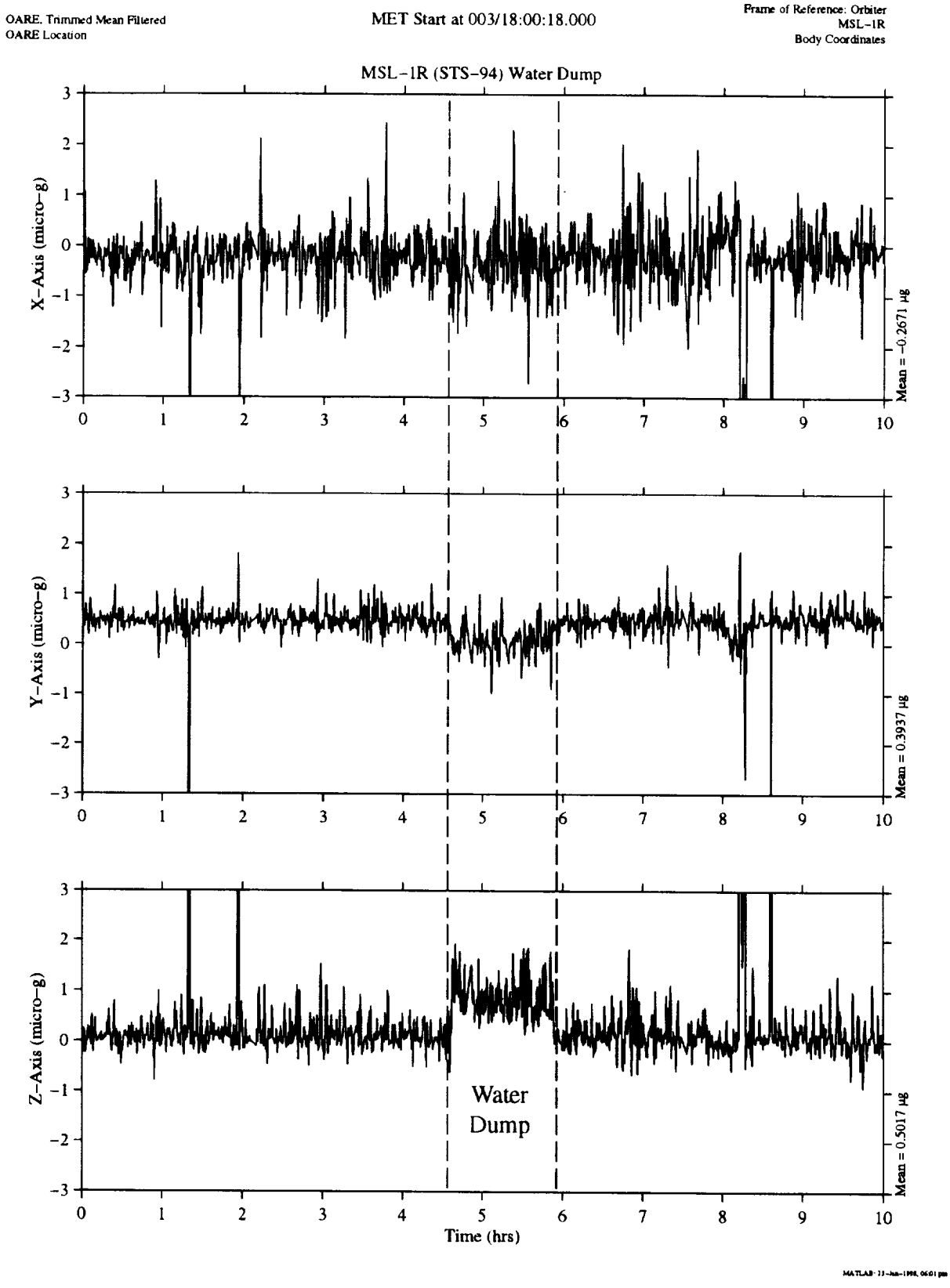


Figure 10. OARE Data Collected During a Supply Water Dump at MET 003/18:00.

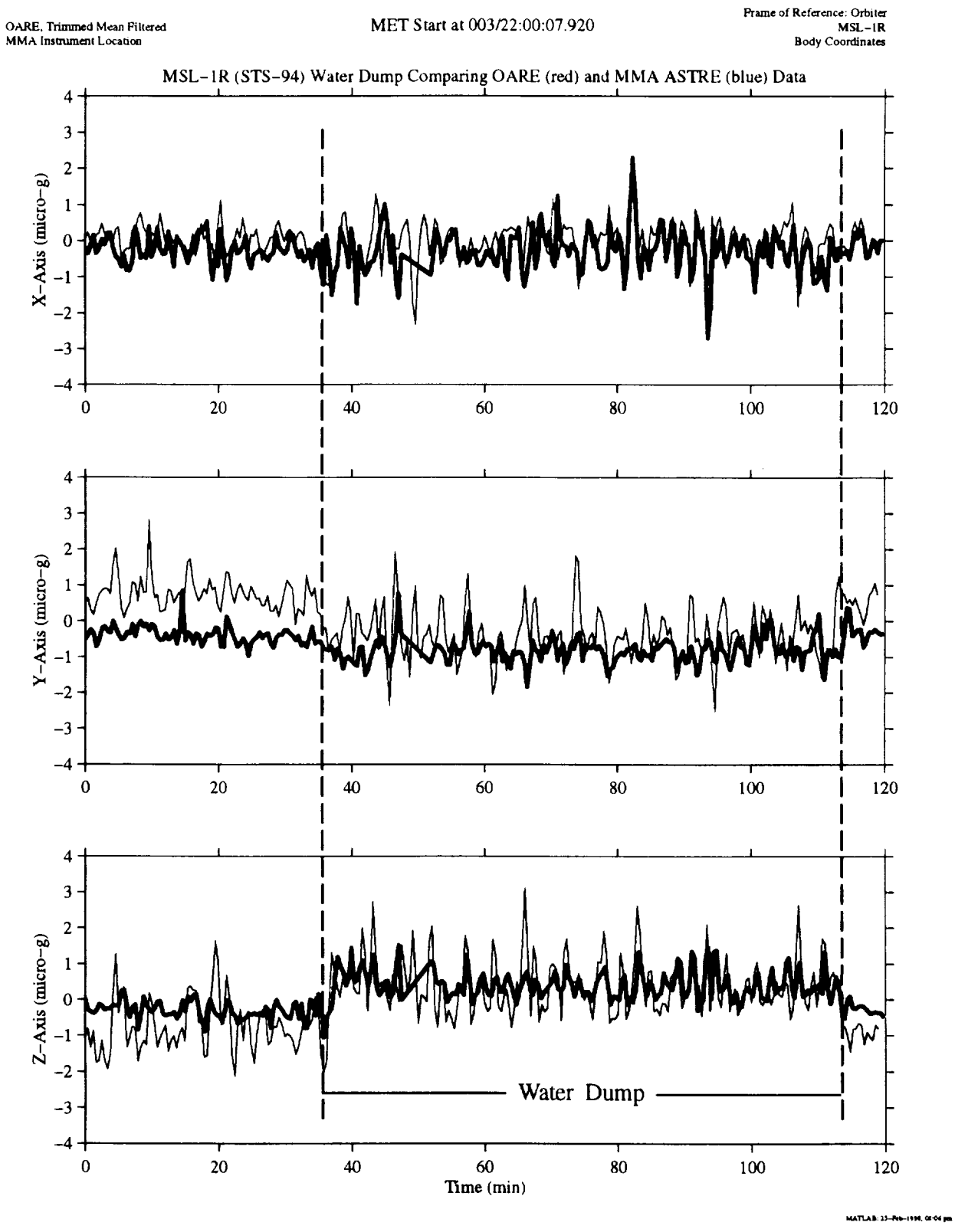


Figure 11. Comparison of OARE and MMA Astre Data During a Supply Water Dump for STS-94.

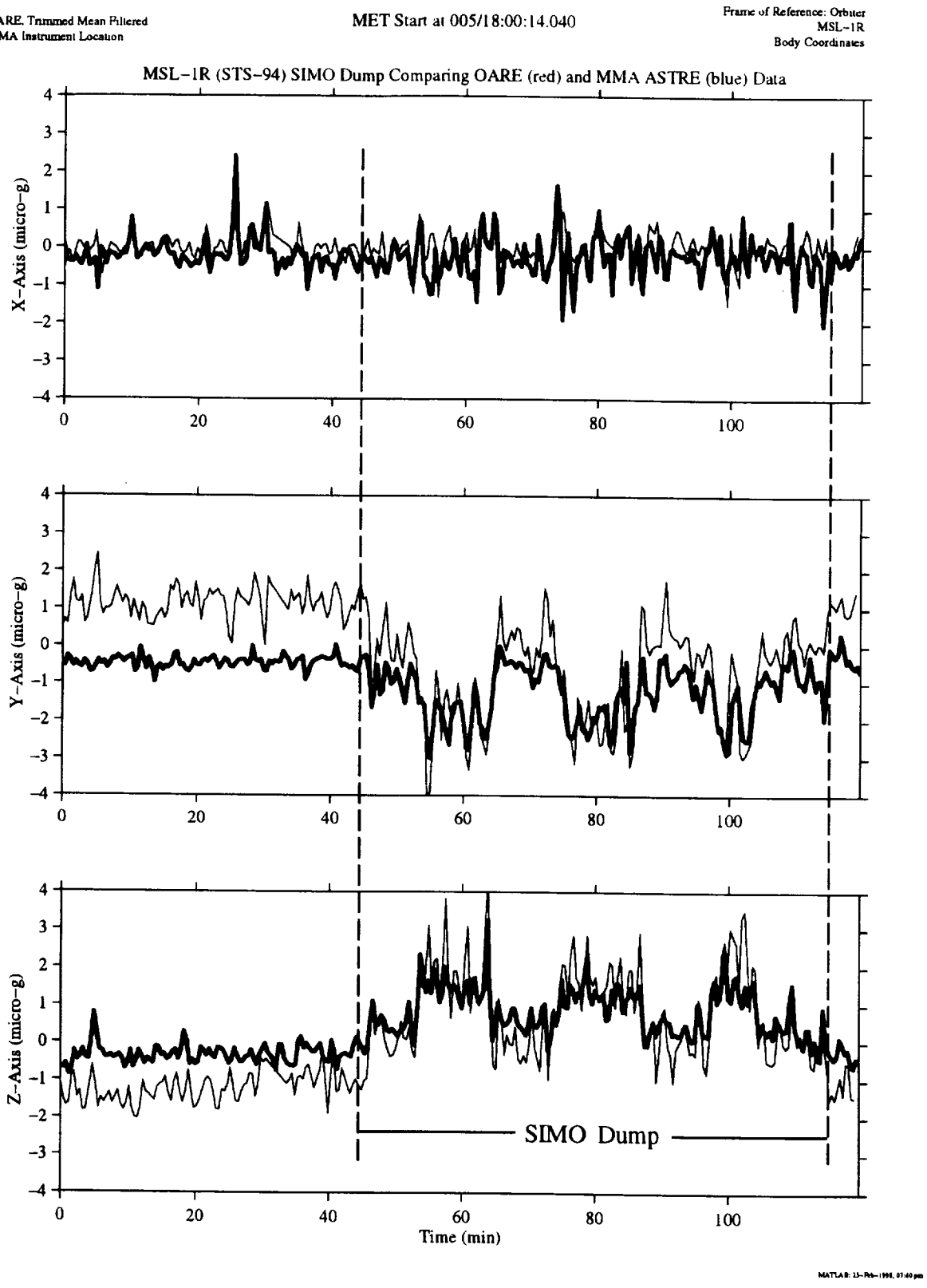


Figure 12. Comparison of OARE and MMA Astre Data During a SIMO Dump for STS-94.

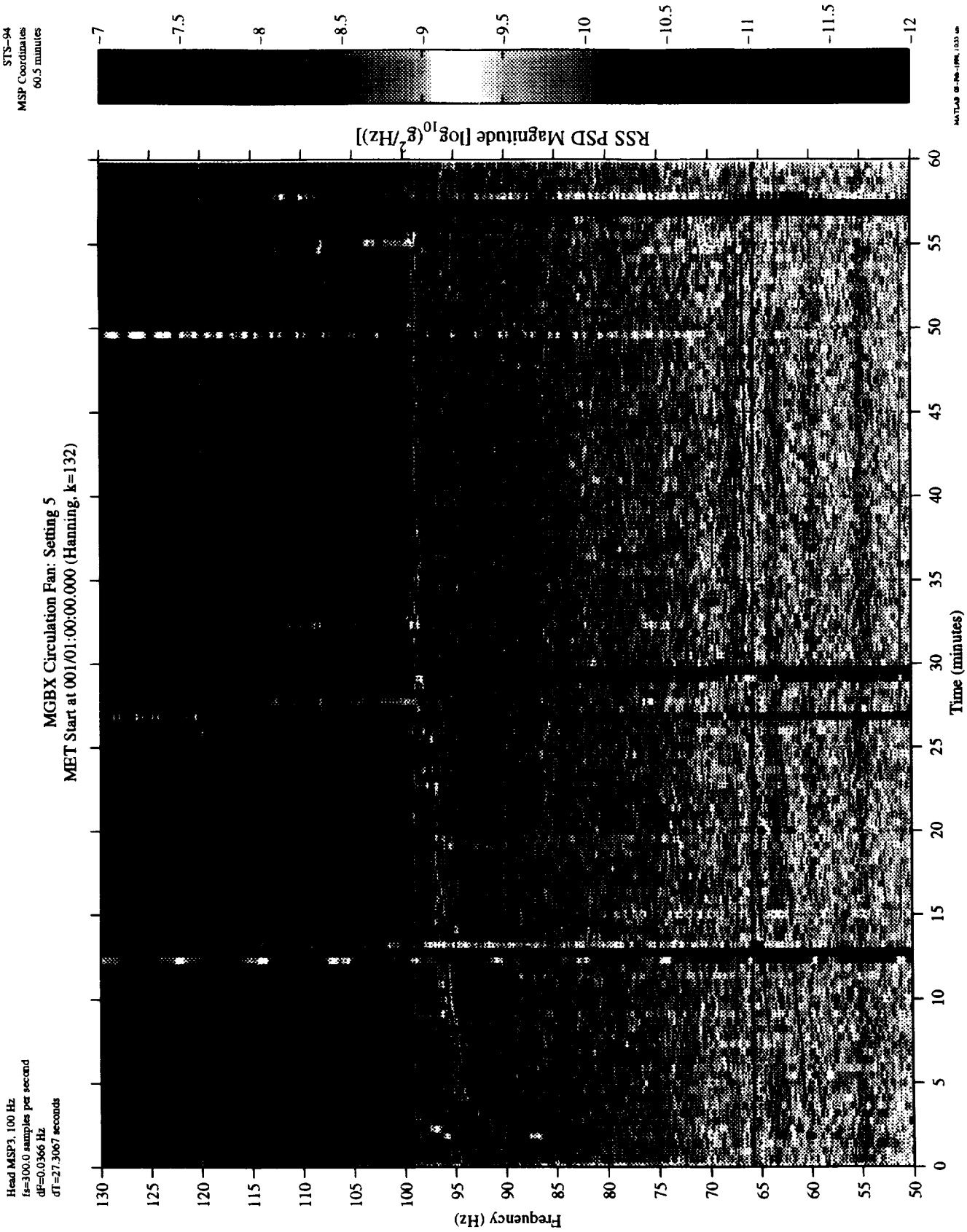


Figure 13. MGBX Circulation Fan (Setting 5), MMA MSP-3 Data, Color Spectrogram.

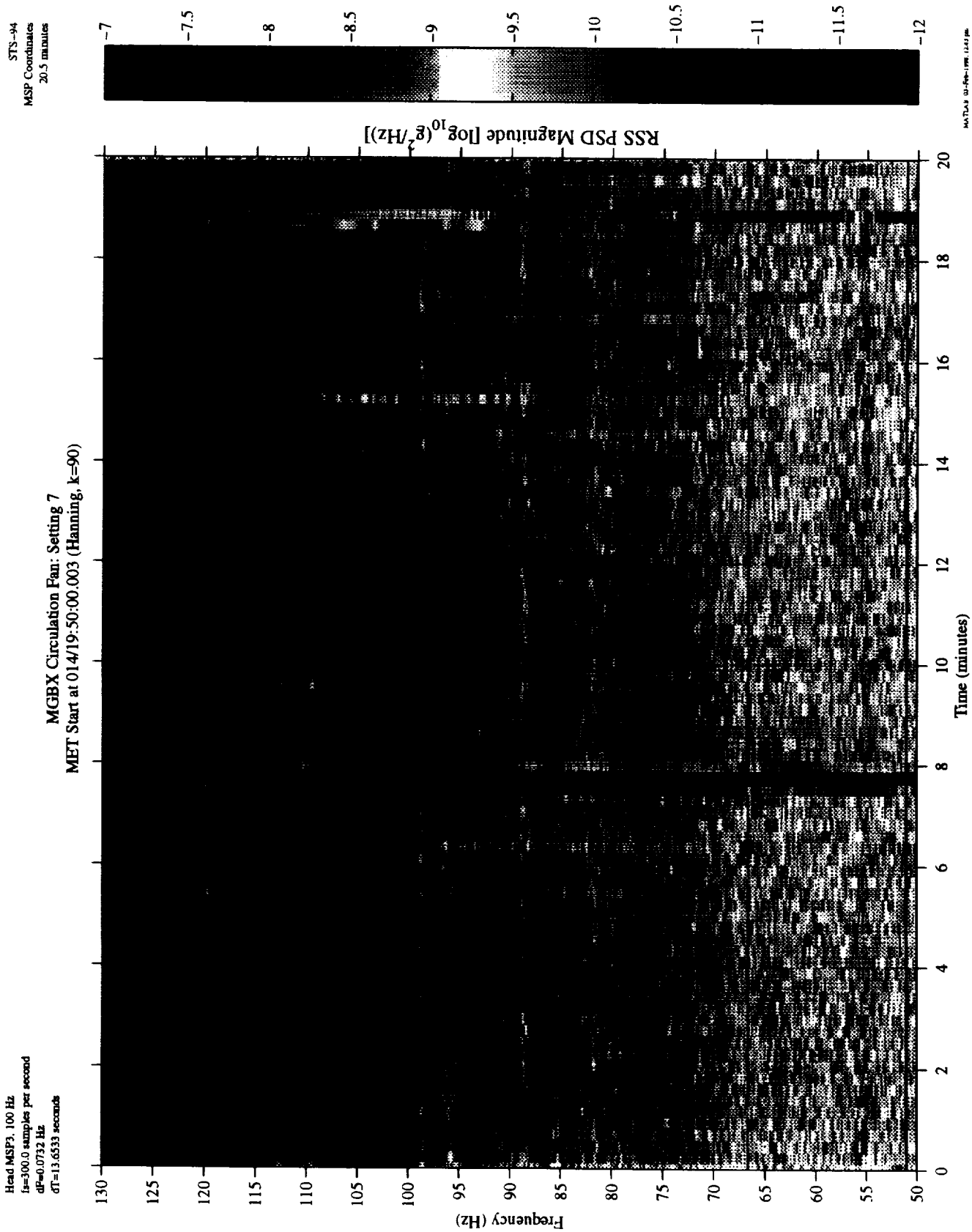


Figure 14. MGBX Circulation Fan (Setting 7), MMA MSP-3 Data, Color Spectrogram.

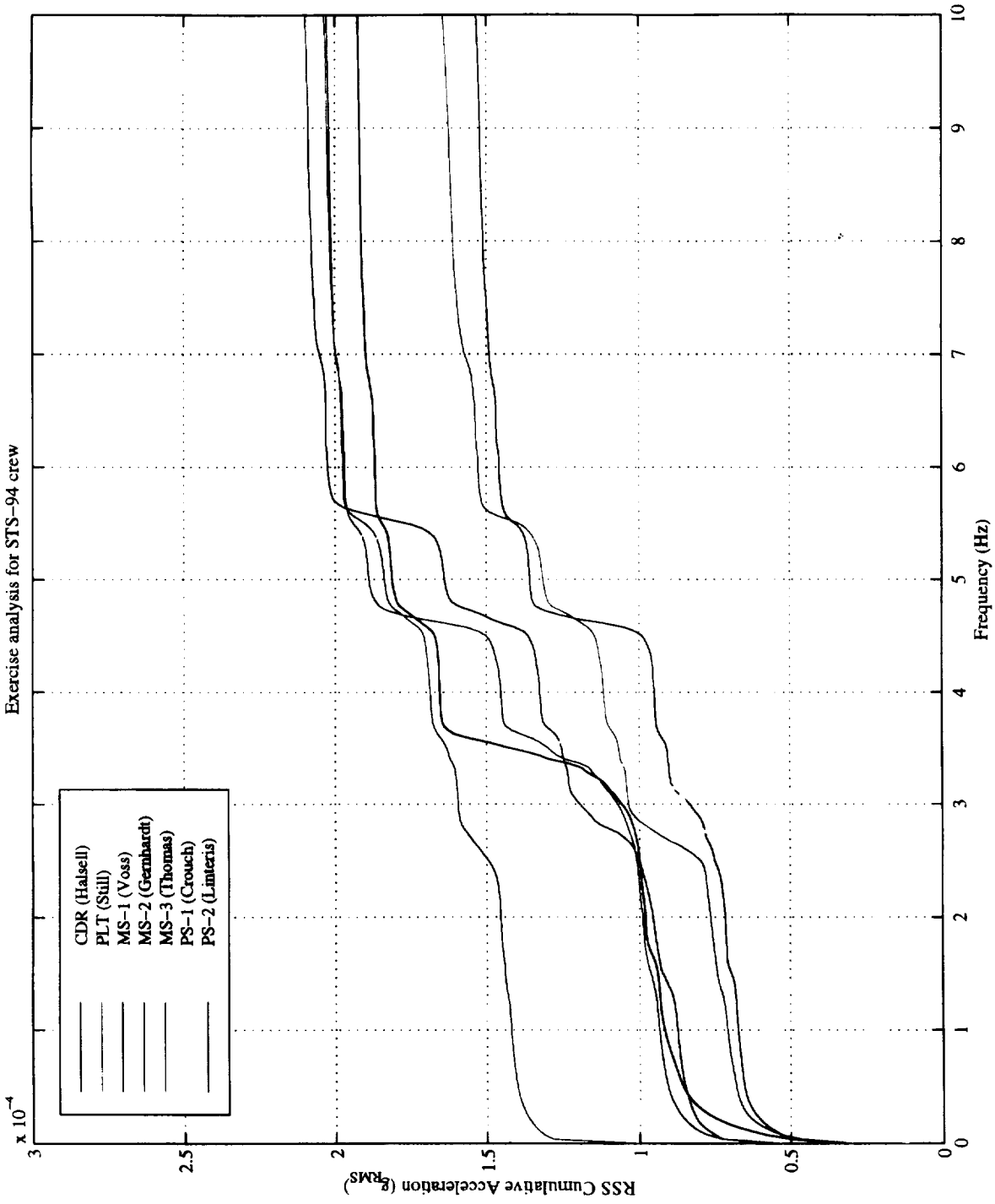


Figure 15. Exercise Analysis from STS-94, MMA MSP-3 Data.

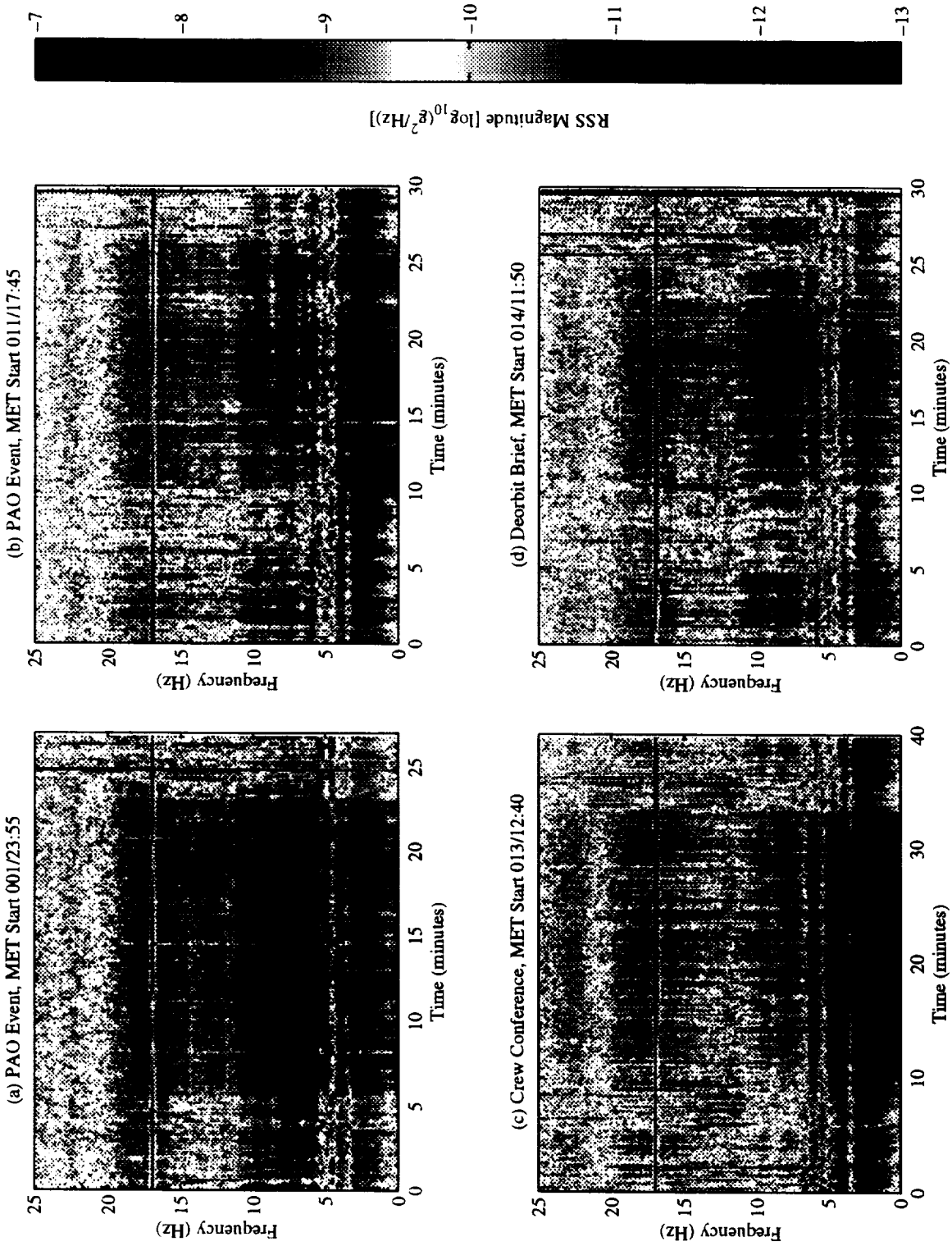


Figure 16. SAMS TSH B Color Spectrograms for PAO Events/Quiet Periods.

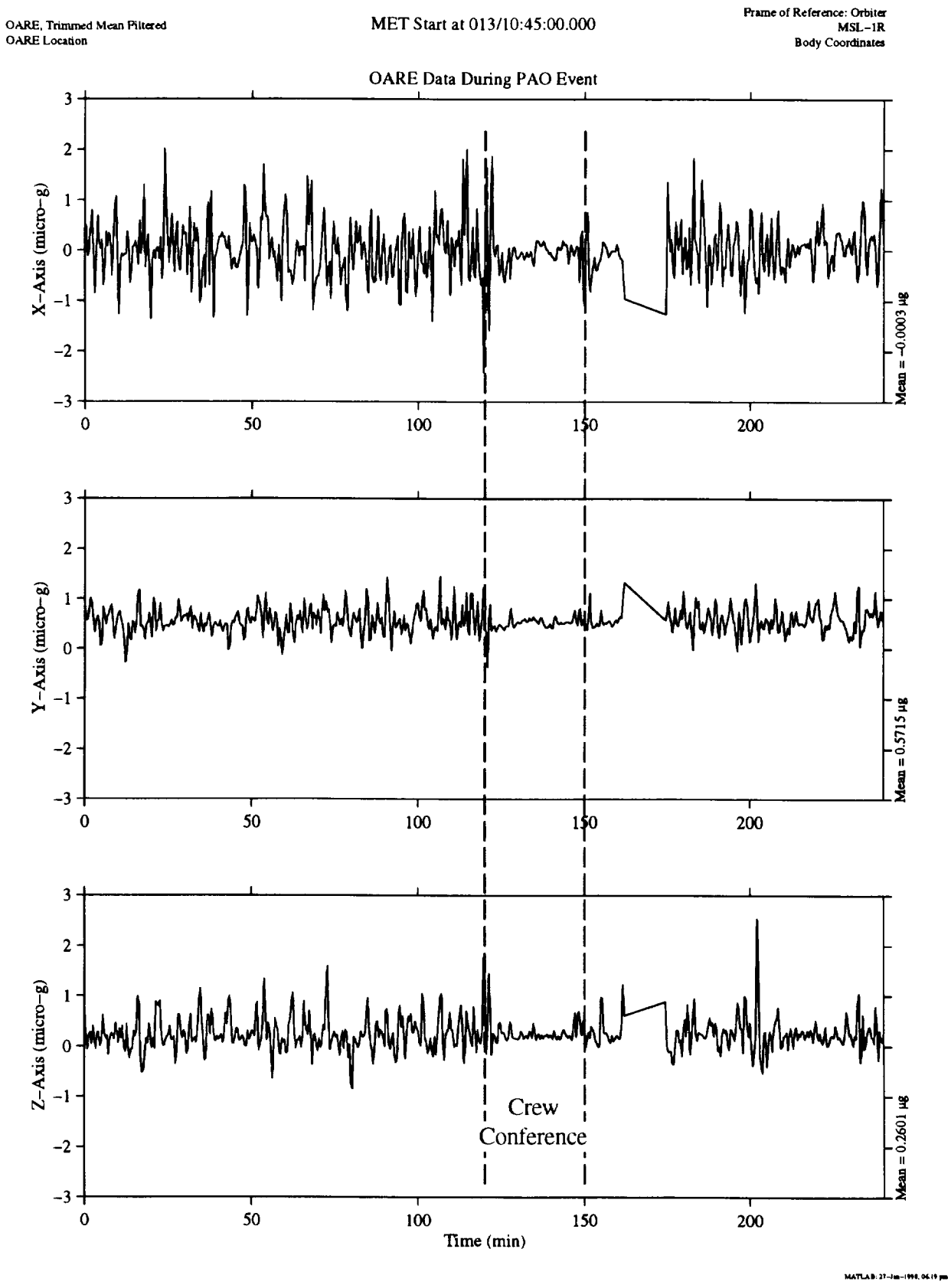


Figure 17. Trimmean Filtered OARE Data Collected During an STS-94 Crew Conference, MET 013/10:45.

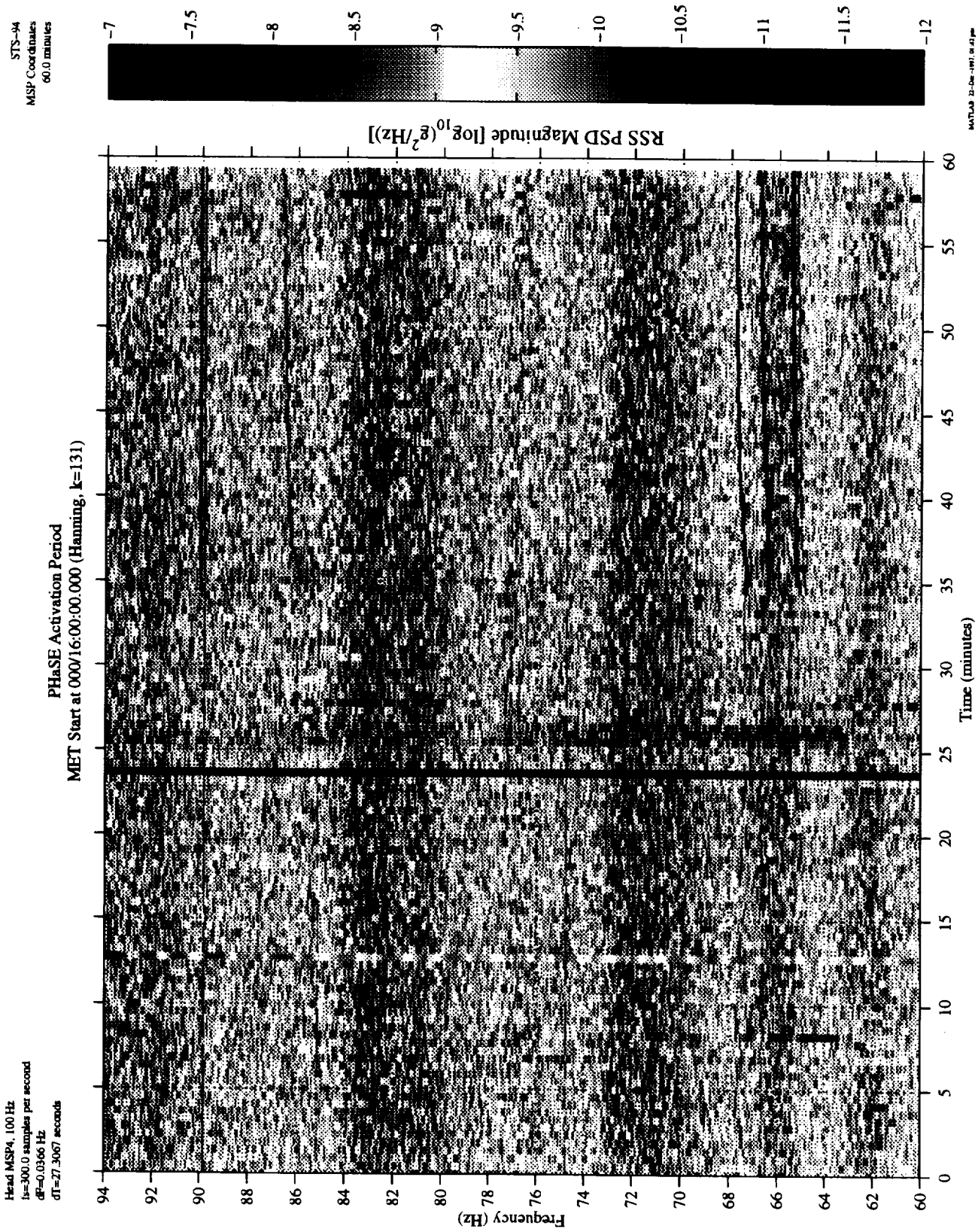


Figure 18. PHaSE Activation: MMA MSP-4 Data, Color Spectrogram.

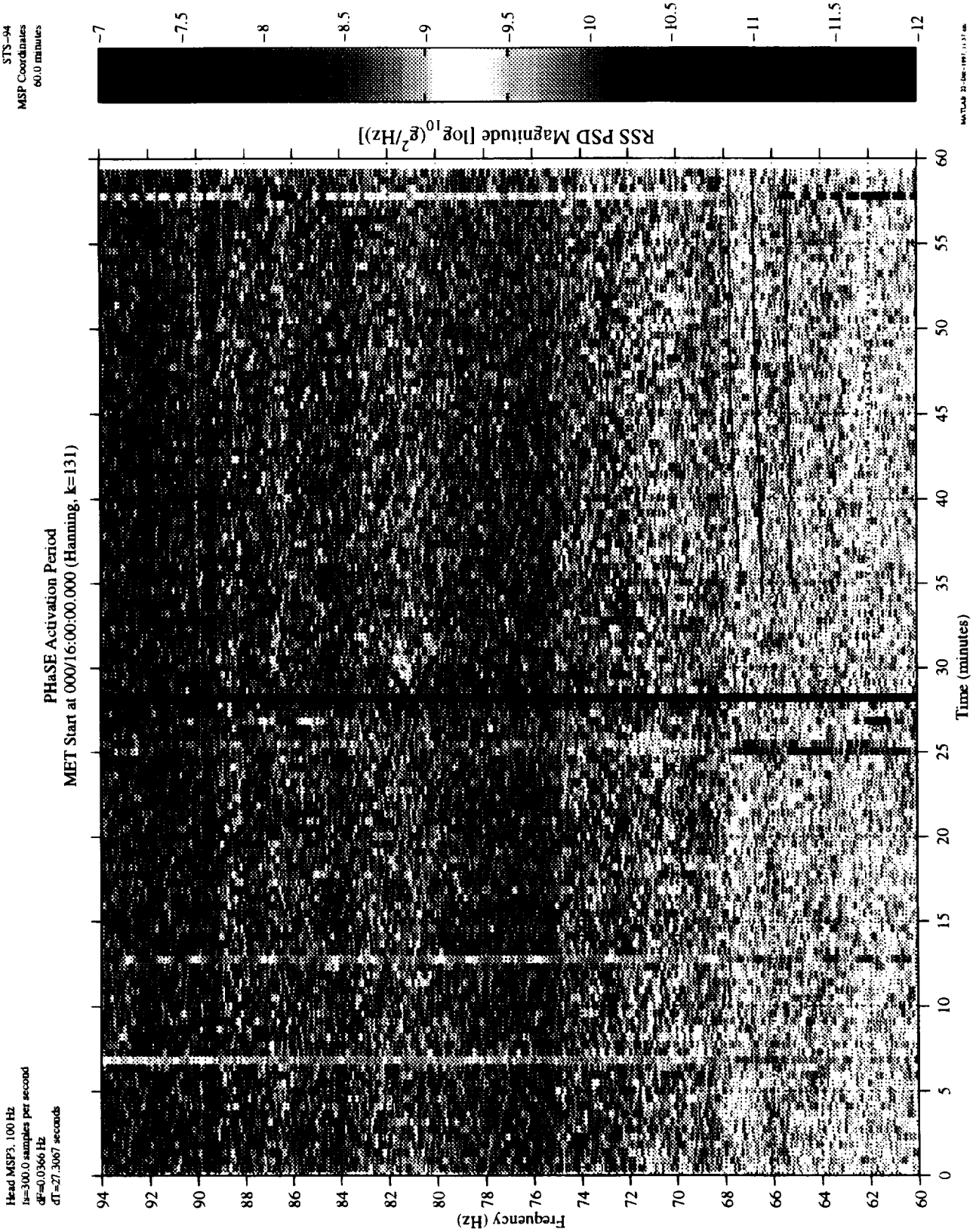


Figure 19. PHaSE Activation: MMA MSP-3 Data, Color Spectrogram.

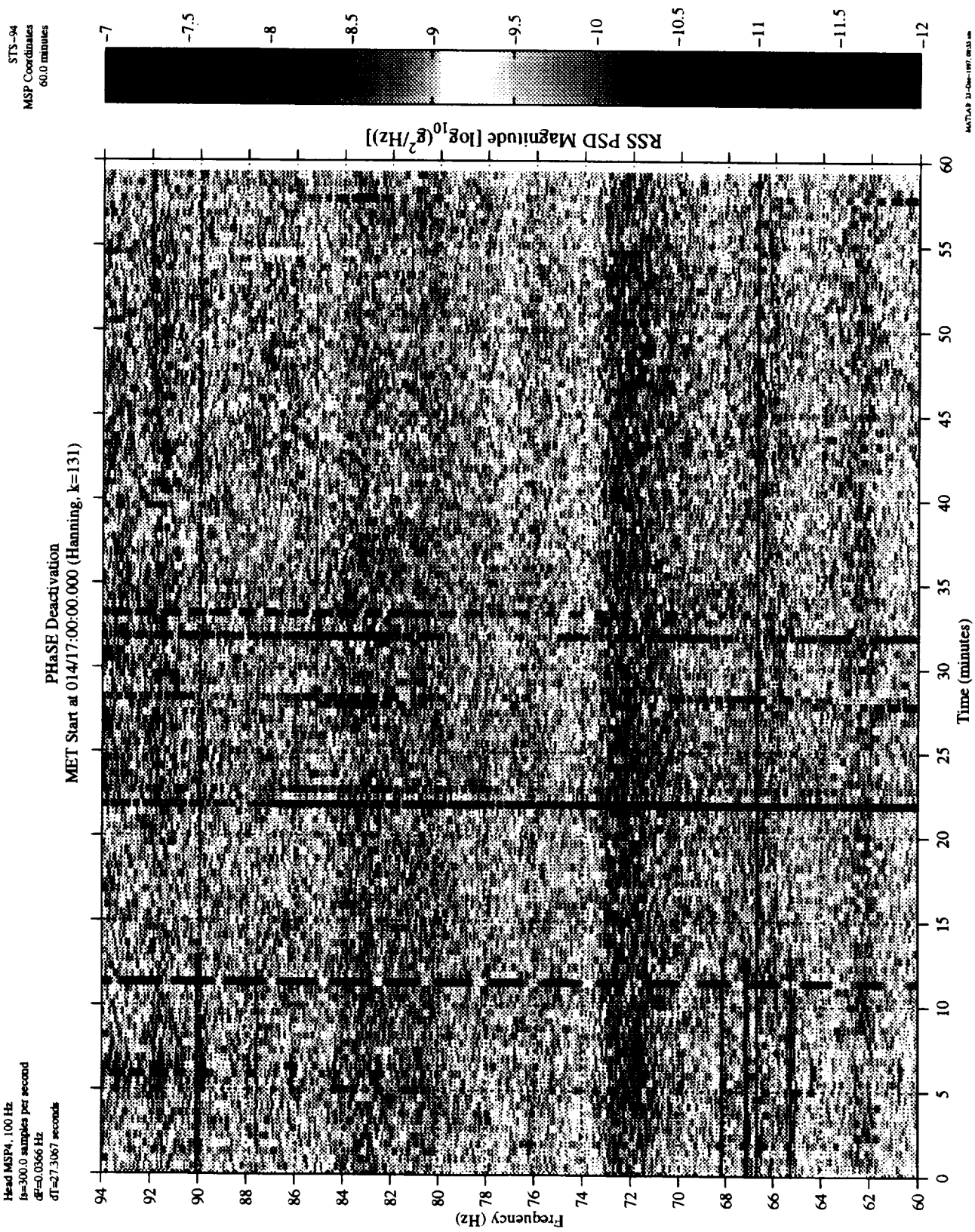


Figure 20. PHaSE Deactivation: MMA MSP-4 Data, Color Spectrogram.

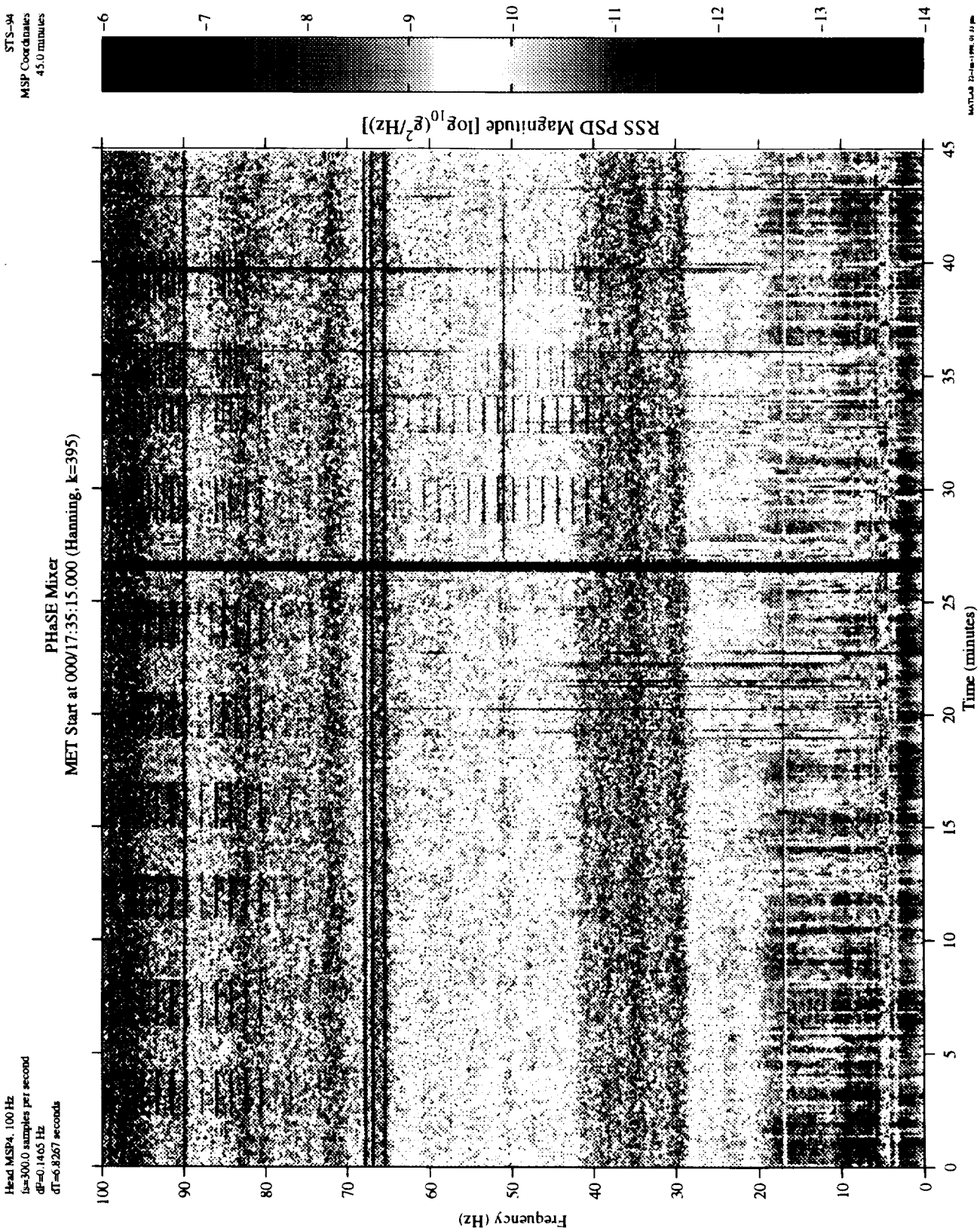


Figure 21. Spectrogram of MMA MSP-4 Data During On/Off Cycling of PHaSE Mixer.

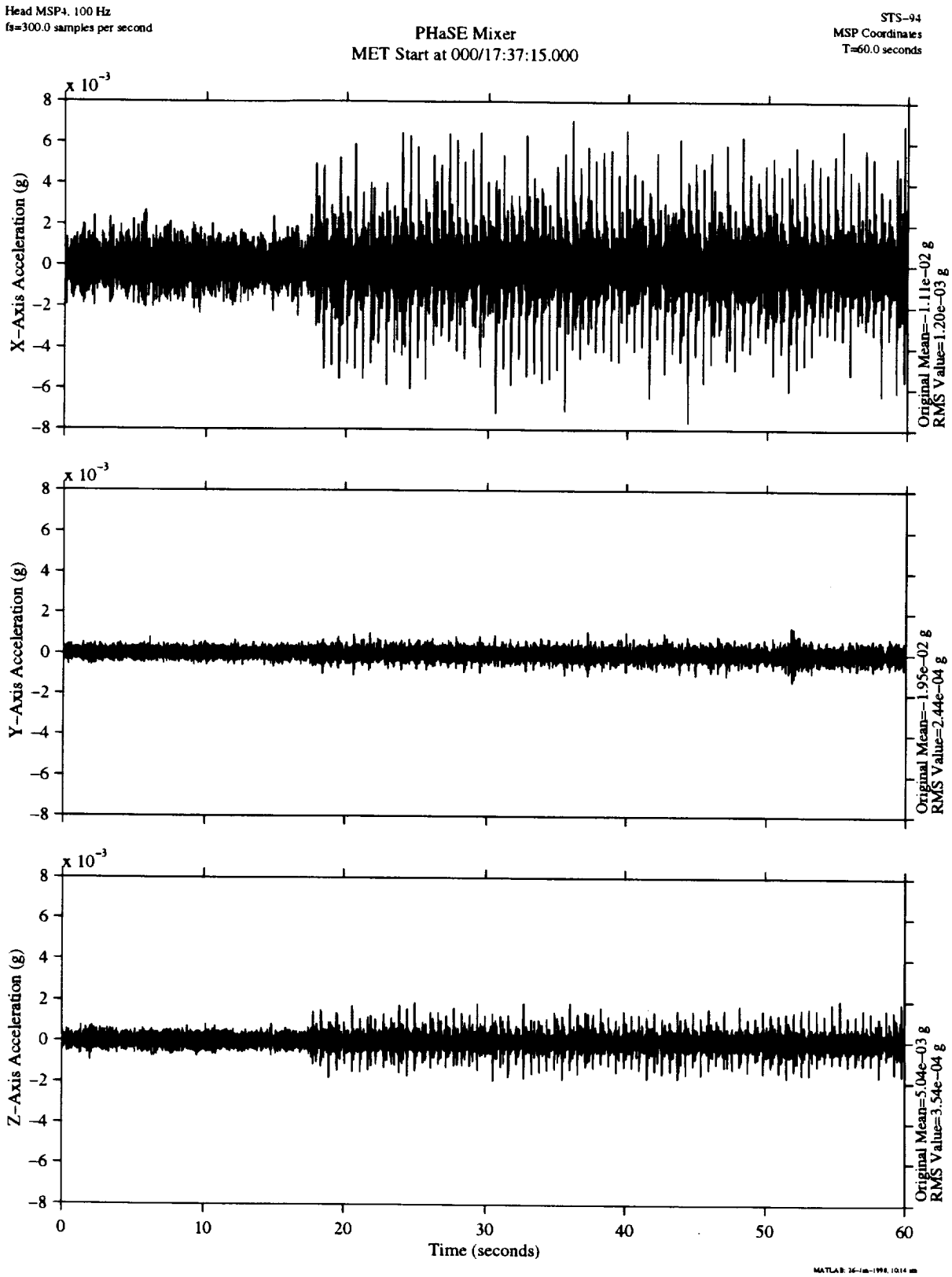


Figure 22. Onset of PHaSE Mixer Operation: MMA MSP-4 Data, Acceleration Versus Time

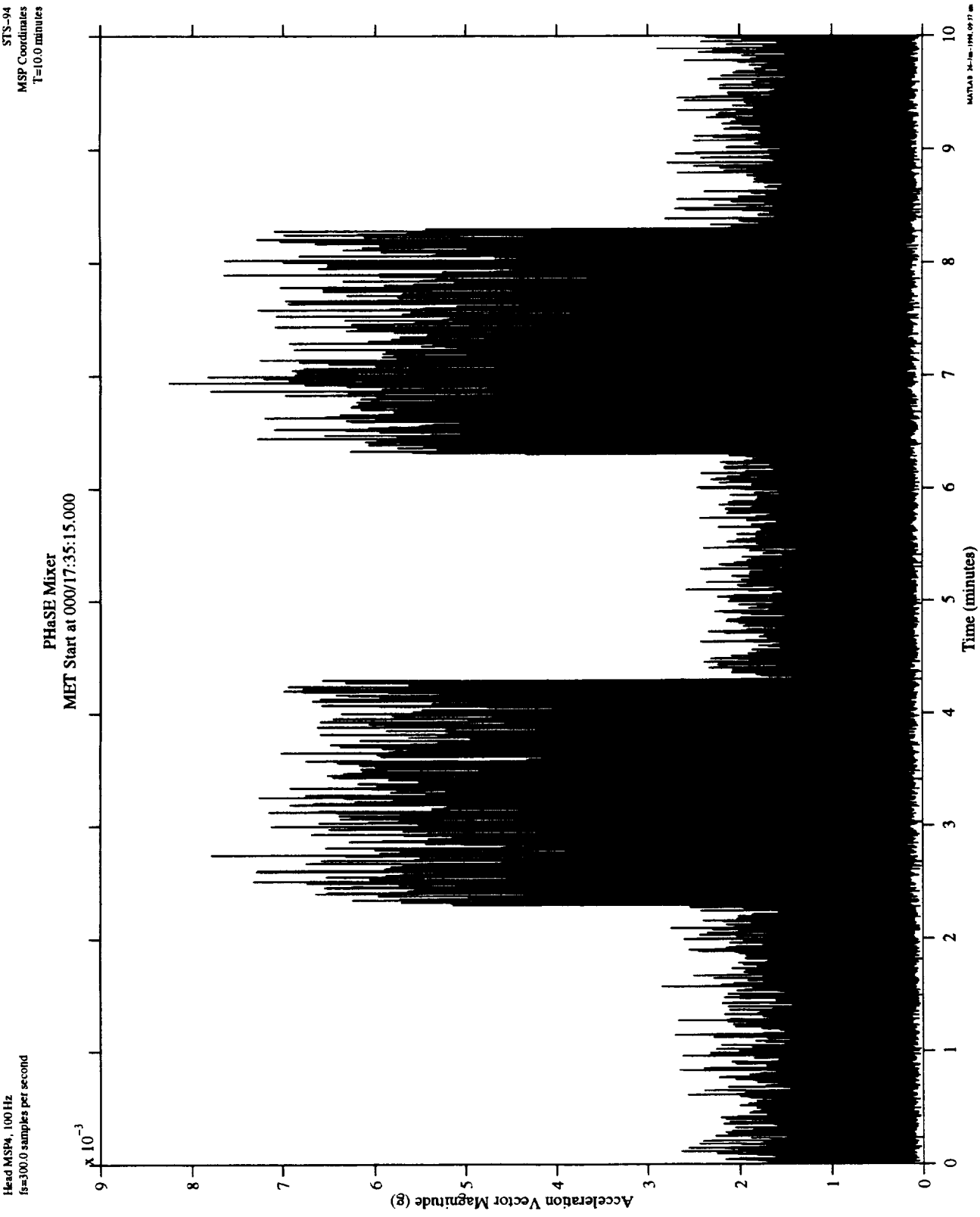


Figure 23. On/Off Cycling of PHaSE Mixer: MMA MSP-4 Data, Acceleration Vector Magnitude

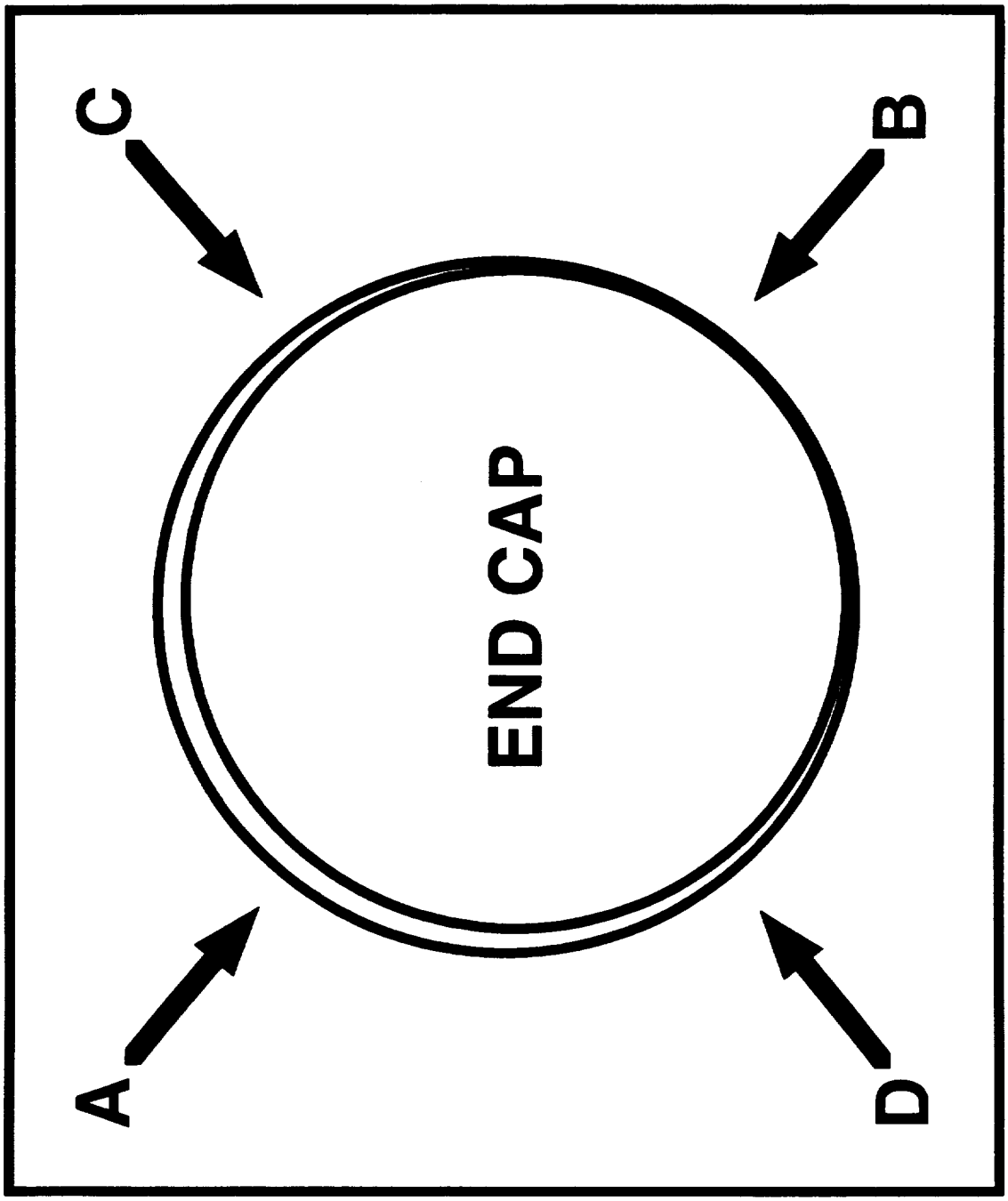


Figure 24. CM-1 Chamber Access (Chamber Close) Diagram

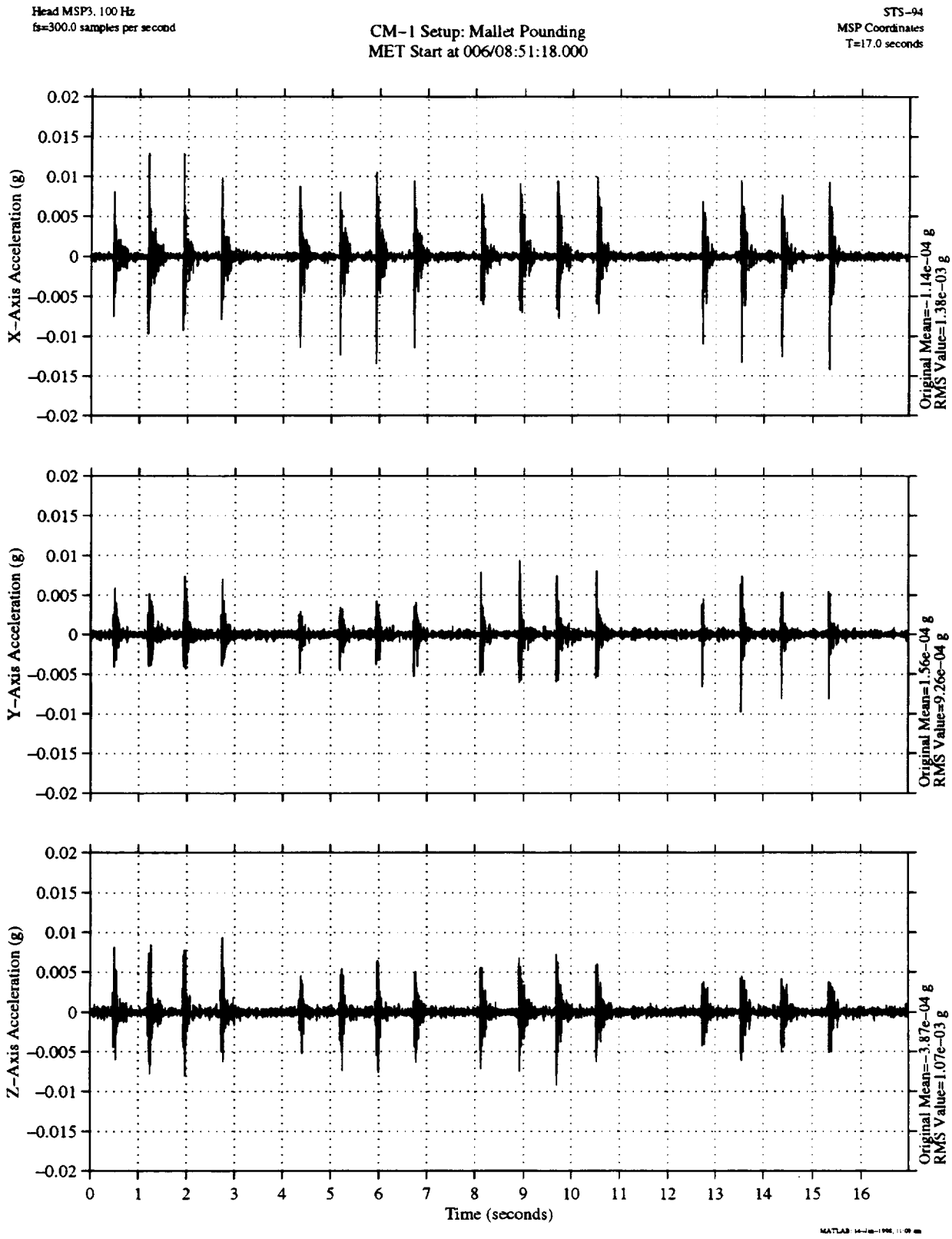


Figure 25. Mallet Pounding for CM-1 Setup: MMA MSP-3 Data.

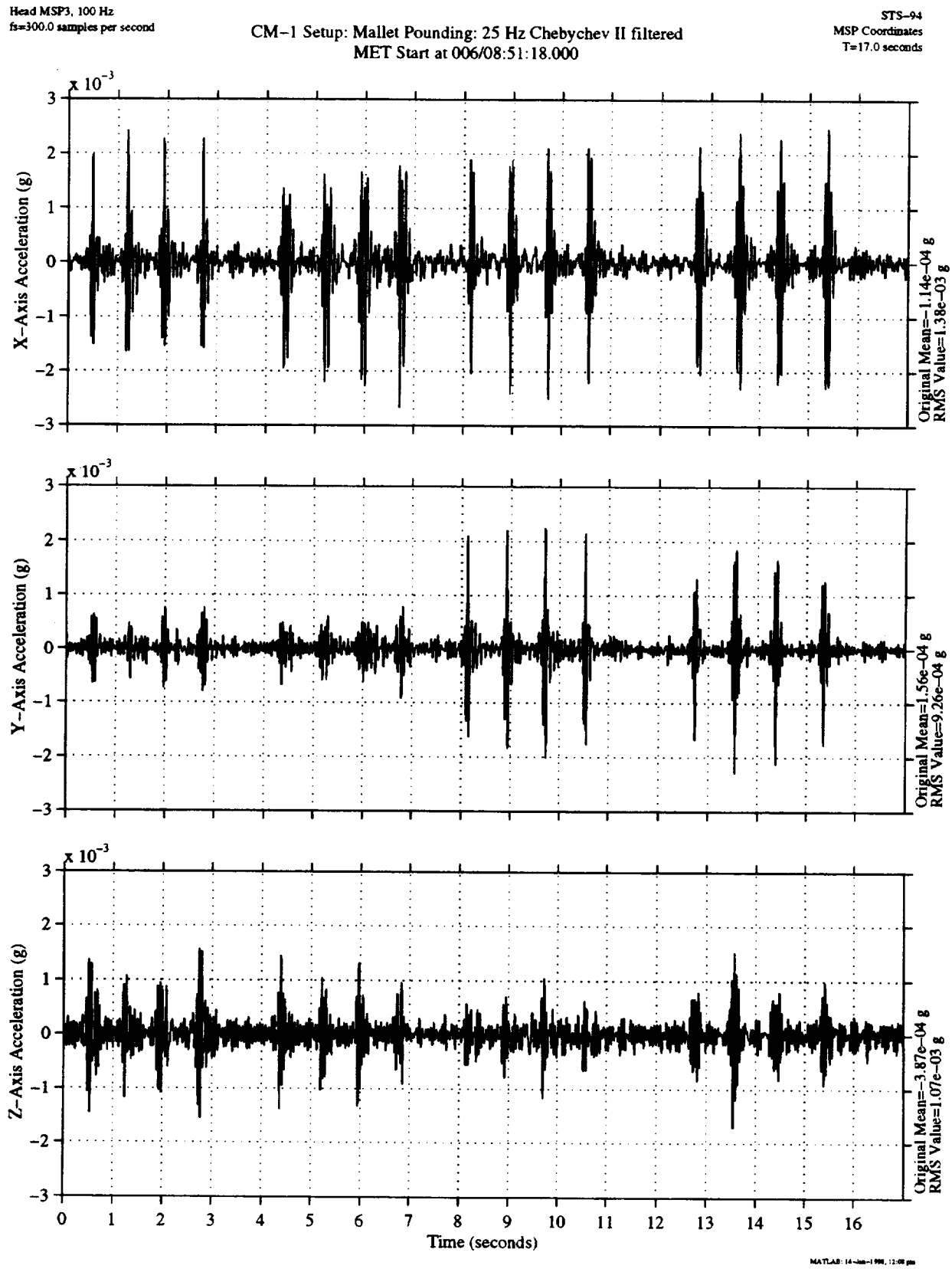


Figure 26. Mallet Pounding for CM-1 Setup: MMA MSP-3 Data, 25 Hz Filtered.

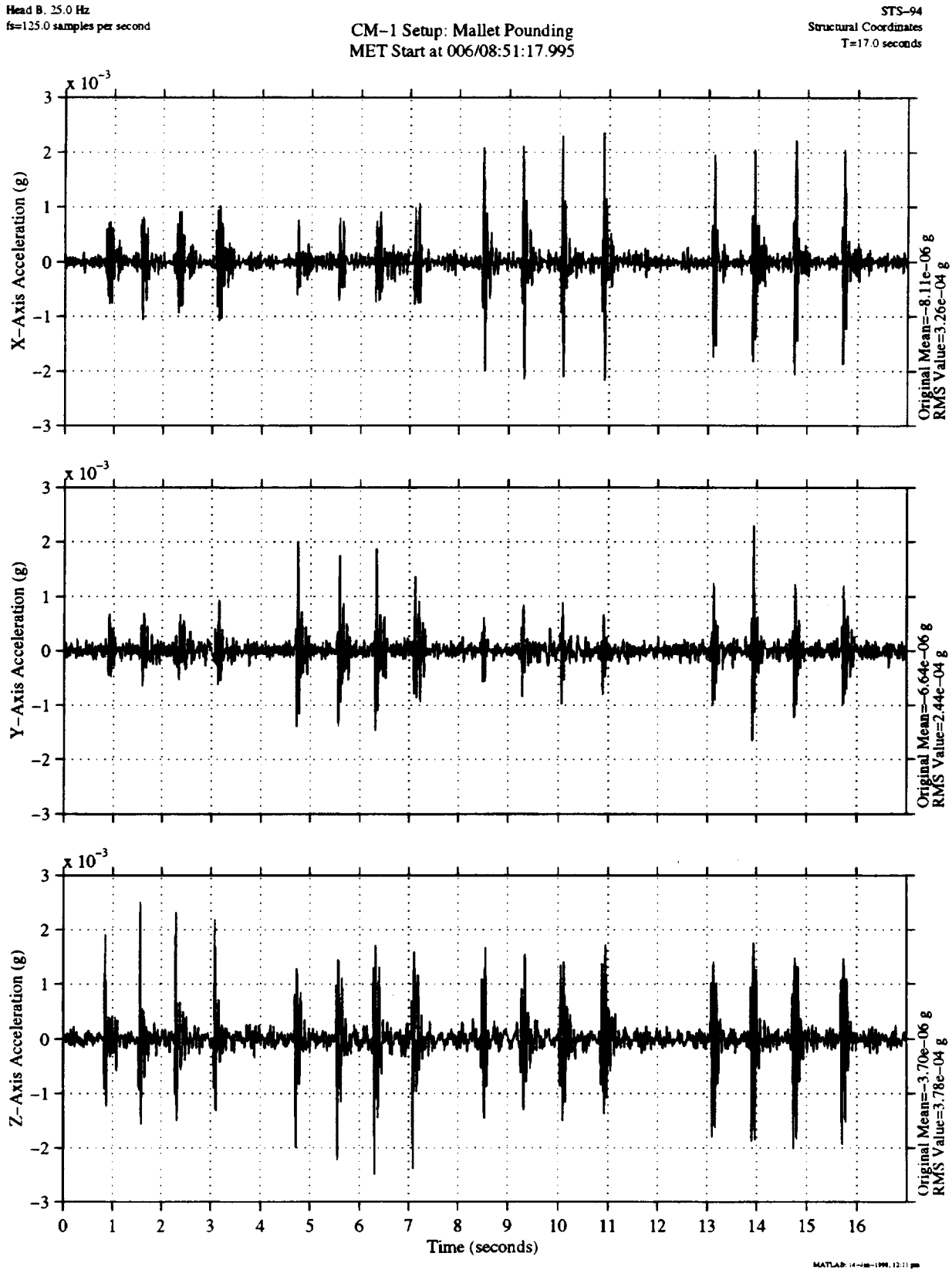


Figure 27. Mallet Pounding for CM-1 Setup: SAMS TSH B Data.

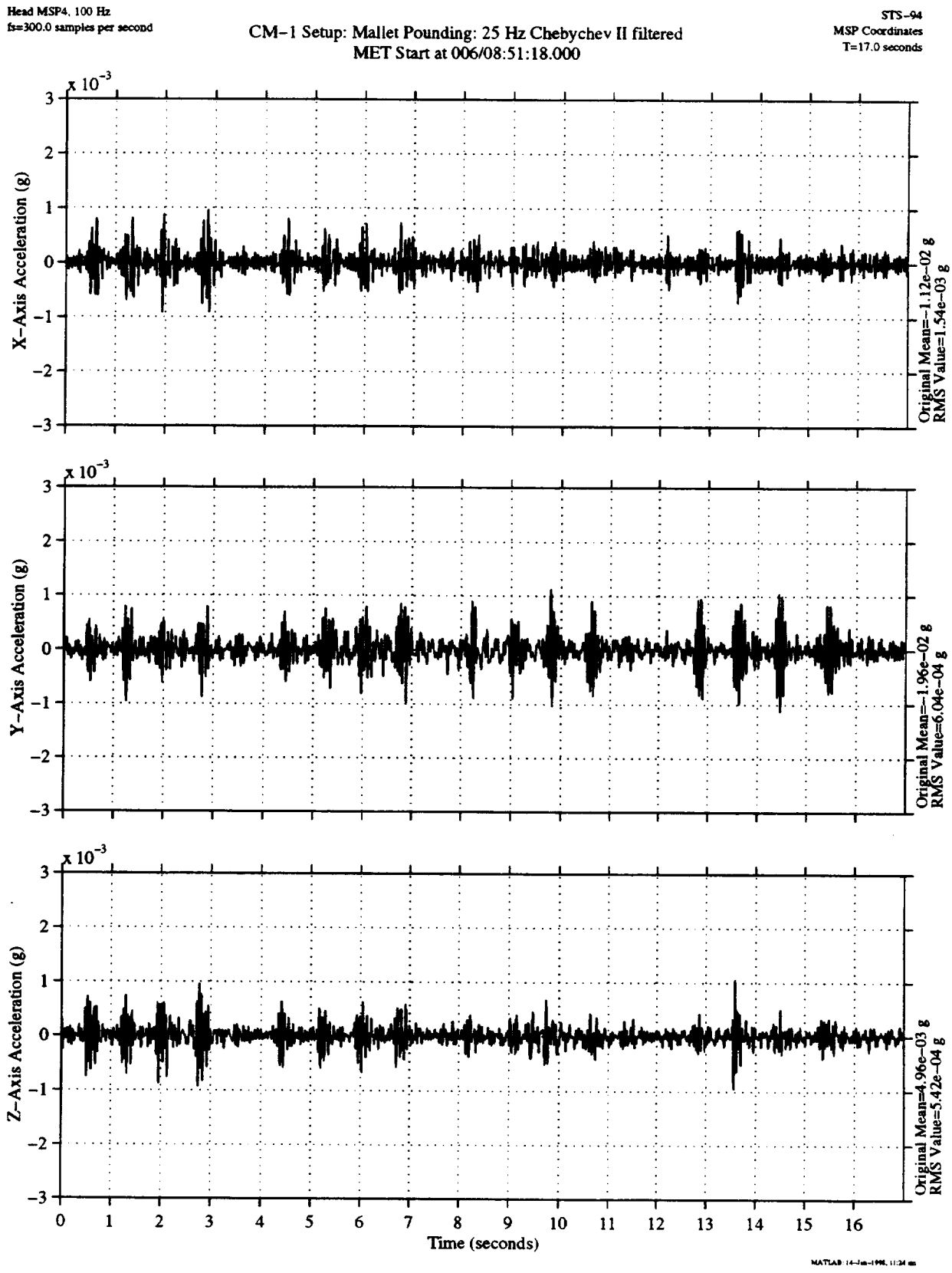


Figure 28. Mallet Pounding for CM-1 Setup: MMA MSP-4 Data, 25 Hz Filtered.

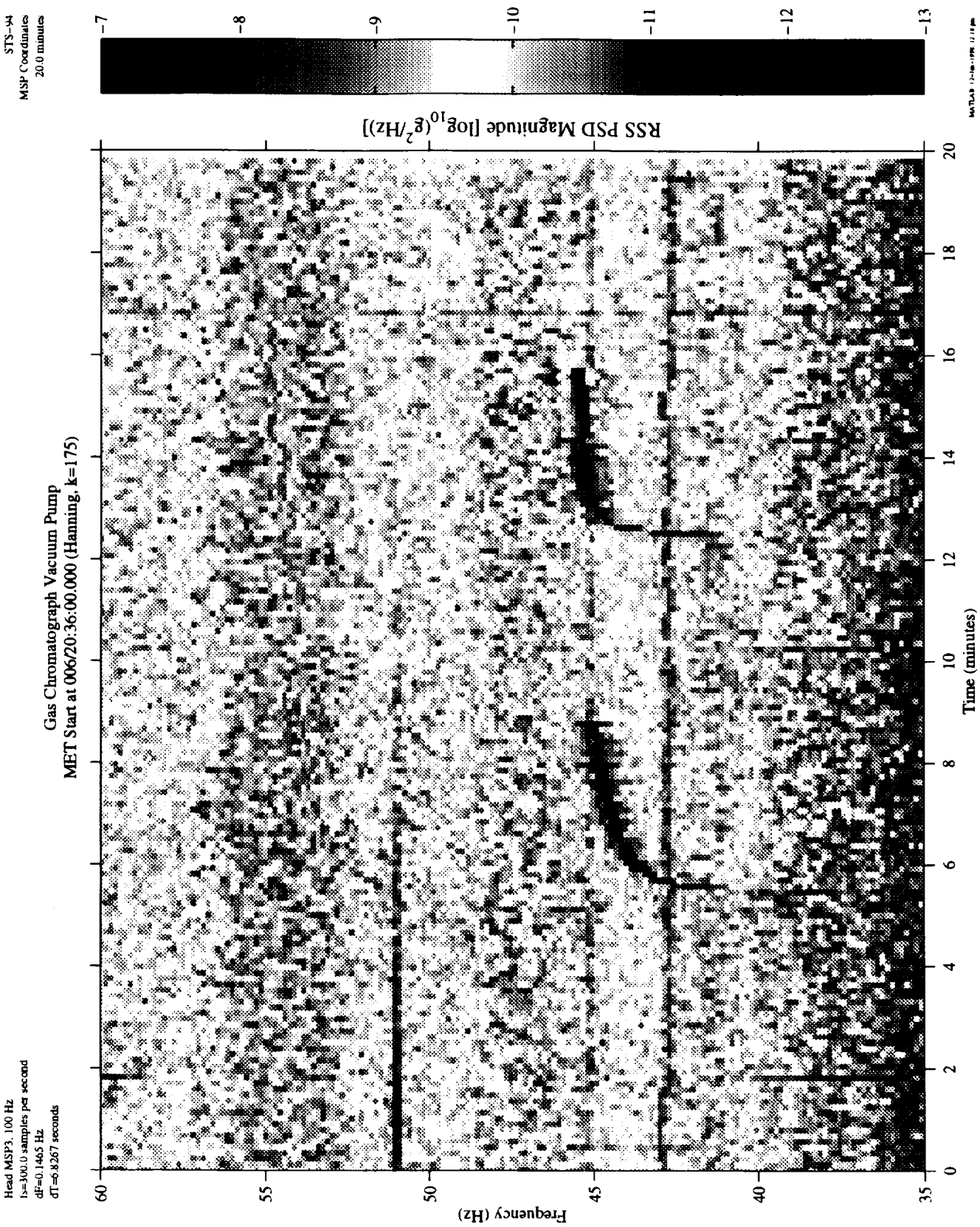


Figure 29. Typical CM-1 Gas Chromatograph Vacuum Pump Operation Sequence.

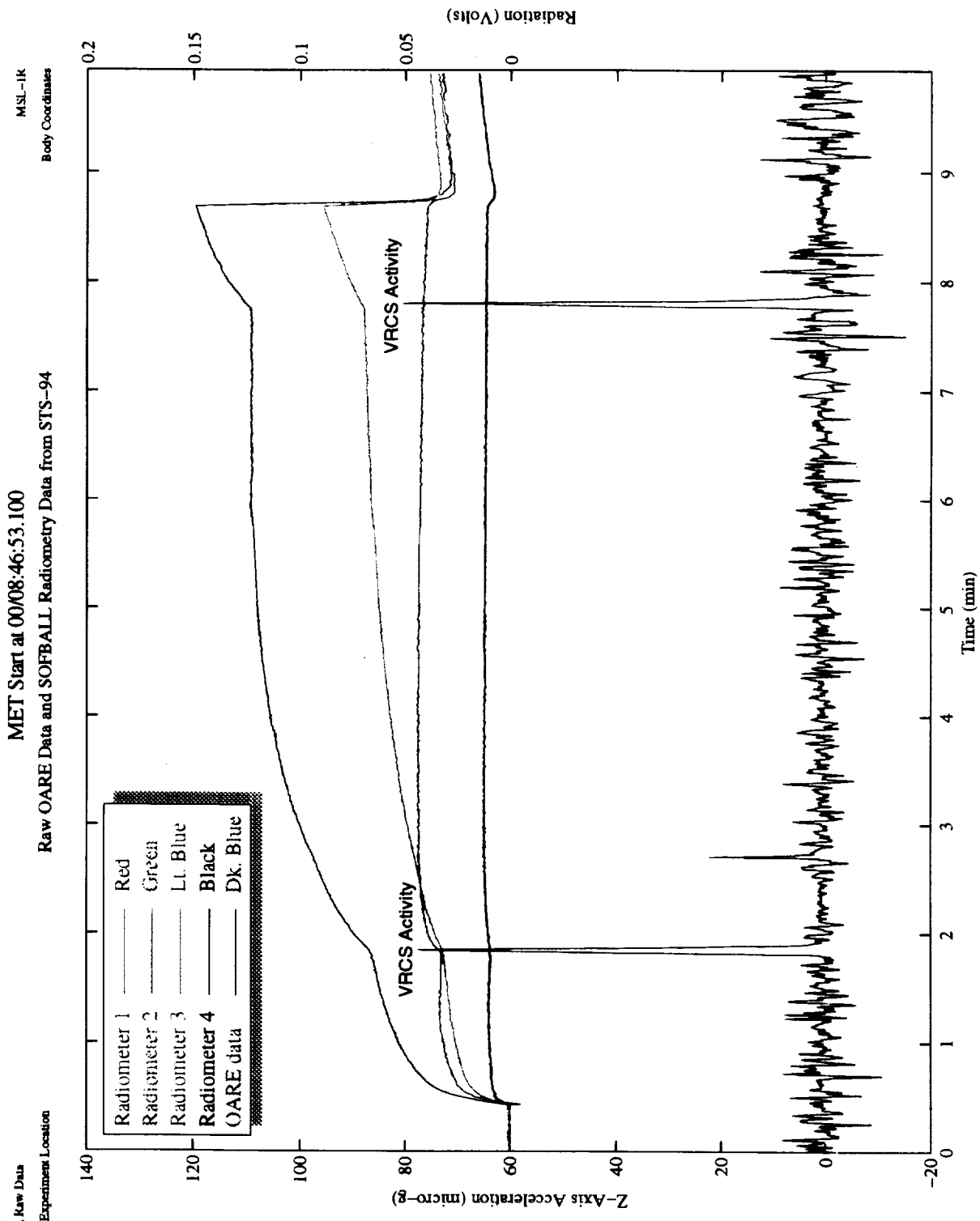


Figure 30. Raw (10 samples per second) OARE Data with SOFBALL Radiometry Data from STS-94, SOFBALL Test Point 14A. MET Start 007/08:46:53.

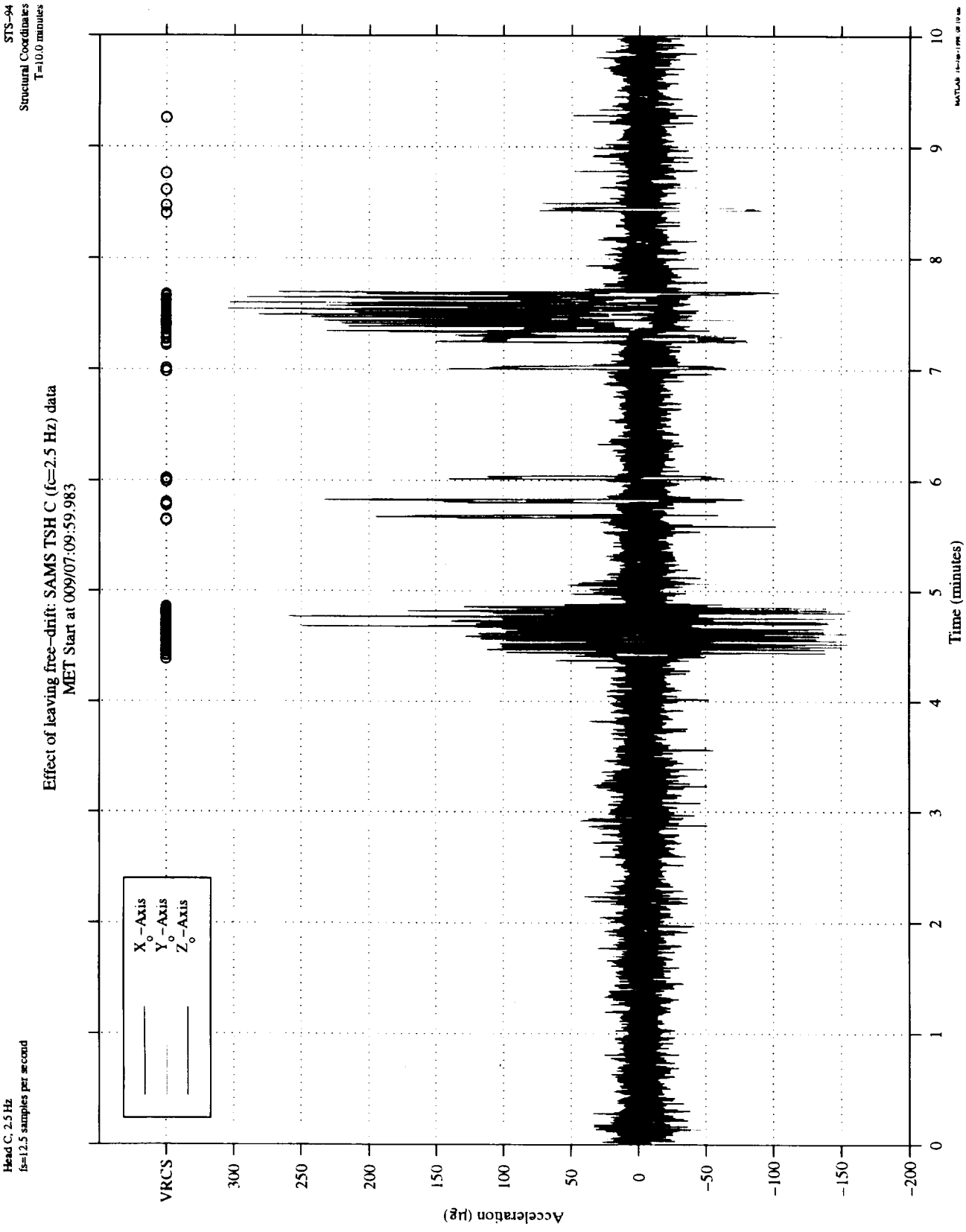


Figure 31. Effect of Leaving Free Drift: SAMS TSH C Data, Acceleration Versus Time.

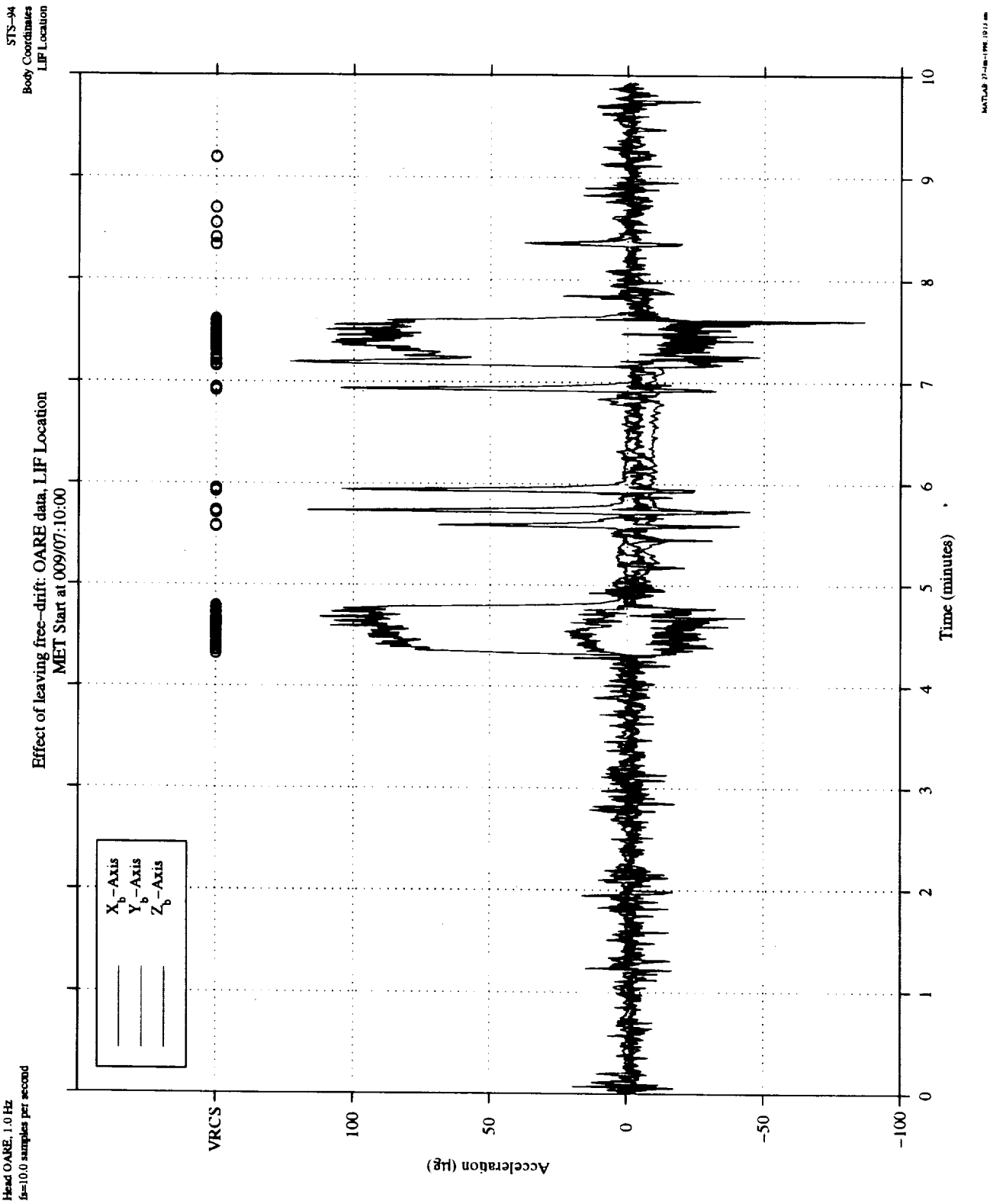


Figure 32. Effect of Leaving Free Drift: OARE Data, Acceleration Versus Time.

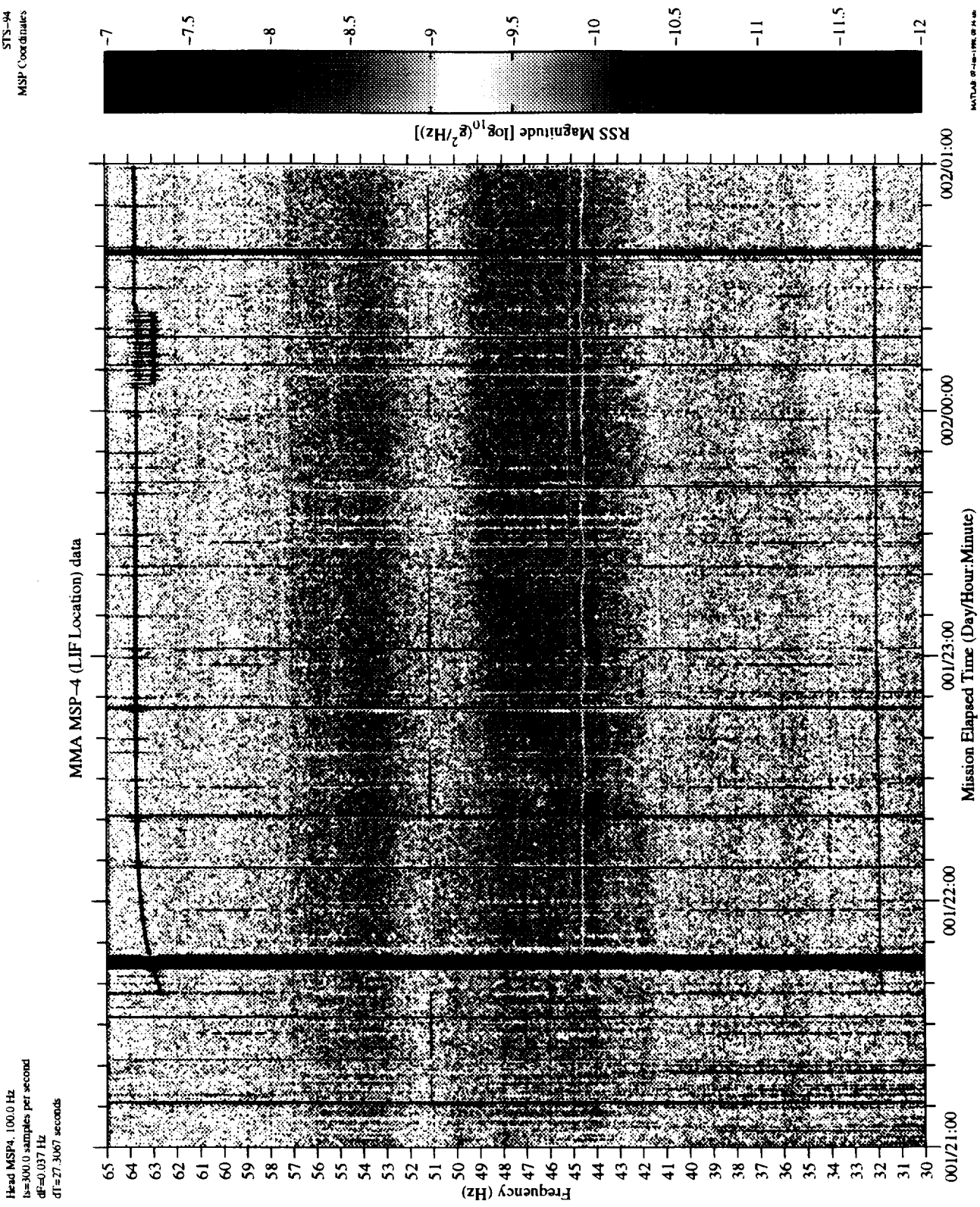


Figure 33. Astro/PGBA Activation: MMA MSP-4 Data, Color Spectrogram.

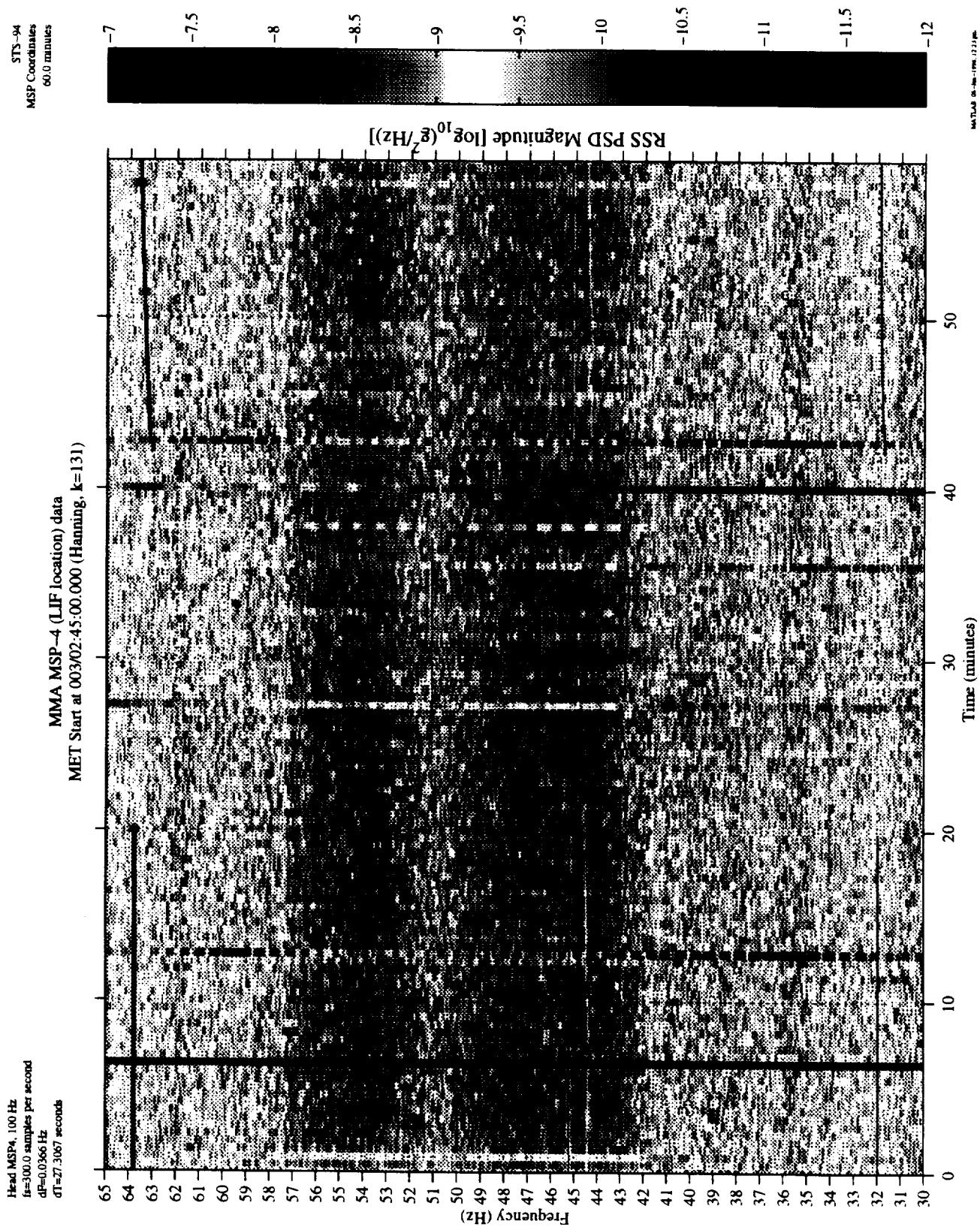


Figure 34. Astro/PGBA Acceleration Signal Turn-off: MMA MSP-4 Data, Color Spectrogram.

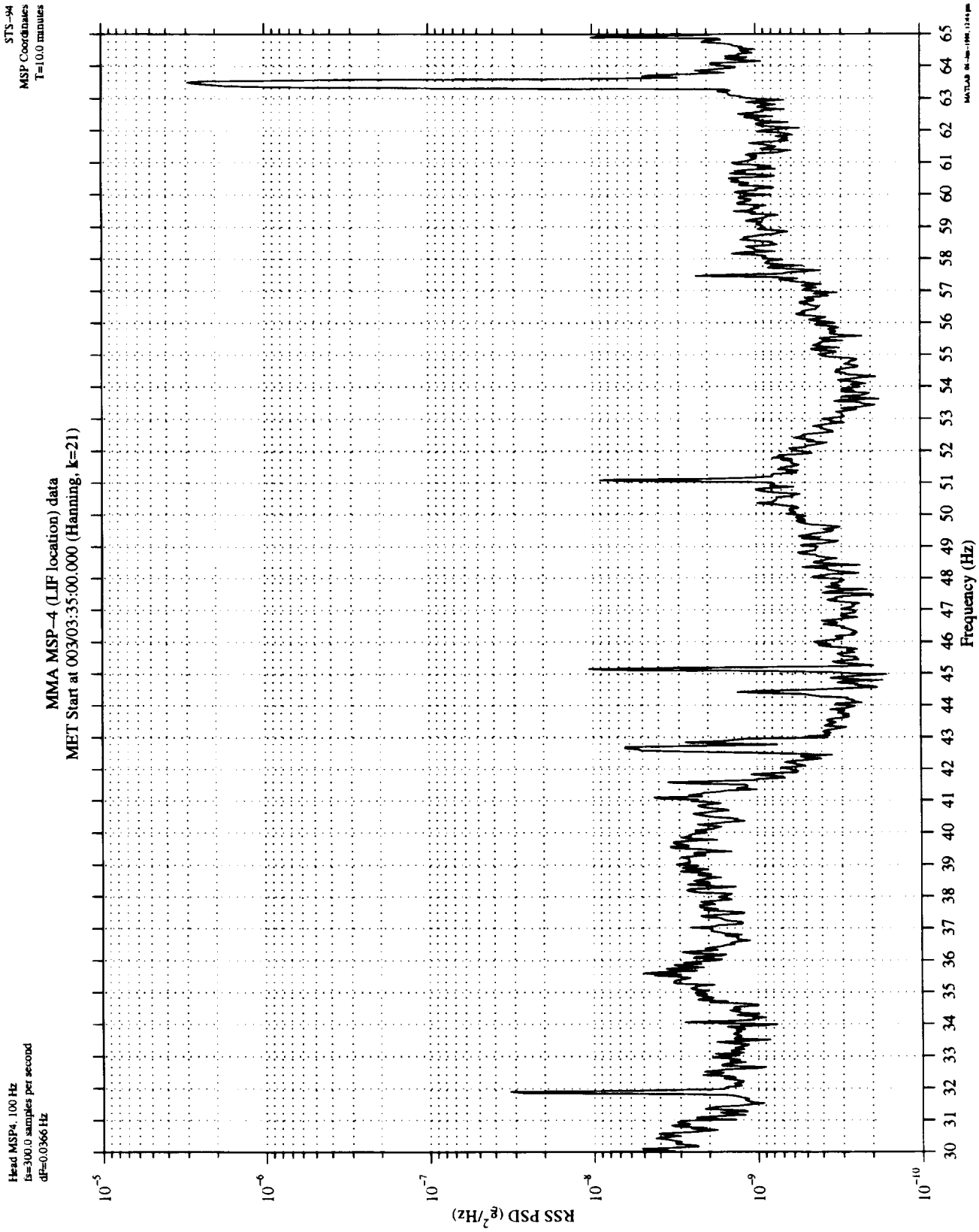


Figure 35. Astro/PGBA Acceleration Signals: MMA MSP-4 Data, Power Spectral Density.

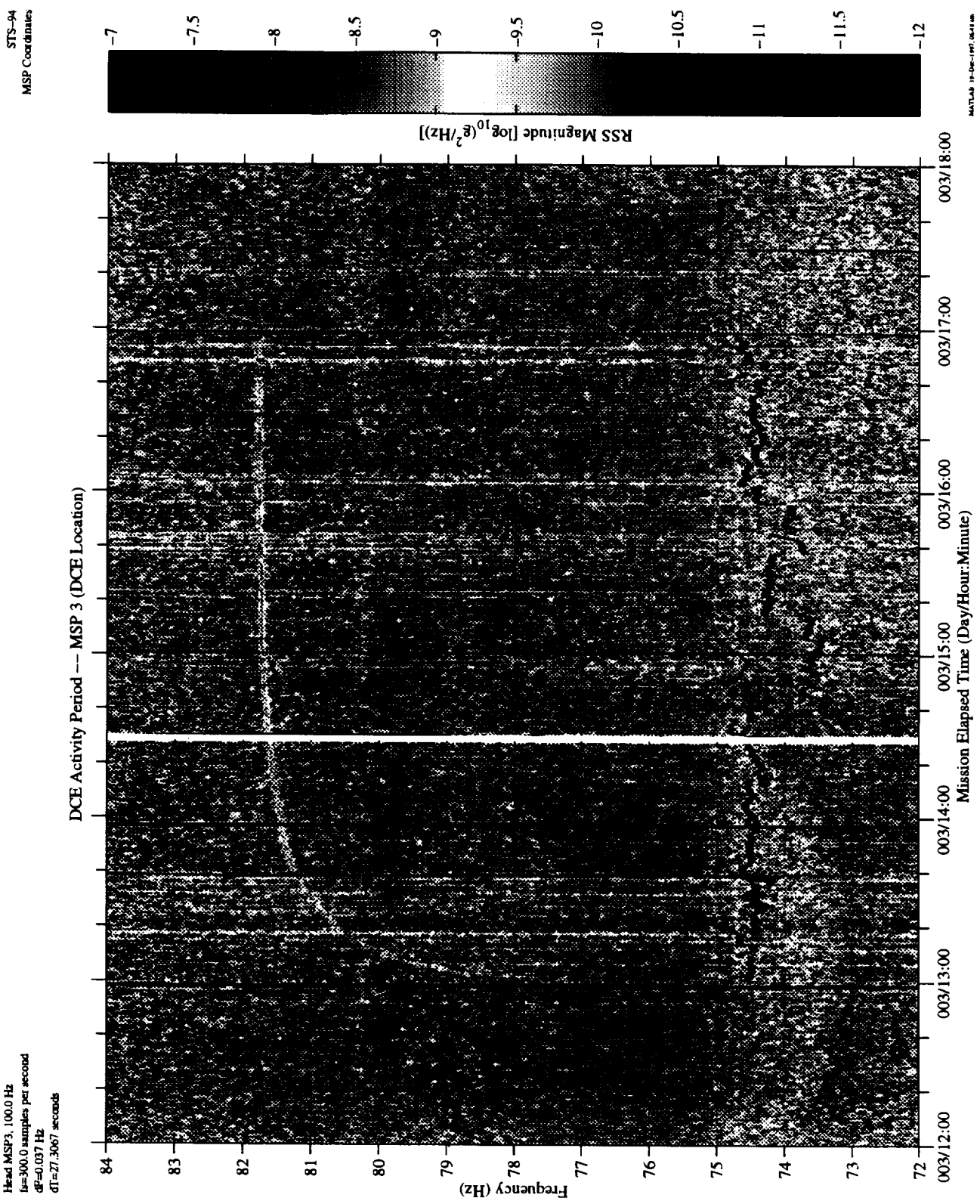


Figure 36. DCE Activity: MMA MSP-3 Data, Color Spectrogram.

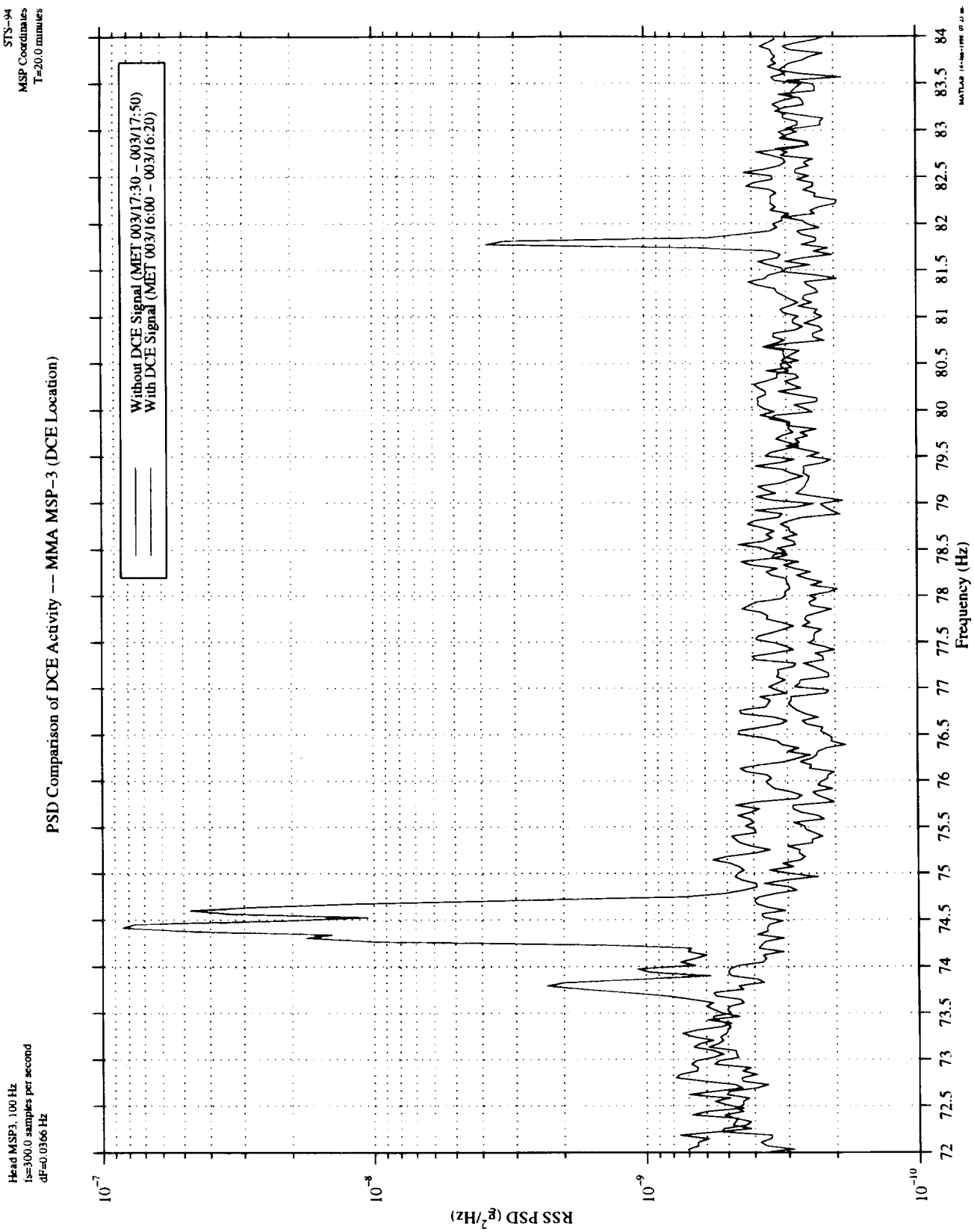


Figure 37. DCE Activity: MMA MSP-3 Data, Comparison of Before and During PSDs.

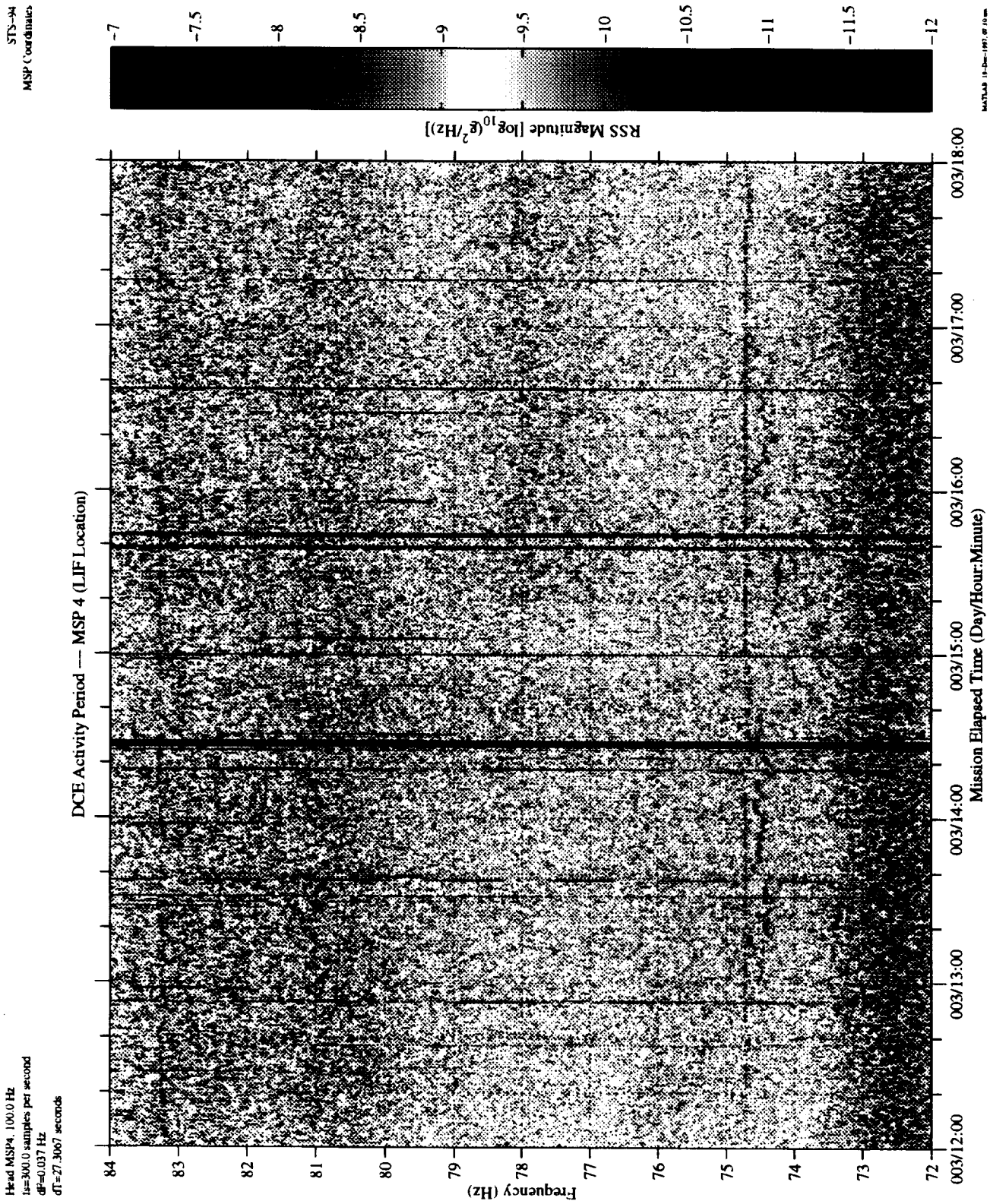


Figure 38. DCE Activity: MMA MSP-4 Data, Color Spectrogram.

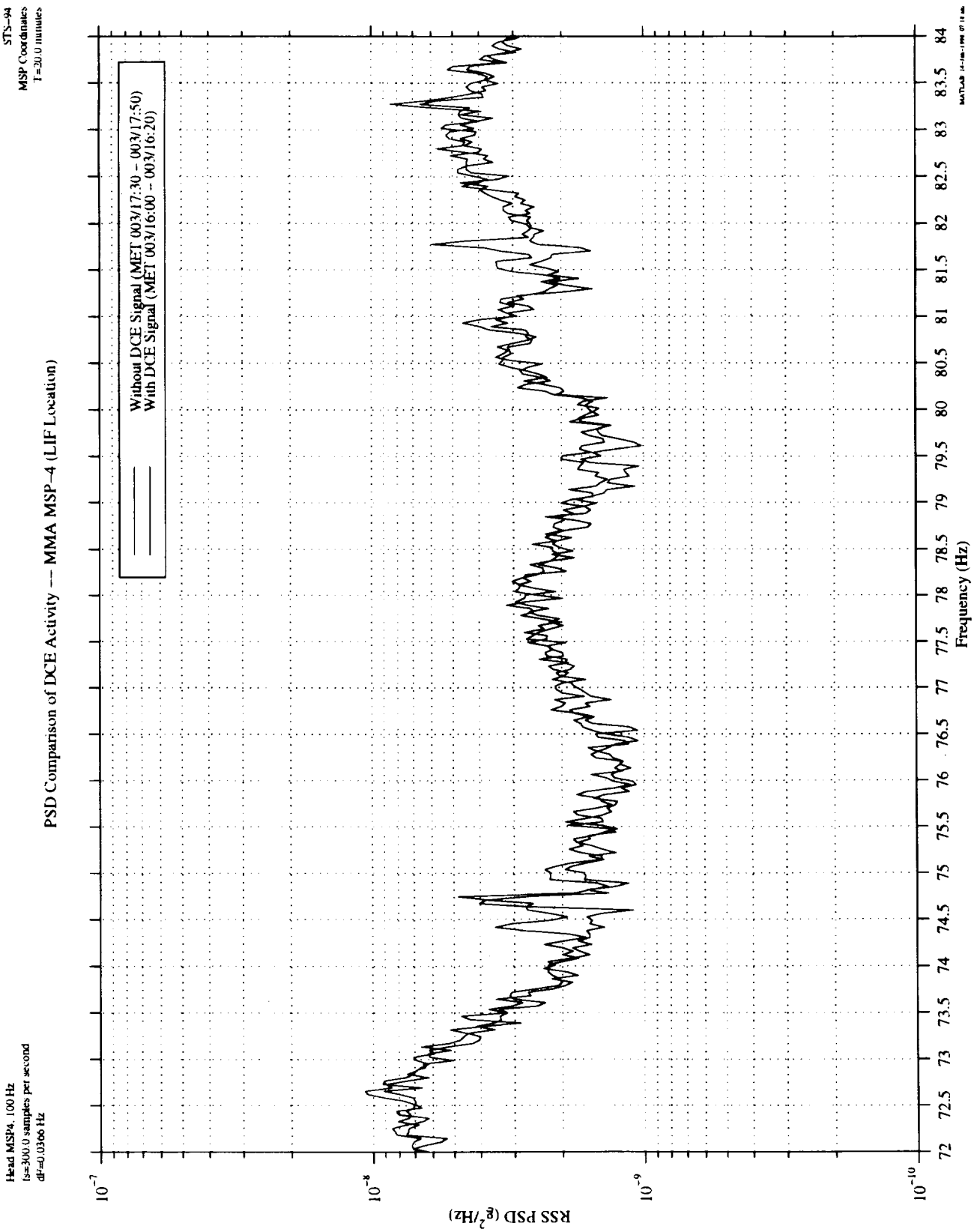


Figure 39. DCE Activity: MMA MSP-4 Data, Comparison of Before and During PSDs.

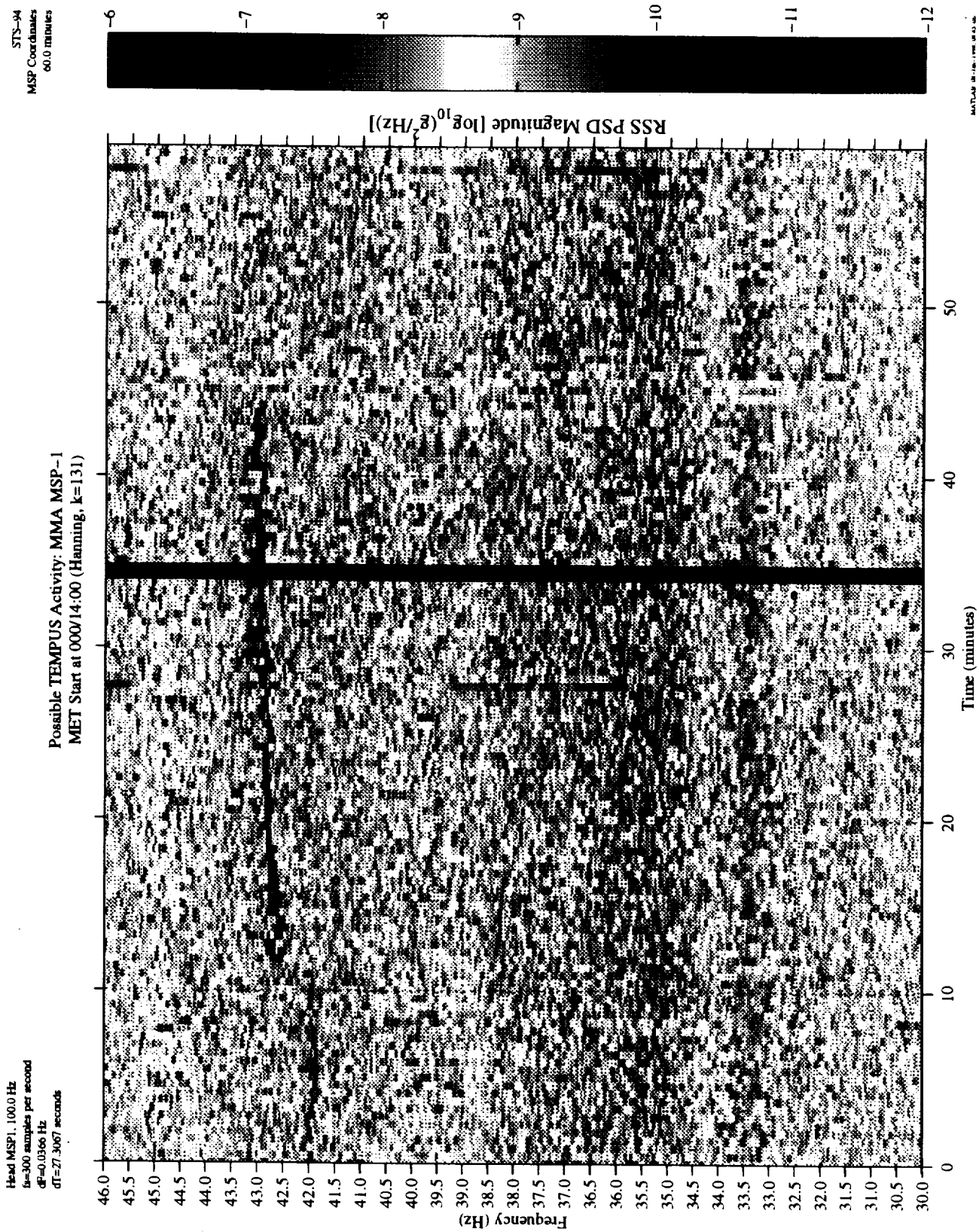


Figure 40. TEMPUS Activity: MMA MSP-1 Data, Color Spectrogram.

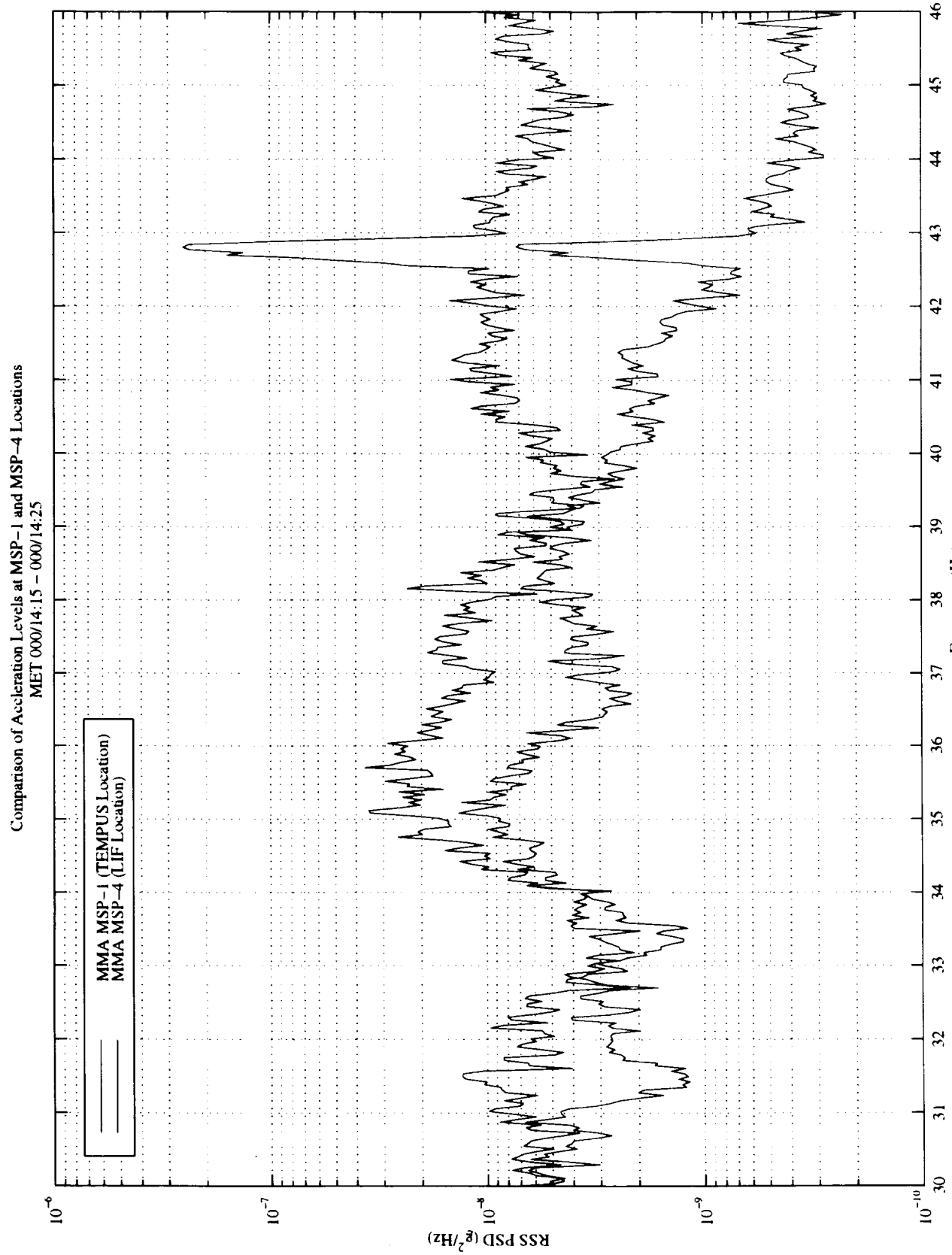


Figure 41. Comparison of Acceleration Levels Due to TEMPUS at MMA MSP-1 and MSP-4 Locations.

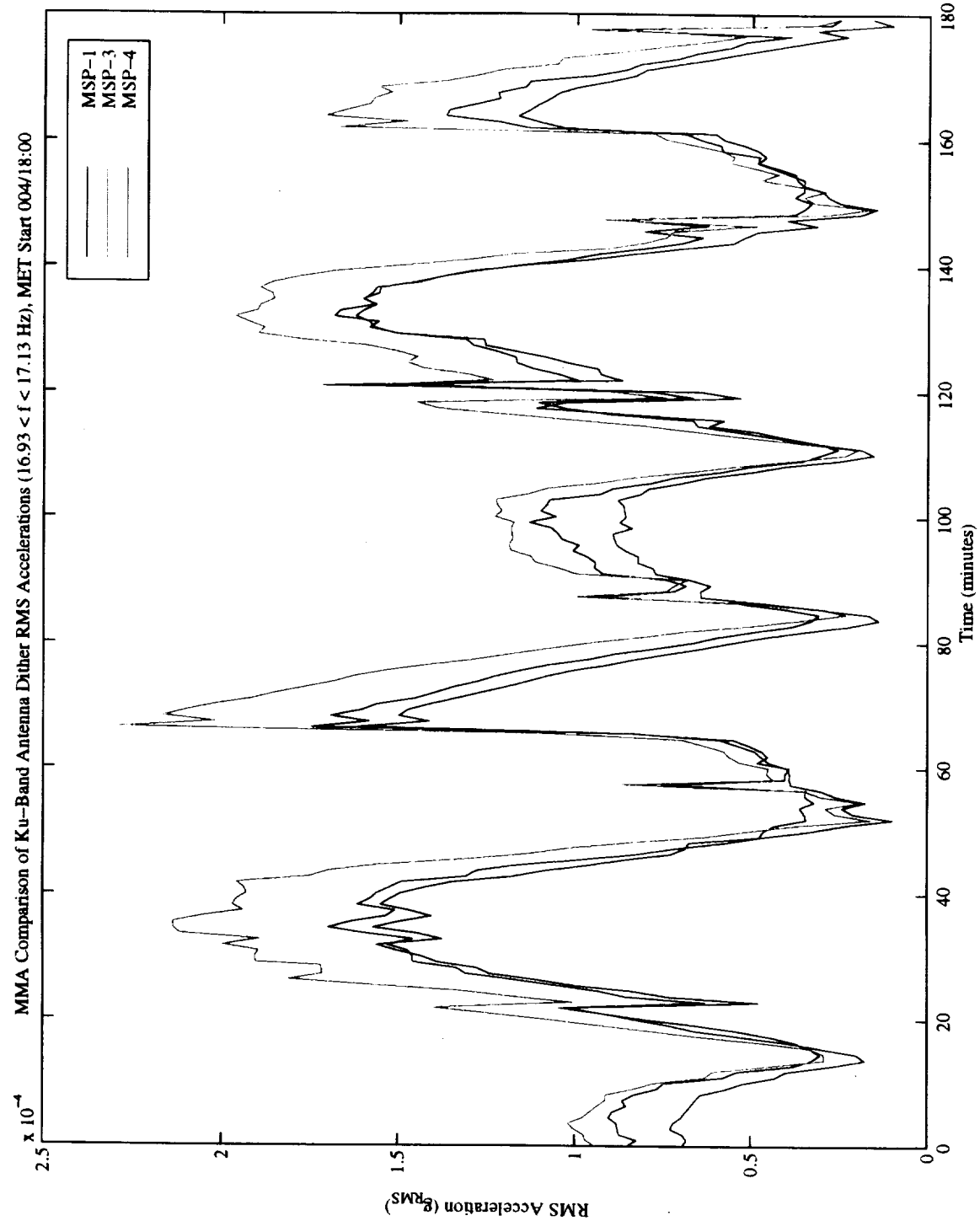


Figure 42. Comparison of Ku-band Antenna Dither RMS Accelerations for MET 004/18:00 - 004/21:00.

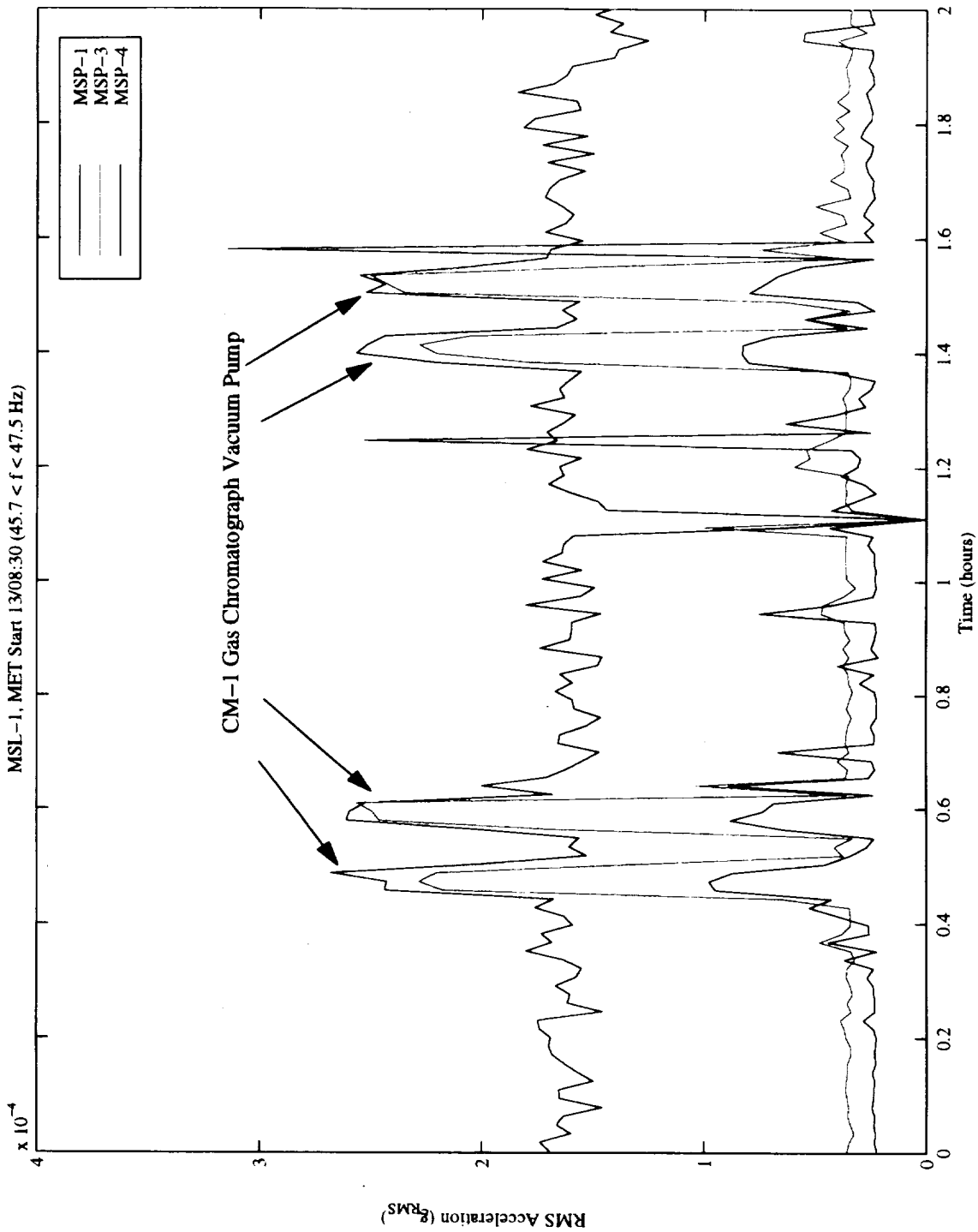


Figure 43. Comparison of CM-1 Gas Chromatograph Vacuum Pump RMS Accelerations for MET 013/08:30 - 013/10:30.

**THIS PAGE INTENTIONALLY LEFT BLANK**

## Appendix A: Accessing Acceleration Data via the Internet

SAMS and OARE data are available over the internet from the NASA LeRC file server (beech.lerc.nasa.gov). Previously, SAMS data were made available on CD-ROM, but distribution of data from current (and future) missions will be primarily through this internet file server.

SAMS data files are arranged in a standard tree-like directory structure. Data are first separated based upon mission. Then, data are further subdivided based upon some portion of the mission, head, year (if applicable), day, and finally type of data file (acceleration, temperature, or gain). Effective November 1, 1996, there has been a minor reorganization of the beech.lerc.nasa.gov file server. There are now two locations for SAMS data: a directory called SAMS-SHUTTLE and a directory called SAMS-MIR. Under the SAMS-SHUTTLE directory, the data are segregated by mission. Under the SAMS-MIR directory, the data are segregated by year. The following figure illustrates this structure.

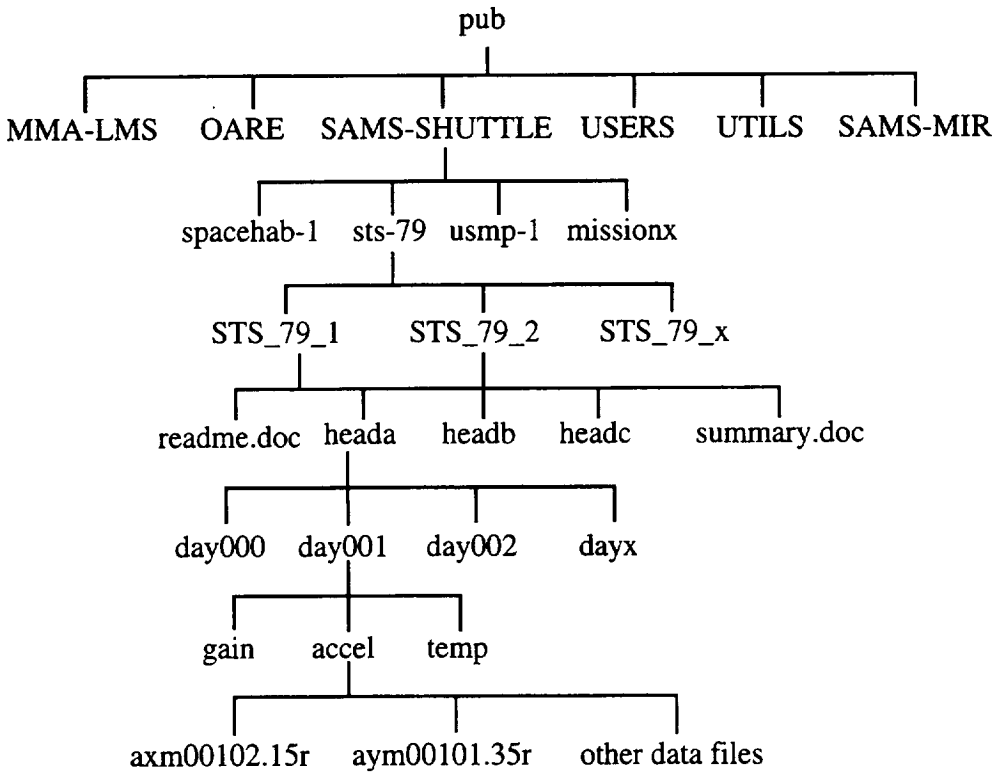


The SAMS data files (located at the bottom of the tree structure) are named based upon the contents of the file. For example, a file named "axm00102.15r" would contain head A data for the x-axis for day 001, hour 02, file 1 of 5. The readme.doc files give a complete explanation of the file naming convention.

OARE data files are also arranged in a tree-like directory structure, but with different branches. The data are first divided based upon mission, and then are divided based upon type of data. The OARE tree structure looks like this:

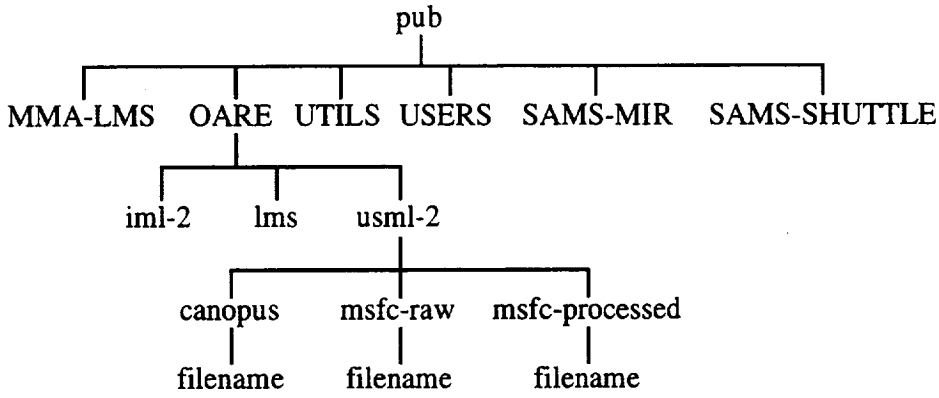


Files under the canopus directory are trimmean filter data, computed by Canopus Systems, Inc. Files under the msfc-raw directory contain the telemetry data files provided to PIMS by the Marshall Space Flight Center's Payload Operations Control Center data reduction group. Files under the msfc-processed directory are raw files containing binary floating point values, listing the MET (in hours), and the x, y, and z axis acceleration in micro-g's.

Data access tools for different computer platforms (MS-DOS, Macintosh, SunOS, and MS-Windows) are available in the /pub/UTILS directory.

The NASA LeRC beech file server can be accessed via anonymous File Transfer Protocol (ftp), as follows:

1) Open an ftp connection to "beech.lerc.nasa.gov"
2) Login as userid "anonymous"
3) Enter your e-mail address as the password
4) Change directory to pub
5) List the files and directories in the pub directory
6) Change directories to the area of interest
7) Change directories to the mission of interest
8) Enable binary file transfers
9) Use the data file structures (described above) to locate the desired files
10) Transfer the desired files

If you encounter difficulty in accessing the data using the file server, please send an electronic mail message to "pims@lerc.nasa.gov". Please describe the nature of the difficulty and also give a description of the hardware and software you are using to access the file server. If you are interested in requesting specific data analysis or information from the PIMS team, also send e-mail to pims@lerc.nasa.gov or call the PIMS Project Manager, Duc Truong at (216) 433-8394.

## Appendix B: MMA MSP-3 Color Spectrograms at Rack 10

The SAMS data have been further processed to produce the plots shown here. Color spectrograms are used to show how the microgravity environment varies in intensity with respect to both the time and frequency domains. These spectrograms are provided as an overview of the frequency characteristics of the SAMS data during the mission. Each spectrogram is a composite of two-hour's worth of data. The time resolution used to compute the spectrograms seen here is 27.307 seconds. This corresponds to a frequency resolution of 0.0366 Hz.

The spectrograms contained herein differ from those spectrograms produced for PIMS mission summary reports prior to January 1996. Previous spectrograms utilized a colormap which had 8 colors. The new spectrograms contain 207 colors. Thus, the magnitude resolution (as represented by the color) shows a significant improvement. Care should be taken to not confuse the current colormap system with that used in reports prior to January 1996. For example, in previous spectrograms, yellow represented a higher magnitude than did red. The new colormap system is opposite when it comes to the yellow-red relation. The user is advised to refer to the colormap key located next to each spectrogram plot.

In order to produce the spectrogram image, Power Spectral Densities (PSDs) were computed for successive time intervals (the length of the interval is equal to the time resolution). For the PSD computation, a Hanning window was applied. In order to combine all three axes into a single plot to show an overall level, a Vector-Magnitude (VM) operation was performed. Stated mathematically:

$$VM = \sqrt{PSD_{x_k}^2 + PSD_{y_k}^2 + PSD_{z_k}^2} .$$

By imaging the base 10 logarithm ($\log_{10}$) magnitude of the PSD as a color and stacking successive PSDs from left to right, variations of acceleration magnitude and frequency are shown as a function of time. Colors are assigned to discrete magnitude ranges, so that there are 207 colors assigned to the entire range of magnitudes shown. Data which fall outside of the maximum and minimum magnitude limits will be imaged as either the highest or lowest magnitude, depending on which side they have saturated. For this report, 1% of the total points lie below the lower limit, and 1% of the total points lie above the upper limit. If an area of interest seems to be saturated, care should be taken in that the actual values may lie above or below the color mapping shown on the plot.

Plot gaps (if any exist) are shown by either white or dark blue areas on the page. Care should be taken to not mistake a plot gap (represented by a dark blue vertical band) with a quiet period. If a plot gap exists for an entire plot (or series of successive plots), a comment is placed on the page to let the user know there is a gap in the data. These "no data available" comments will not show exact times for which the data are not available, but will only indicate missing plots.

Due to the nature of spectrograms, care should be taken to not merely read a color's numeric value as being the acceleration level at a given frequency. In order to get this type of information, the PSDs must be integrated between two frequencies. These frequencies (lower and upper) form the band of interest

$$g_{RMS} = \sqrt{\int_{f_1}^{f_2} PSD \cdot df.}$$

The result of this integration is the $g_{RMS}$ acceleration level in the $[f_{lower}, f_{upper}]$ band.

The PIMS group is able to provide this type of analysis on a per-request basis. To request this additional analysis, send an e-mail to pims@lerc.nasa.gov, or FAX a request to (216) 433-8545.

## Appendix C: MMA MSP-4 Color Spectrograms at Rack 9

The SAMS data have been further processed to produce the plots shown here. Color spectrograms are used to show how the microgravity environment varies in intensity with respect to both the time and frequency domains. These spectrograms are provided as an overview of the frequency characteristics of the SAMS data during the mission. Each spectrogram is a composite of two-hour's worth of data. The time resolution used to compute the spectrograms seen here is 27.307 seconds. This corresponds to a frequency resolution of 0.0366 Hz.

The spectrograms contained herein differ from those spectrograms produced for PIMS mission summary reports prior to January 1996. Previous spectrograms utilized a colormap which had 8 colors. The new spectrograms contain 207 colors. Thus, the magnitude resolution (as represented by the color) shows a significant improvement. Care should be taken to not confuse the current colormap system with that used in reports prior to January 1996. For example, in previous spectrograms, yellow represented a higher magnitude than did red. The new colormap system is opposite when it comes to the yellow-red relation. The user is advised to refer to the colormap key located next to each spectrogram plot.

In order to produce the spectrogram image, Power Spectral Densities (PSDs) were computed for successive time intervals (the length of the interval is equal to the time resolution). For the PSD computation, a Hanning window was applied. In order to combine all three axes into a single plot to show an overall level, a Vector-Magnitude (VM) operation was performed. Stated mathematically:

$$VM = \sqrt{PSD_{x_k}^2 + PSD_{y_k}^2 + PSD_{z_k}^2} .$$

By imaging the base 10 logarithm ($\log_{10}$) magnitude of the PSD as a color and stacking successive PSDs from left to right, variations of acceleration magnitude and frequency are shown as a function of time. Colors are assigned to discrete magnitude ranges, so that there are 207 colors assigned to the entire range of magnitudes shown. Data which fall outside of the maximum and minimum magnitude limits will be imaged as either the highest or lowest magnitude, depending on which side they have saturated. For this report, 1% of the total points lie below the lower limit, and 1% of the total points lie above the upper limit. If an area of interest seems to be saturated, care should be taken in that the actual values may lie above or below the color mapping shown on the plot.

Plot gaps (if any exist) are shown by either white or dark blue areas on the page. Care should be taken to not mistake a plot gap (represented by a dark blue vertical band) with a quiet period. If a plot gap exists for an entire plot (or series of successive plots), a comment is placed on the page to let the user know there is a gap in the data. These "no data available" comments will not show exact times for which the data are not available, but will only indicate missing plots.

Due to the nature of spectrograms, care should be taken to not merely read a color's numeric value as being the acceleration level at a given frequency. In order to get this type of information, the PSDs must be integrated between two frequencies. These frequencies (lower and upper) form the band of interest

$$g_{RMS}=\sqrt{\int_{f_1}^{f_2} \mathrm{PSD} \cdot \mathrm{df}.}$$

The result of this integration is the $g_{RMS}$ acceleration level in the $[f_{lower}, f_{upper}]$ band.

The PIMS group is able to provide this type of analysis on a per-request basis. To request this additional analysis, send an e-mail to pims@lerc.nasa.gov, or FAX a request to (216) 433-8545.

## Appendix D: MMA MSP-1 Color Spectrograms at Rack 3

The SAMS data have been further processed to produce the plots shown here. Color spectrograms are used to show how the microgravity environment varies in intensity with respect to both the time and frequency domains. These spectrograms are provided as an overview of the frequency characteristics of the SAMS data during the mission. Each spectrogram is a composite of two-hour's worth of data. The time resolution used to compute the spectrograms seen here is 27.307 seconds. This corresponds to a frequency resolution of 0.0366 Hz.

The spectrograms contained herein differ from those spectrograms produced for PIMS mission summary reports prior to January 1996. Previous spectrograms utilized a colormap which had 8 colors. The new spectrograms contain 207 colors. Thus, the magnitude resolution (as represented by the color) shows a significant improvement. Care should be taken to not confuse the current colormap system with that used in reports prior to January 1996. For example, in previous spectrograms, yellow represented a higher magnitude than did red. The new colormap system is opposite when it comes to the yellow-red relation. The user is advised to refer to the colormap key located next to each spectrogram plot.

In order to produce the spectrogram image, Power Spectral Densities (PSDs) were computed for successive time intervals (the length of the interval is equal to the time resolution). For the PSD computation, a Hanning window was applied. In order to combine all three axes into a single plot to show an overall level, a Vector-Magnitude (VM) operation was performed. Stated mathematically:

$$VM = \sqrt{PSD_{x_k}^2 + PSD_{y_k}^2 + PSD_{z_k}^2} .$$

By imaging the base 10 logarithm ($\log_{10}$) magnitude of the PSD as a color and stacking successive PSDs from left to right, variations of acceleration magnitude and frequency are shown as a function of time. Colors are assigned to discrete magnitude ranges, so that there are 207 colors assigned to the entire range of magnitudes shown. Data which fall outside of the maximum and minimum magnitude limits will be imaged as either the highest or lowest magnitude, depending on which side they have saturated. For this report, 1% of the total points lie below the lower limit, and 2% of the total points lie above the upper limit. If an area of interest seems to be saturated, care should be taken in that the actual values may lie above or below the color mapping shown on the plot.

Plot gaps (if any exist) are shown by either white or dark blue areas on the page. Care should be taken to not mistake a plot gap (represented by a dark blue vertical band) with a quiet period. If a plot gap exists for an entire plot (or series of successive plots), a comment is placed on the page to let the user know there is a gap in the data. These "no data available" comments will not show exact times for which the data are not available, but will only indicate missing plots.

Due to the nature of spectrograms, care should be taken to not merely read a color's numeric value as being the acceleration level at a given frequency. In order to get this type of information, the PSDs must be integrated between two frequencies. These frequencies (lower and upper) form the band of interest

$$g_{RMS} = \sqrt{\int_{f_1}^{f_2} PSD \cdot df.}$$

The result of this integration is the $g_{RMS}$ acceleration level in the $[f_{lower}, f_{upper}]$ band.

The PIMS group is able to provide this type of analysis on a per-request basis. To request this additional analysis, send an e-mail to pims@lerc.nasa.gov, or FAX a request to (216) 433-8545.

## Appendix E: Accelerometer Systems Contacts

| *Accelerometer* | *Location* | *Contact* | *Affiliation* |
|---|---|---|---|
| Microgravity Measurement Assembly (MMA) | Spacelab Rack 3 | Maurizio Nati | European Space Agency (ESA) |
| Orbital Acceleration Research Experiment (OARE) | Keel Bridge | William Wagar | NASA Lewis Research Center, Cleveland, OH |
| Space Acceleration Measurement System (SAMS) | Spacelab Center Aisle | Ron Sicker | NASA Lewis Research Center, Cleveland, OH |
| Quasi-steady Acceleration Measurement (QSAM) System | Spacelab Rack 3 | Hans-Ewald Richter | German Aerospace Research Establishment (DLR) |

**THIS PAGE INTENTIONALLY LEFT BLANK**

## Appendix F: User Comment Sheet

We would like you to give us some feedback so that we may improve the Mission Summary Reports. Please answer the following questions and give us your comments.

1. Do the Mission Summary Reports fulfill your requirements for acceleration and mission information?
   _____Yes _____No

If not why not?

Comments: _____

_____

2. Is there additional information which you feel should be included in the Mission Summary Reports?
   _____Yes _____No

If so what is it?

Comments: _____

_____

3. Is there information in these reports which you feel is not necessary or useful?

   _____Yes _____No

If so, what is it?

Comments: _____

_____

4. Do you have internet access via: ( ____ )ftp ( ____ )WWW ( ____ )gopher ( ____ )other? Have you already accessed SAMS data or information electronically?

   _____Yes _____No

Comments: _____

_____

Completed by: Name:_____ Telephone:_____

Address:_____ Facsimile:_____

_____ E-mail:_____

**Return this sheet to:**
**Duc Truong**
**NASA Lewis Research Center**
**21000 Brookpark Road MS 500-216**
**Cleveland, OH 44135**

**or**
**FAX to PIMS Project: 216-433-8660**
**e-mail to: pims@lerc.nasa.gov.**

# REPORT DOCUMENTATION PAGE

*Form Approved*
*OMB No. 0704-0188*



| 1. AGENCY USE ONLY (*Leave blank*) | 2. REPORT DATE | 3. REPORT TYPE AND DATES COVERED |
|---|---|---|
| | May 1998 | Technical Memorandum |

**4. TITLE AND SUBTITLE**

Summary Report of Mission Acceleration Measurements for MSL–1
STS–83, Launched April 14, 1997
STS–94, Launched July 1, 1997

**5. FUNDING NUMBERS**

WU–963–60–0D–00

**6. AUTHOR(S)**

Milton E. Moskowitz, Kenneth Hrovat, Peter Tschen, Kevin McPherson, Maurizio Nati, and Timothy A. Reckart

**7. PERFORMING ORGANIZATION NAME(S) AND ADDRESS(ES)**

National Aeronautics and Space Administration
Lewis Research Center
Cleveland, Ohio 44135–3191

**8. PERFORMING ORGANIZATION REPORT NUMBER**

E–11134

**9. SPONSORING/MONITORING AGENCY NAME(S) AND ADDRESS(ES)**

National Aeronautics and Space Administration
Washington, DC 20546–0001

**10. SPONSORING/MONITORING AGENCY REPORT NUMBER**

NASA TM—1998-206979

**11. SUPPLEMENTARY NOTES**

Milton E. Moskowitz, Ken Hrovat, and Timothy Reckart, Tal-Cut Company, 24831 Lorain Road, Suite 203, North Olmsted, Ohio 44070; Peter Tschen and Kevin McPherson, NASA Lewis Research Center; Maurizio Nati, European Space Research and Technology Center, Noordwijk, The Netherlands. Responsible person, Ken Hrovat, organization code 6727, (216) 433–3564.

**12a. DISTRIBUTION/AVAILABILITY STATEMENT**

Unclassified - Unlimited
Subject Categories: 20, 35, and 18 Distribution: Nonstandard

This publication is available from the NASA Center for AeroSpace Information, (301) 621–0390.

**12b. DISTRIBUTION CODE**

**13. ABSTRACT** ***(Maximum 200 words)***

The microgravity environment of the Space Shuttle Columbia was measured during the STS–83 and STS–94 flights of the Microgravity Science Laboratory (MSL–1) mission using four different accelerometer systems: the Orbital Acceleration Research Experiment (OARE), the Space Acceleration Measurement System (SAMS), the Microgravity Measurement Assembly (MMA), and the Quasi-Steady Acceleration Measurement (QSAM) system. All four accelerometer systems provided investigators with acceleration measurements downlinked in near-real-time. Data from each system was recorded for post-mission analysis. The OARE measured the Shuttle's acceleration with high resolution in the quasi-steady frequency regime below about 0.1 Hz. The SAMS provided investigators with higher frequency acceleration measurements up to 25 Hz. The QSAM and MMA systems provided investigators with quasi-steady and higher frequency (up to 100 Hz) acceleration measurements, respectively. The microgravity environment related to various Orbiter maneuvers, crew activities, and experiment operations as measured by the OARE and MMA is presented and interpreted in section 8 of this report.

| 14. SUBJECT TERMS | 15. NUMBER OF PAGES |
|---|---|
| Microgravity environment; SAMS; Shuttle; Orbiter; NASA; Acceleration measurement | 112 |
| | 16. PRICE CODE A06 |

| 17. SECURITY CLASSIFICATION OF REPORT | 18. SECURITY CLASSIFICATION OF THIS PAGE | 19. SECURITY CLASSIFICATION OF ABSTRACT | 20. LIMITATION OF ABSTRACT |
|---|---|---|---|
| Unclassified | Unclassified | Unclassified | |